



Joint Authorities for  
Rulemaking on Unmanned  
Systems

# JARUS guidelines on SORA

## Annex F

### Theoretical Basis for Ground Risk Classification and Mitigation

DOCUMENT IDENTIFIER : JAR-DEL-SRM-SORA-F-2.5

<b>Edition Number</b>	<b>2.5</b>
<b>Edition Date</b>	<b>13.05.2024</b>
<b>Status</b>	<b>Release</b>
<b>Intended for</b>	<b>Publication</b>
<b>Category</b>	<b>Guidelines</b>
<b>WG</b>	<b>SRM</b>

# DOCUMENT CHARACTERISTICS

TITLE		
<b>Specific Operations Risk Assessment (SORA) Annex F</b>		
<b>Publications Reference:</b>		JAR_doc_29
		<b>ID Number:</b>
<b>Document Identifier</b>	<b>Edition Number:</b>	2.5
JAR-DEL-SRM-SORA-F-2.5	<b>Edition Date:</b>	13.05.2024
Abstract		
<p>This document presents a theoretical basis for the ground risk model used in SORA. It provides a quantitative underpinning for the Steps #2 and #3. It also covers the containment model of SORA with regards to its ground risk component.</p>		
Keywords		
<p>SORA, SAIL, Specific, Ground Risk, Containment</p>		
<b>Contact Person(s)</b>	<b>Tel</b>	<b>Unit</b>
Jörg Dittrich – DLR / Germany Leader Work Group Safety Risk Management		WG-SRM

STATUS, AUDIENCE AND ACCESSIBILITY					
Status		Intended for		Accessible via	
Working Draft	<input type="checkbox"/>	General Public	<input checked="" type="checkbox"/>	Intranet	<input type="checkbox"/>
Final	<input checked="" type="checkbox"/>	JARUS members	<input type="checkbox"/>	Extranet	<input type="checkbox"/>
Proposed Issue	<input type="checkbox"/>	Restricted	<input type="checkbox"/>	Internet ( <a href="http://jarus-rpas.org">http://jarus-rpas.org</a> )	<input checked="" type="checkbox"/>
Released Issue	<input type="checkbox"/>	Internal/External consultation <input type="checkbox"/>			

## DOCUMENT APPROVAL

The following table identifies the process successively approving the present issue of this document before public publication.

PROCESS	NAME AND SIGNATURE WG leader	DATE
WG	Lorenzo Murzilli	22.05.2020
Internal Consultation	Lorenzo Murzilli	12.02.2021
External Consultation	Lorenzo Murzilli	08.11.2022
Publication	Jörg Dittrich	13.05.2024

## DOCUMENT CHANGE RECORD

The following table records the complete history of the successive editions of the present document.

EDITION NUMBER	EDITION DATE	REASON FOR CHANGE	PAGES / SECTIONS AFFECTED
0.1	22.05.2020	Version for WG internal consultation	First edition
0.2	12.02.2021	Version for JARUS WG-SRM internal consultation	All, Additional section on measuring population density. Appendices for abbreviation and variables, and for defining Loss of Control
0.3	08.11.2022	Version for JARUS External consultation	All sections for internal comment resolution, Adjustment of the assumptions for ground risk resulting in a change of population density limits in the GRC table. Removal of M3 mitigation Expanded explanatory material on improvements to iGRC cell resolution.
2.5	13.05.2024	Public release	All sections for external comment resolution, Adjustment of the assumptions for ground risk resulting in a change of population density limits in the GRC table, Addition of grid size determination based on flight altitude, New section for containment added which was previously consulted as part of the Explanatory Note for SORA 2.5. Alternative containment method is based on the External Consultation Version of SORA 2.5.

## DOCUMENT CONTRIBUTORS

<b>WG-SRM Lead</b>	
From December 2022	Jörg Dittrich – DLR / Germany
before December 2022	Lorenzo Murzilli – FOCA / Switzerland
<b>Task Force Ground Risk Quantitative Methods Lead</b>	
Terrence Martin – Revolution Aerospace	
<b>Task Force Ground Risk Quantitative Methods</b>	
Alberto Cunial – EASA	Lilian Daelemans – EASA
Cheryl Dorsey – Aurora Flight Sciences	Anders La Cour-Harbo – Aalborg University
Henri Hohtari – Wingtra	Tony Nannini – Wing
Andreea Perca – FOCA / Switzerland	Tom Putland – Revolution Aerospace

As multiple WG-SRM members have assumed new responsibilities and changed affiliations over the years of document development, all contributors are listed with their affiliation at the time of their last contribution.

# Contents

<b>1</b>	<b>Introduction</b>	<b>10</b>
1.1	Scope	10
1.2	Basis for Ground Risk Assessment in the SORA	11
1.2.1	Establishing a Target Level of Safety	11
1.2.2	Determining the Ground Fatality Rate	12
1.2.3	SORA iGRC Table	13
1.2.4	Relation to SAIL	13
1.3	Calculating iGRC with Population and Critical Area	14
1.4	Finalised iGRC Table	14
1.5	Reduced iGRC Allocation Errors	15
1.6	Mitigation and the iGRC	17
1.7	iGRC value – a step-by-step approach	18
1.7.1	Determine the approach method for finding iGRC	18
1.7.2	Using the iGRC table directly	19
1.7.3	Limiting values for iGRC cells	20
1.7.4	Trade-off tables	20
1.7.5	Casex online tool	21
1.7.6	Casex Python package	21
1.7.7	The JARUS model	21
1.7.8	Operations with unusual parameters	22
1.7.9	Further observations	22
1.8	JARUS model step-by-step	22
1.8.1	Case 1: UA width above or equal to 8 meters	23
1.8.2	Case 2: UA width between 1 m and 8 m	24
1.8.3	Case 3: UA width smaller than 1 m	24
1.8.4	Finding the iGRC value	24
<b>2</b>	<b>Intrinsic Ground Risk Framework</b>	<b>25</b>
2.1	Relationship between $\lambda_{GI}$ , $D_{pop}$ , $A_C$ and TLOS	25
2.2	iGRC Design Considerations	26
2.3	Basics of Critical Area Determination	26
2.3.1	Models	27
2.3.2	Critical area used in Annex F	28
2.4	Initial Threshold Selections for Population and Wingspan Bands	29
2.5	Step-by-step Progression in the development of the nominal iGRC Table	30
2.5.1	Unmitigated Casualty Expectation given Nominal $D_{pop}$ and $A_C$ Values	30
2.5.2	Maximum Allowable loss of control of the operation rate ( $\lambda_{GI}$ ) for nominal $D_{pop}$ and $A_C$ Values	31
2.5.3	Mapping from SAIL to iGRC values	31
2.5.4	Intrinsic Ground Risk Class for nominal $D_{pop}$ and $A_C$ Values	31
2.5.5	Raw iGRC Formulation	32
2.5.6	Rounding Policy	33
2.6	Progression from $A_C$ to Wingspan and Velocity in the final iGRC Table	34
<b>3</b>	<b>Determination of Population to Support iGRC</b>	<b>35</b>
3.1	Introduction	35
3.2	Step by Step Process to iGRC Map Selection and Modification	36
3.2.1	Dealing with erroneous static data in designated population density maps	36
3.3	Selecting which Population Density to use in the iGRC footprint	38
3.3.1	Determining the Population Density for Flight over Heterogeneous iGRC Footprints	39

3.3.2	Short Exposure Flight Over Higher Population Segments	41
3.3.3	Higher Population Densities in the Ground Risk Buffer	41
3.4	Common Methods Used to Create Population Density Maps	42
3.4.1	Census Data and the Modifiable Areal Unit Problem (MAUP)	42
3.4.2	Spatial Interpolation	45
3.4.3	Areal Interpolation	46
3.4.4	Pycnophylactic Interpolation	47
3.4.5	Dasymetric Mapping	48
3.4.6	Smart Interpolation	49
3.5	Temporal Accuracy	49
3.5.1	Human movement: Residential and Business Properties	49
3.5.2	Human Movement: Temporary changes due to events	50
3.5.3	Mobile Phone Data for Use in Population Maps	50
3.6	Settlement Maps and Density Smoothing	51
3.6.1	Background	51
3.6.2	Establishing Consensus over Definitions and Methodology	51
3.6.3	DEGURBA Incorporation in GHS-SMOD	52
3.7	Understanding the Original Intent of a Map Generation	54
3.7.1	Underlying Intent of the Mapping Product	55
3.7.2	Population Counts: Underlying Data and Methodology	55
3.7.3	Ancillary Data Assumptions	55
3.8	Common Mapping Products	55
3.9	Appropriate grid resolution to accurately measure population density	57
3.9.1	Map resolution as a function of intended operating altitude	60
3.10	Hybrid Mapping products created by the Applicant	62
<b>4</b>	<b>Mitigations</b>	<b>64</b>
4.1	Overview of Available Mitigations	64
4.2	M1(A) - Strategic Mitigations for Ground Risk - Sheltering	65
4.3	M1(B) - Strategic Mitigations for Ground Risk - Operational Restriction	66
4.4	Achievable iGRC Reductions using strategic mitigations	66
4.5	M1(C)- Tactical Mitigations - ground observation	67
4.6	M2 - Effects of ground impact are reduced	67
4.6.1	Criterion 1 - Technical Design	67
4.6.2	Criterion 2 - Procedures (if applicable)	68
4.6.3	Criterion 3 - Training (if applicable)	68
4.7	Summary of Mitigation Reductions	69
4.8	Optional JARUS Model Trade-offs	69
<b>5</b>	<b>Adjacent Areas and Containment</b>	<b>71</b>
5.1	Adjacent Area Ground Risk Assumptions	71
5.1.1	Adjacent Area Ground Risk Assumptions and sizing	71
5.1.2	Adjacent Area Size Justifications	71
5.1.3	Maximum Size of Adjacent Area	71
5.1.4	Evaluating Gathering of People in the Adjacent Areas	75
5.2	Expected Ground Risk Casualty Rate Model in the Adjacent Area	81
5.2.1	Containment Requirements as a Function of Final GRC in the Adjacent Area	82
5.2.2	Inherent Probability of Entering the Adjacent Area	83
5.2.3	Mitigated Probability of Entering the Adjacent Area	84
5.2.4	Low, Medium, and High Robustness Containment Objectives	84
5.2.5	Low Robustness Containment Assumptions	84
5.2.6	Medium Robustness Containment Assumptions	85
5.2.7	High Robustness Containment Assumptions	85

5.2.8	Containment Objectives Based Upon the Risk of the Adjacent Area	86
5.3	Alternative Method to Compute Ground Risk Containment Requirements	87
5.3.1	Introduction	87
5.3.2	Outcome	87
5.3.3	Task Description	87
5.3.4	Additional Guidance	91
5.3.5	Guidance on the application of the ground risk mitigations in the adjacent area	91
<b>A</b>	<b>Critical Area to Wingspan and Speed Calculations</b>	<b>92</b>
A.1	Addition of Velocity Constraints in the Column Headers	92
A.2	Determining Appropriate Values for the iGRC Table	93
A.2.1	Impact Angle and Speed	93
A.2.2	Altitude for ballistic descent	94
A.2.3	Descent scenarios	94
A.2.4	Lighter-than-air aircraft	95
A.3	Critical Area Model Parameters	95
A.3.1	Maximum Speed	96
A.3.2	Ratio of Glide to Maximum Speed	96
A.3.3	Coefficient of Restitution	96
A.3.4	Coefficient of Friction	97
A.3.5	Lethal kinetic energy	97
A.3.6	Drag coefficient	97
A.3.7	Ballistic Descent Calculations	98
A.3.8	Concession on smaller critical area for rotorcraft	99
A.4	Mapping Impact Speed and Impact Angle	100
A.4.1	Speed and angle relation for fixed critical area	100
A.4.2	iGRC Maximum Speed Limit Values	101
A.5	Special Cases	101
A.5.1	The First iGRC column (UAS characteristic dimension < 1 m)	101
A.5.2	Obstacles stopping an aircraft	102
A.5.3	Obstacles versus sheltering	104
A.5.4	Density of obstacles	106
A.6	Creating the Final iGRC Table	106
A.6.1	Introduction	106
A.6.2	Critical Area Calculations	107
A.6.3	Finalisation of iGRC Table	109
<b>B</b>	<b>Critical area modelling</b>	<b>110</b>
B.1	Existing Model Comparison	110
B.1.1	Bounce and splatter/cratering	110
B.1.2	Secondary effects	111
B.1.3	Explosions	111
B.1.4	Deflagration	111
B.1.5	Blade throw	112
B.1.6	High-energy rotating parts	112
B.2	Mathematics behind models	113
B.2.1	RCC model	113
B.2.2	RTI model	114
B.2.3	FAA model	114
B.2.4	NAWCAD model	115
B.2.5	Deflagration model	116
B.3	JARUS critical area model	116
B.4	Critical area reduction due to obstacles	117

B.4.1	Obstacles	117
B.4.2	CA reduction simulation	118
B.4.3	CA reduction modelling	121
B.4.4	Applying reduced CA	122
<b>C</b>	<b>Hazard terminology in the context of Annex F</b>	<b>124</b>
C.1	UAS operation out of control in context	125
<b>D</b>	<b>Abbreviations and variables</b>	<b>127</b>
D.1	Abbreviations	127
D.2	Variables	128
<b>E</b>	<b>CasEx package</b>	<b>129</b>
E.1	Introduction	129
E.2	Installation and use	129
E.3	Online calculator	129

# 1 Introduction

## 1.1 Scope

Annex F supports the Joint Authorities for Rulemaking of Unmanned Systems (JARUS) Specific Operations Risk Assessment (SORA). Specifically, Annex F provides the principles, calculations, and assumptions used in the SORA ground assessment process (i.e., SORA Steps #2 and #3). The high-level goal for this annex is to ensure that for most cases, there is a path to operational approval when ground risk is conservatively mitigated to an acceptable level of safety, commensurate with manned aviation and reflects the variety of UAS operations in the Category B/Specific Category as described in JARUS document, "UAS Operational Categorisation" [1]. In addition, the inputs needed for the risk assessment are meant to be able to be reasonably obtained by the applicant and verified by the authority. This intent is achieved by providing:

- Quantitative traceability between the SORA Specific Assurance and Integrity Levels (SAIL) embedded within the Operational Safety Objectives (OSO) and how the technical characteristics of a platform and its intended operation use subsequently affect the associated risk of a ground collision.
- A mechanism to establish whether the actual risk of the operation is aligned with the nominal iGRC classification (Step #2 of SORA) by providing a detailed analytical basis.
- A quantitative framework that outlines the effect of population, platform characteristics, and mitigations (Step #3 of SORA) on ground risk.
- A list of assumptions used in the above calculations. For circumstances where those assumptions are not applicable to a particular system or operation, a process is detailed (including equations), by which an applicant or authority can manually calculate the expected ground risk class.

This annex is divided into five sections and five appendices that describe the analytic and quantitative approach for the Ground Risk assessment process. The structure of this Annex is as follows:

### Sections

- Section 1 - Provides a high-level overview of the quantitative basis underpinning the JARUS SORA Ground Risk process.
- Section 2 – Furthers Section 1 by detailing the underlying principles of the iGRC and iGRC matrix, including how it is calculated.
- Section 3 - Provides information on determining the overflowed population density.
- Section 4 – Provides information on the two ground risk mitigations in the SORA.
- Section 5 - Provides information on the ground risk model applies to the adjacent area and containment.

### Appendices

- Appendix A - Justifies the substitution of cruise velocity for kinetic energy to the iGRC table.
- Appendix B - Describes the mathematical basis used in the critical area models fundamental to the critical area calculation and the model for ground obstacles.

- Appendix C - Clarifies the meaning for “*loss of control of the operation*” in the context of Annex F
- Appendix D - Provides a consolidated list of acronyms and variables used throughout the document.
- Appendix E - Introduction to CasEx, the Python package developed alongside Annex F to allow for the recreation of figures and for operators and competent authorities to do their own calculations.

Applicable assumptions and constraints are identified in the relevant sections throughout this Annex. Unless stated otherwise, all units in this Annex are metric.

## 1.2 Basis for Ground Risk Assessment in the SORA

### 1.2.1 Establishing a Target Level of Safety

To quantitatively determine if an unmanned operation is appropriately safe, an acceptable level of safety needs to be defined. Annex F uses the top-level principles cited in Section 5 in the Scoping Paper to AMC RPAS 1309 Issue 2 [2] to determine a justifiable Target Level of Safety (TLOS) for drone operations. In particular, we use Section 5(g)(2) as a foundational principle for the TLOS:

**RPAS must not present a greater risk to persons or property on the ground or in the air than that attributable to manned aircraft of equivalent category.**

The equivalent ground risk category for the TLOS is based on manned General Aviation (GA) risk to third parties on the ground. For these third parties, TLOS is measured in expected third-party ground fatalities per hour. This is a critical difference to conventional aviation risk measurement, measured in *accidents per flight hour*.

In conventional aviation, because persons are onboard (either as crew or passengers), safety targets focus on **events** that affect the people on board in some capacity (i.e., serious injury accidents, fatal accidents). When dealing with risk to third parties, the harm only occurs **if** a third party is harmed when an accident, which results in ground impact, occurs. This means the focus of the TLOS should be on the harm to those third parties rather than the aircraft accident itself.

Additionally, as the risk is focused on a population at risk rather than the persons on board an aircraft, the temporal metric must reflect the risk to the population. This means that instead of using the conventional aviation “per flight hour” metric, a “per hour” risk metric associated with a given population must be used. Please see Section 3.3 for more information.

The TLOS is determined by understanding the current fatality rate that occurs due to general aviation incidents using the following equation:

$$\text{TLOS} = \lambda_{\text{GA}_{\text{Accident}}} \cdot N_{\text{fatality}|\text{GA}_{\text{Accident}}} , \quad (1)$$

where

- $\lambda_{\text{GA}_{\text{Accident}}}$  is the generally accepted manned general aviation accident rate. Annex F uses  $10^{-4}$  accidents per flight hour for general aviation as discussed in section 11.3(c) of the Scoping Paper and
- $N_{\text{fatality}|\text{GA}_{\text{Accident}}}$  is the expected ground fatalities per general aviation aircraft accident. Annex F uses  $10^{-2}$  fatalities per manned GA accident rate, as discussed in section 11.2(c) of the Scoping Paper.

Multiplying out the terms in Equation (1) provides a value of  $10^{-6}$  fatalities per flight hour (or 1 fatality every 1 million flight hours), which UAS operations should not exceed. In order to prevent unusual averaging arguments, this is treated as a "per hour" rate, with expansion on the topic provided in Subsection 3.3.1. It is highlighted, however, that the TLOS detailed above for GA is the risk to third parties on the ground and does not include the risk to people on board the aircraft.

Although the aforementioned TLOS is consistent with manned aircraft ground risk, assessing risks/events that could compromise the TLOS may not be identical. As with all valid safety processes, after the TLOS is established, the events and associated risks that could undermine that TLOS must be identified, quantified, and sufficiently mitigated.

### 1.2.2 Determining the Ground Fatality Rate

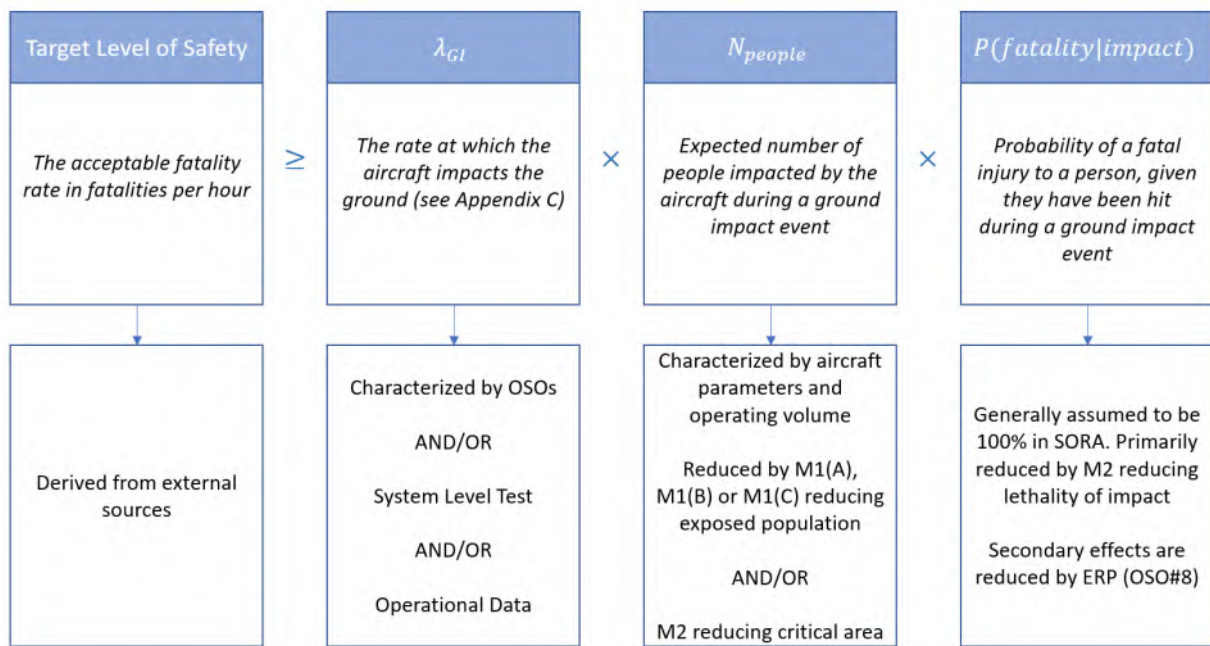


Figure 1: A graphical representation of the relation in Equation (2).

The SORA Ground Risk TLOS is set to the expected number of fatalities on the ground per flight hour for the UAS operation, as outlined in Section 1.2. The components underpinning this TLOS are broken out as

$$\lambda_{\text{fatality}} = \lambda_{\text{GI}} \cdot N_{\text{people}} \cdot P(\text{fatality}|\text{collision, GI}), \quad (2)$$

where

- $\lambda_{\text{fatality}}$  is the expected ground fatality rate per flight hour for the operation.
- $\lambda_{\text{GI}}$  is the expected number of times the UAS operation enters into a loss of control of the operation state, which will result in a ground impact only, per flight hour. This parameter takes into account both aircraft's technical and operational failures. The meaning of "loss of control" of the operation" is discussed in Appendix C.1.
- $N_{\text{people}}$  is the expected number of people impacted by the UAS during a loss of control of the operation event. People who are involved in the operation are not included in this value.
- $P(\text{fatality}|\text{collision, GI})$  is the probability of the UAS causing a fatality to each impacted person on the condition that the aircraft has failed into a loss of control of the operation state and has collided with that person(s).

Furthermore,  $N_{\text{people}}$  is decomposed into population density, population exposure factor, and critical area to get

$$\lambda_{\text{fatality}} = \lambda_{\text{GI}} \cdot D_{\text{pop}} \cdot F_{\text{exp}} \cdot A_C \cdot P(\text{fatality}|\text{collision, GI}) , \quad (3)$$

where

- $D_{\text{pop}}$  is the assumed maximum population density [measured in people per square meter, or ppl/m<sup>2</sup>] within the ground risk footprint (see Section 3 for details).
- $F_{\text{exp}}$  is the fraction of people exposed to harm from the operation, equivalent to (1 minus sheltering factor. See Section 4.2 for more detail ). Note that the value depends on the aircraft and the operation since it is the fraction of people who can indeed be reached by a crashing aircraft, even if they are under a tree, roof, etc.
- $A_C$  is the critical area (measured in m<sup>2</sup>) of the aircraft, which is the ground area where a person would be expected to be impacted by the aircraft in the event of a loss of control of the operation event (see Section 2.3 for details).

Figure 1 illustrates how the different aspects of the SORA Ground Risk process apply to the expected number of fatalities as given in Equation (2).

### 1.2.3 SORA iGRC Table

Step #2 of the JARUS SORA outlines the process to be used by operators and competent authorities to determine an intrinsic Ground Risk Class (iGRC), supported by the use of the iGRC table. Here, the operator establishes their iGRC value by finding the cell corresponding with the intersection for the maximum population density they plan to overfly and two aircraft parameters: wingspan and maximum cruise velocity.

The iGRC is a simplified metric providing a conservative starting value for the **unmitigated ground risk** that an operation poses to persons situated within the operational volume and ground risk buffer on the condition that a failure has occurred.

For the iGRC matrix, it is assumed that everyone within the defined area is uniformly distributed within that area and fully exposed to the risk. This means that  $\lambda_{\text{fatality}}$  is the same everywhere in the ground risk footprint and that  $F_{\text{exp}} = 1$ . It is also assumed that any contact between the aircraft and a person is fatal (i.e.,  $P(\text{fatality}|\text{collision, GI}) = 1$ ), unless otherwise stated<sup>1</sup>. Given these assumptions, the expected number of fatalities in the event of a loss of control of the operation event is

$$E_C(\text{unmitigated}) = D_{\text{pop}} \cdot A_C , \quad (4)$$

which is the number of people expected to be in the critical area.

### 1.2.4 Relation to SAIL

With no further action, the iGRC becomes the final Ground Risk Class (GRC) that, along with the Air Risk Class (ARC), would determine the SAIL. The SAIL links the “*loss of control*” of the operation rate to operational, organizational, personnel, and UAS technical requirements. When implemented correctly, these measures ensure that the probability of losing control of the operation meets the TLOS.

<sup>1</sup>For example in Section A.5.2,  $P(\text{fatality}|\text{collision, GI})$  during slide for < 1 m platforms is ignored

The relationship between the SAIL objective levels of robustness and the expected maximum probability of loss of control of the operation has been developed as a multinational effort of aviation experts working through the JARUS WG-SRM panel to develop robustness requirements for the operational, organizational, personnel, and technical threat barriers that can be implemented to reduce the probability that an operation loses control.

The higher the SAIL score, the less probable a loss of control of the operation event is expected to be. Table 1 shows the mapping between SAIL and the maximum expected rate,  $\lambda_{GI}$ , of a loss of control of the operation event to meet the TLOS still.

Table 1: Mapping between SAIL and maximum acceptable Operation Failure Rate (loss of control of the operation)

SAIL level	I	II	III	IV	V	VI
<b>operation failure rate</b> $\lambda_{GI}$ (Rate of loss of control of the operation per flight hour)	$10^{-1}$	$10^{-2}$	$10^{-3}$	$10^{-4}$	$10^{-5}$	$10^{-6}$

Since it may be impractical for many operations to determine the actual loss of control of the operation rate  $\lambda_{GI}$  with system-level testing or operational data, the qualitative SAIL system has been developed by JARUS to superimpose increasingly more rigorous OSOs commensurate with increasing risk as a means of ensuring levels of design, maintenance, operational procedures and crew training are appropriate for the risk posed by the operation<sup>2</sup>. It is designed such that as the SAIL level increases, the expected probability of loss of control of the operation decreases due to the increased robustness of the OSOs.

Note that the final SAIL is defined by taking the larger contribution from the air and ground risk. For this Annex, only ground risk is considered, acknowledging that the final SAIL level may be higher due to the air risk component.

### 1.3 Calculating iGRC with Population and Critical Area

Based on the link between TLOS, loss of control of the operation rates, SAIL, and fatality rate in Equation (3), it is detailed in Section 2.1 that the iGRC value is a function that exists for all population densities and critical area combinations, and which ultimately can be written as

$$iGRC = \max\left(1, \lceil 7 + \log_{10}(D_{pop} \cdot A_C) - 0.5 \rceil\right). \quad (5)$$

The left and right half brackets mean rounding up to the nearest integer, and the constant 0.5 is a modifying constant further detailed in Section 2.5.6. The  $\max$  ensures that the iGRC value is at least 1 (for very small population densities or critical areas).

### 1.4 Finalised iGRC Table

Equation 5 was applied to a selection of aircraft parameters and population density bands to produce the finalized iGRC table which is shown in Table 2. The iGRC is found at the intersection of the applicable maximum population density and the left most column matching both criteria, the maximum UA characteristic dimension and the maximum speed in 2. The applicant can provide substantiation to the competent authority for a different iGRC. See Appendix A to this Annex for further guidance.

The key updates to previous iGRC table published in SORA 2.0, are as follows:

<sup>2</sup>At higher SAILs, there is a combination of qualitative and quantitative requirements to be met.

Table 2: Finalised iGRC Table.

Intrinsic Ground Class Value						
Max UAS Characteristic Dimension	1 m	3 m	8 m	20 m	40 m	
	Maximum speed*	25 m/s	35 m/s	75 m/s	120 m/s	200 m/s
Max population density [ppl/km <sup>2</sup> ]	Controlled	1	1	2	3	3
	< 5	2	3	4	5	6
	< 50	3	4	5	6	7
	< 500	4	5	6	7	8
	< 5000	5	6	7	8	9
	< 50,000	6	7	8	9	10
	> 50,000	7	8	Not part of SORA		

1. Supplementing UAS wingspan with Maximum Speed\* variable. This is conservatively defined as the maximum possible commanded airspeed of the UA, as defined by the designer<sup>3</sup>.
2. Replacing the qualitative descriptors for population densities with quantitative bands.
3. Addition of an extra column for platforms greater than 20m, but less than 40m wingspan<sup>4</sup>.
4. Significant improvements in the information on mitigations, underpinned by a more rigorous quantitative basis.
5. The iGRC table no longer includes rows associated with VLOS operations. However, operators can claim a minus 1 in most cases for operations where ground observation is possible. This change acknowledges that there is no inherent difference between unmitigated VLOS and BVLOS operations in terms of the intrinsic ground risk they present. The ability to obtain a minus 1 is a recognition that aspects of operations **with ground observation** serve to mitigate ground risk and reduce the likelihood of fatality. Further details are provided in Section 4.5.

Whilst this table simplifies the application of ground risk determination for operators and authorities alike, the theoretical principles linking aircraft characteristics and population to aircraft SAIL scores are associated with a substantial body of work. To expand on this effort, section 2 provides a summary of the role critical area ( $A_C$ ) and population density ( $D_{pop}$ ) played in motivating Items 1 to 3, whilst section 4 expands on mitigation in general, with section 4.5 providing specifics on the criteria to gain credit for VLOS mitigation.

## 1.5 Reduced iGRC Allocation Errors

A key benefit of upgrading the iGRC table is that there are fewer instances where applicants will be allocated an inappropriate iGRC score. To highlight this benefit, it is first necessary to highlight how

<sup>3</sup>This is not the mission specific maximum commanded airspeed of the UA as reducing the mission airspeed may not necessarily reduce the impact area. Mitigations that limit airspeed below the maximum speed value during an impact can be accounted for in Annex B, part of Step #3

<sup>4</sup>In principle, the iGRC table could be extended to encompass larger critical areas or more populous areas. However, these combinations are likely to produce iGRC values that are too high to reasonably warrant that platform or operation being conducted under the auspices of the Specific category. It is expected that operations associated with this level of iGRC would require certification of the aircraft system, crew, and organizations due to the extremely low maximum allowable  $\lambda_{GI}$  required to meet the acceptable target level of safety

iGRC scores vary as  $D_{pop}$  and  $A_C$  change. Figure 2 provides a series of iso-iGRC bands, calculated using Equation 5 provided earlier.

The Critical Area values ( $A_C$ ) are shown at the bottom on the horizontal axes, whilst the coinciding wingspan and velocity doublets used in the determination for the shown critical areas are provided above the figure. Population density is depicted on the vertical axes. The cell boundaries depicted in white and the coinciding values aligned with those shown in the final iGRC values in Table 2.

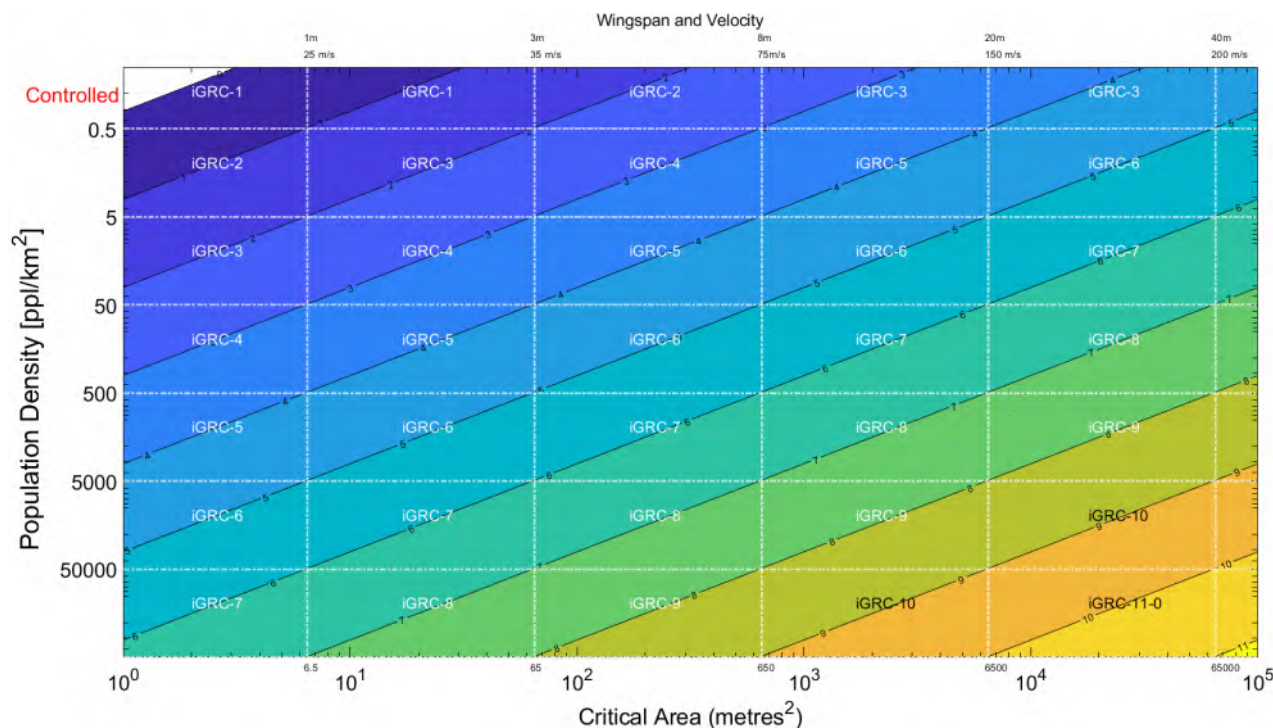


Figure 2: Iso-parametric iGRC bands as a function of variation in Population and Critical Area. Note that iGRC Score Rounding has been applied, that both axes have logarithmic scaling, and that the population density axis has units of ppl/km<sup>2</sup>, while critical area is expressed in m<sup>2</sup>. Care should be taken to employ the correct unit in calculations.

It is emphasized that the iso-iGRC values shown here already have rounding applied. In the event applicants seek to have their iGRC lowered based on Figure 2, competent authorities should not allow further concessions for applicants close to the cell boundaries, as concessions are already embedded via the rounding policy. Further detail on the rounding approach is provided in Section 2.5.6

To emphasize the strengths of the new iGRC table, the same layer of iso-iGRC scores has been superimposed onto the old iGRC table from SORA V2.0, with the result shown in Figure 3<sup>5</sup>. Reasonable numerical values were assigned to each of the qualitative descriptors used for population (shown in red). They are purely to highlight the reduction in quantization error and should not be interpreted as an alternate set of boundaries, as the SORA V2.0 iGRC table will be superseded upon publication of Annex F with coinciding updates to the SORA main body document.

For both figures, each grid square (quanta) is bound by a white line with the allocated iGRC value indicated in white within the cell.

Contrasting the realized iso-GRC scores within the new Version (Figure 2) with the old (Figure 3) it is clear that the new SORA version has more cells or "quanta"<sup>6</sup>. For example, consider the

<sup>5</sup>VLOS elements have been redacted

<sup>6</sup>even accounting for an extra column dedicated to platforms with 40 m wingspan

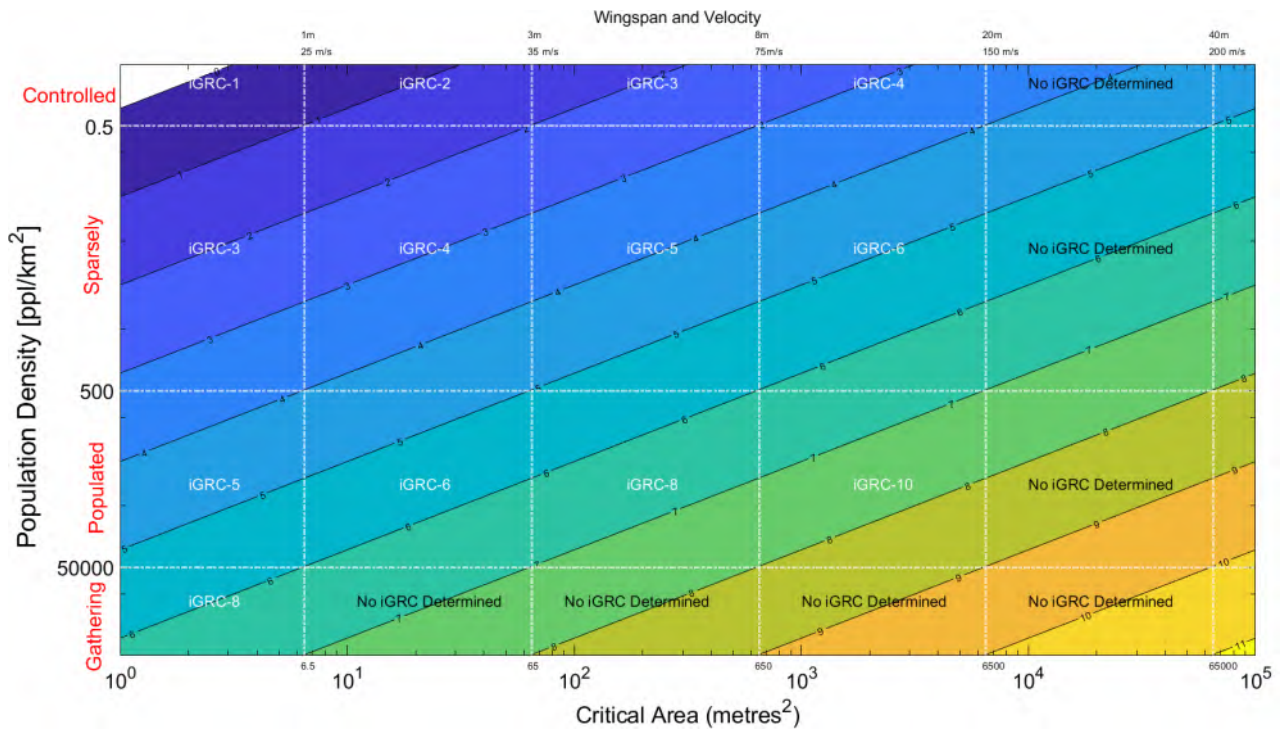


Figure 3: The SORA V2.0 iGRC table (BVLOS values) is superimposed on the same iso-bands as shown in the previous figure. The red text is the descriptors of population density from the SORA V2.0 iGRC table.

iGRC-4 cell (displayed in white) in the second column of Figure 2. It can be seen that this cell has significantly fewer iGRC bands compared to the corresponding iGRC-4 cell in Figure 3.

The key benefit of the improved cell resolution is that there is a lower chance of any particular aircraft being misclassified into an incorrect band.

An additional benefit of the information contained in Figure 2 is that it helps applicants quickly isolate any instances where their combination of wingspan, velocity, and critical area may warrant a lowering of their assessed iGRC score derived in Table 1.4.

## 1.6 Mitigation and the iGRC

Currently, the SORA identifies four possibilities for reducing the iGRC score via mitigation:

- M1(A): reducing the number of people at risk on the ground via shelter.
- M1(B): reducing the number of people at risk using operational restrictions.
- M1(C): reducing the number of people at risk tactically by observing the ground area and adapting the operation to avoid areas of higher population.
- M2: reducing the effect of the ground impact

An applicant has to conform with the integrity requirements for the mitigation claimed and **may** have to present evidence to the competent authority. The term may is used because for some low robustness requirements, there may not be a requirement for the evidence to be presented to the competent authority. This conservatively ensures the TL0S of  $10^{-6}$  fatalities per hour is maintained. Once the effect of mitigations is calculated the result is the "final" ground risk class (fGRC).

Section 4 provides more detailed guidance on how the listed mitigations can be applied to help reduce the assessed iGRC scores from Table 2.

## **1.7 iGRC value – a step-by-step approach**

This section provides a step-by-step guide for using Annex F to determine an iGRC for an operation. While all the different approaches are indeed explained in detail in this Annex, it may be overwhelming for someone not well-versed in mathematics or without a background in modeling to figure out how to go about finding the iGRC. For that reason, we provide an overview of all the different approaches in a compressed format.

### **1.7.1 Determine the approach method for finding iGRC**

When determining the iGRC for an operation, the operator can choose between a number of approaches. To make it easier for operators, Figure 4 provides a flow diagram that can be used to select the best approach. The diagram starts with the most simple but also least granular approach and ends with the JARUS model.

The flow diagram is intended to assist in determining the best approach, but the text in each of the color-coded decision boxes is limited, so below is a more detailed explanation of each of them. The number in the small boxes in Figure 4 refers to the sections below.

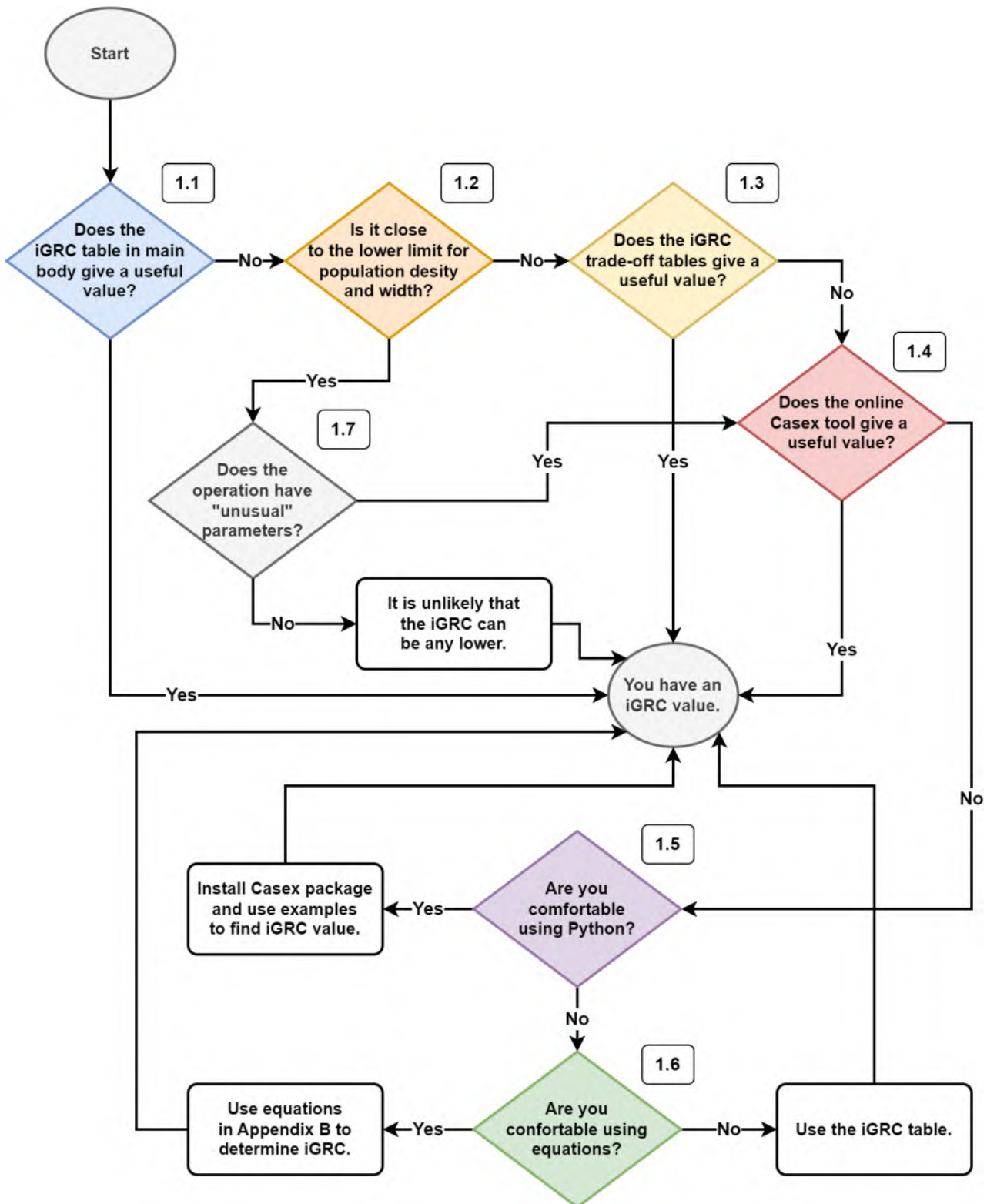


Figure 4: Flow diagram for finding the best approach for determining iGRC value for an operation.

### 1.7.2 Using the iGRC table directly

The iGRC table provided in the main body is simple to use and should always be the first step for establishing the iGRC Value. If the table provides an acceptable value, this will be the easiest for both the operator and the NAA.

### 1.7.3 Limiting values for iGRC cells

The iGRC table is, by design, conservative. Consequently, it can occasionally result in an overestimate of the real iGRC because of the “*quantisation*” error described earlier. For instances where the aircraft size/velocity and population density for the operation are close to the lower limits for a given iGRC table cell, it is likely that using a more fine-grained approach to find the iGRC can result in a lower value. This is also shown in Figure 5, exemplified with one of the cells from the iGRC table.

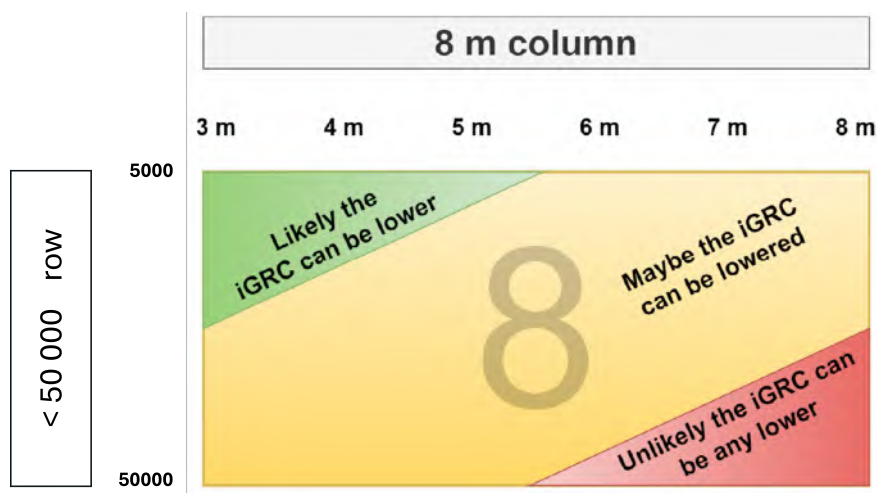


Figure 5: Every cell in the iGRC table captures a range of both aircraft width and population density (the figure shows one particular cell with iGRC 8 as an example). For operations with parameters in the upper-left corner, say 3.8 m width and a population density of 6000, it is likely that the iGRC can be lowered (in this case, from 8 to 7) using either trade-off tables or direct computations. As the parameters move toward the lower right corner of the cell, the probability decreases. This applies to all cells except for controlled ground area.

This is because each cell covers a fairly large range of both aircraft size and population density to make the table manageable. Consequently, the “location” in the cell matters for the possibility of getting a lower iGRC value.

It should be noted that there is a red lower-right corner of the cell in the figure, where it is unlikely that the operations can achieve a lower iGRC value. This is because the iGRC table in the main body features a reduction of 0.5 in the iGRC score to compensate for the conservativeness of the coarse approach. This reduction is also implemented in the trade-off tables. It is not permissible to use this reduction when using the Casex online tool, the Python package, or in any custom implementation. For more details on this reduction, see section 2.5.6 on rounding policy.

There are basically two steps in the more fine-grained approach: the trade-off tables and the mathematical equations (either directly or via Python). Both are explained in more detail in the following sections.

### 1.7.4 Trade-off tables

The iGRC table in the main body is based on a series of choices for combinations of aircraft size, speed, and population density. Therefore, it is only one out of several different possible tables where the size, speed, and population density can vary. To facilitate operators with other options, six other tables are proposed, as described in Section 4.8 and quantified in Table 13. They are called trade-off tables because when decreasing one parameter, say speed, there is a trade-off to one of the other parameters, say size. These trade-offs allow the operator to relatively easily use alternatives

that may give a lower iGRC value (i.e., the operation may fall into another cell with a lower iGRC value) without the hassle of using the JARUS model equations.

If, however, the trade-off tables also do not fit a given operation, the operator may use the model equations directly. This can be done in three different ways, as explained in the following sections.

### **1.7.5 Casex online tool**

The easiest approach for plugging the operational parameters in the model is to use the Casex online tool, which provides a simple interface for the model. It is available at [www.casex.one](http://www.casex.one). Here it is possible to use the actual size, speed, and other values for the intended operations to see the actual iGRC as resulting from the model.

This approach has another advantage. The iGRC is given with one decimal place of precision, allowing readers to easily determine how close the iGRC value is to potentially being lowered by changes to the operations. If the resulting iGRC is, say, 6.8 (and thus should be rounded up to 7), then it is unlikely that any tweaking with size, speed, population density, or impact angle will bring the iGRC down to 6. If, however, the iGRC value is 6.1, then using a slightly lower population density or a slightly lower impact speed (or some other minor change) may well result in an iGRC of 6.0. Obviously, such changes must also be implemented in the operation and/or on the aircraft.

### **1.7.6 Casex Python package**

The Casex online tool is using the Casex Python package behind the scenes. No knowledge of math or coding in Python is required to use the online tool. But if the operator is interested in going beyond the capabilities of the web interface, it is possible to download the Casex package from the standard Python package repository and use it directly in the operator's own Python code. This does require some knowledge of Python. However, the package comes with documented examples, so it should be easy for anyone with a little experience in Python to compute iGRC values. Guidance for installing and using the package is provided via links on [www.casex.one](http://www.casex.one).

The Python package includes a number of additional features not available in the online iGRC calculator. The effect of obstacles is fixed in the iGRC table and online tool but can be changed and applied to a specific operation using the obstacle modeling in the Casex Python package. If the operator finds that ballistic descent is significantly more likely, the iGRC table or trade-off tables are overly conservative, and by using the ballistic model in the Casex package, it is possible to get a more realistic, and almost certainly lower, iGRC value. To use these two features, start by looking at the obstacle and descent examples in the Casex package. Still, be prepared to do some work in Python to produce useful iGRC values.

### **1.7.7 The JARUS model**

An alternative to using the Casex online tool or Python package is implementing the model in whatever form the operator finds appropriate. While all the necessary equations are provided in this Annex, it still requires some limited math skills plus some programming skills (in C++, Java, Matlab, Excel, or whatever environment is chosen). As guidance for how the computations should proceed, the calculations used to construct the iGRC table are given in section [A.6](#), while a step-by-step guide for using the model is provided in section [1.8](#).

It should be noted that, unlike the JARUS model for the computation of critical area, the obstacle and ballistic descent models are not easily reproduced in "simple" equations. As such, these two

features are not presented in mathematical terms in Annex F but should be found in the referenced literature.

### **1.7.8 Operations with unusual parameters**

If the parameters for an operation are far from the values in the table (e.g., the aircraft's maximum speed is significantly lower than the values in the table, or the impact angle is always very shallow), the table will provide either an overly conservative iGRC score or a rather optimistic score, depending on the type of deviation from normal parameters. In this case, the only option is to use the model to obtain an iGRC value via Casex or a custom implementation of the model. Since the Annex F model is not designed to accommodate extreme operations, the operator needs to proceed with caution and carefully consider the appropriateness of the result.

### **1.7.9 Further observations**

For "normal" operations where the parameters are close to the ones used when generating the iGRC table, the operator should not expect to be able to lower the iGRC by more than one. And in many cases, this will not even be possible. Using the model, either through Casex or directly, only provides a more fine-grained analysis of a given operation, not a method for changing the risk.

When an operator uses the Casex online tool for iGRC value, the precise values for all parameters should be clearly presented to the NAA to allow the reproduction of the results.

For "unusual" operations, where the parameters are far from the ones used for the iGRC table (extremely large wing span, very low mass, very high impact speed, etc.), the Annex F model may provide a somewhat different iGRC value (both higher and lower, depending on circumstances). In many cases, this will indeed indicate the associated risk, and for each such case, the operator should provide thorough documentation and reasoning to enable the NAA to determine the validity of the approach.

It may seem like an exploitation of the methodology laid out in Annex F to shop around in the various ways of finding an iGRC value. It is not. The shopping around only searches for the least conservative result. As long as the operation conforms with the parameters used for finding the iGRC value, the risk is acceptably low.

## **1.8 JARUS model step-by-step**

The following is a step-by-step guide to using the equations for the JARUS model to obtain an iGRC value without an explanation of the origin of the equations. For operators not well-versed in mathematics, this approach may be useful. For details on the JARUS model, please see Appendix B.

Obtaining the iGRC is done in two steps. First determine the critical area and then determine the iGRC. The calculation of the critical area has been done for three different cases based on the width of the UA.

The following parameter values are used throughout the three Use Cases below.

Table 3: Values used for Key Parameters in Critical Area Model

$r_{\text{person}}$	Radius of a person	0.3 m
$h_{\text{person}}$	Height of a person	1.8 m
$e$	Coefficient of restitution	0.65 <sup>7</sup>
$\theta$	Angle of impact	35°
$C_g$	Coefficient of friction	0.75
$g$	Gravitational acceleration	9.8 m/s <sup>2</sup>
$K_{\text{non-lethal}}$	Non-lethal kinetic energy limit	290*J
$\pi$	Pi	3.1415
$d_{\text{glide}}$	Glide distance given as $h_{\text{person}} / \tan(\theta)$	2.57 m

\* The slide portion of all 1m class UAs is assumed non-lethal and so Kinetic Energy ( $K_{\text{non-lethal}}$ ) is not relevant to the calculation. For all aircraft larger than 1m, impact with a person is assumed to be lethal and the Non-Lethal Kinetic Energy ( $K_{\text{non-lethal}}$ ) is set to 290J. However, as the size of the aircraft increases beyond 1m, the impact of setting ( $K_{\text{non-lethal}}$ ) to 290J has diminishing impact on the size of the critical area.

However, applicants do have the option via M2 to reduce the lethality of a drone on impact, with subsequent influence to slide speeds and the non-lethal kinetic energy. The non-lethal kinetic energy used here (290J) is **not appropriate** for general arguments of non-lethality, as this value applies to lower limbs only.

First, determine the horizontal impact velocity as

$$v_{\text{horizontal}} = v \cos \theta ,$$

where  $v$  is the maximum speed of the aircraft. Second, find the value

$$r_D = r_{\text{person}} + \frac{w}{2} ,$$

where  $w$  is the width of the aircraft.

Now, find the case that fits the aircraft in either section 1.8.1, 1.8.2, or 1.8.3.

### 1.8.1 Case 1: UA width above or equal to 8 meters

The critical area is composed of a glide area and a slide area where a person could be potentially impacted. The area is computed as

$$A_C = 2r_D(d_{\text{glide}} + d_{\text{slide, reduced}}) + \pi(r_D)^2 .$$

The value for  $d_{\text{slide, reduced}}$  is computed in two steps. First, determine the slide velocity at which the kinetic energy is reduced to  $K_{\text{non-lethal}}$ , using

$$v_{\text{non-lethal}} = \sqrt{\frac{2K_{\text{non-lethal}}}{m}} ,$$

where  $m$  is the mass of the aircraft in kilograms. Then, compute how long it takes to go from impact velocity to  $v_{\text{non-lethal}}$ , using

$$t_{\text{safe}} = \frac{e \cdot v_{\text{horizontal}} + v_{\text{non-lethal}}}{C_g g} .$$

And now we can determine the reduced slide distance as

$$d_{\text{slide, reduced}} = e \cdot v_{\text{horizontal}} \cdot t_{\text{safe}} - \frac{1}{2} C_g g (t_{\text{safe}})^2 .$$

<sup>7</sup>Setting  $e = 0.65$  is based on an assumption that impact angle is 35 degrees (See Eqn 51).

### 1.8.2 Case 2: UA width between 1 m and 8 m

The critical area is computed using a slightly changed equation compared to case 1, namely

$$A_C = 0.6(2r_D(d_{\text{glide}} + d_{\text{slide, reduced}}) + \pi(r_D)^2) .$$

where the factor 0.6 accounts for the probability of impacting ground obstacles. All the components of the equation can be found above.

$t_{\text{safe}}$  and  $d_{\text{slide, reduced}}$  are computed in an equivalent manner to Case 1.

### 1.8.3 Case 3: UA width smaller than 1 m

In this case, it is assumed that the slide is non-lethal. Therefore, the equation for the critical area is simplified to

$$A_C = 2r_D \cdot d_{\text{glide}} + \pi(r_D)^2 .$$

### 1.8.4 Finding the iGRC value

Now that we have a value for the critical area  $A_C$ , it is possible to determine the iGRC value using

$$\text{iGRC} = \lceil 7 + \log_{10}(D_{\text{pop}} \cdot A_C) \rceil .$$

This means multiplying the critical area by the population density (ensuring the units for area are the same between the critical area and the population density), then taking the base 10 logarithm, adding 7, and rounding the result to the nearest integer.

To see some examples of finding the critical area, visit Table 31, which shows the computations for the five width classes. This table includes all of the above computations (except for iGRC since this requires a known population density).

## 2 Intrinsic Ground Risk Framework

### 2.1 Relationship between $\lambda_{GI}$ , $D_{pop}$ , $A_C$ and TLOS

This section provides more detail on the development of the iGRC framework first introduced in Section 1. For operators and regulators, it illustrates how the TLOS for the operation is derived.

First, the parameters from Equation (3) and Table 1 are manipulated to derive a basis for the maximum allowable loss of control of the operation rate,  $\lambda_{GI}$ , as

$$TLOS = \lambda_{GI} \cdot D_{pop} \cdot A_C , \quad (6)$$

This assumes the most conservative case where  $P(\text{fatality}|\text{collision}, GI)$  and populated exposed factor ( $F_{exp}$ ) from Equation (3) are unity. Transposing we obtain

$$\lambda_{GI} = \frac{TLOS}{D_{pop} \cdot A_C} . \quad (7)$$

Applying the requirement for a TLOS of  $10^{-6}$  fatalities per flight hour, we obtain

$$\lambda_{GI} = \frac{10^{-6}}{D_{pop} \cdot A_C} . \quad (8)$$

This facilitates the identification of the maximum allowable loss of control of the operation rate for each combination of  $D_{pop}$  and  $A_C$ , which can subsequently be mapped back to SAIL scores in accordance with Table 1. It will be shown that wingspan and velocity can be used as proxies for  $A_C$ , so Equation (8) can alternatively be written as

$$\lambda_{GI} = \frac{10^{-6}}{D_{pop} \cdot A_C(WS, Vel)} . \quad (9)$$

where  $A_C(WS, Vel)$  denotes  $A_C$  as a function of wingspan and maximum velocity. This formulation underpins the use of Wingspan, Maximum Speed, and Population in the final iGRC values shown in Table 2<sup>8</sup>.

The remainder of this section steps through the process in more detail:

1. **Section 2.2** briefly describes the design intent underpinning the replacement of the SORA 2.0 iGRC table with the SORA 2.5 version, highlighting some key considerations in balancing its structure.
2. **Section 2.3** briefly explains what Critical Area is and identifies key components used in its determination. A more detailed explanation of its derivation is provided in Appendix A.
3. **Section 2.4** outlines the challenges involved with selecting suitable thresholds for population and critical area for the iGRC Table.
4. **Section 2.5** provides a step-by-step walk-through of the process to develop a nominal iGRC Table, illustrating the relationships in Equations (4), (8), alongside Table 5 where:
  - **Table 4** illustrates the impact on Casualty Expectation when  $A_C$  and  $D_{pop}$  vary, in accordance with Equation (4),

---

<sup>8</sup>Appendix A outlines the justification for velocity rather than kinetic energy

- **Table 5** illustrates how the maximum allowable loss of control of the operation rate is determined in accordance with Equation (7)
  - **Table 6 and 7** depicts how each cell or quanta determined via the  $A_C$ ,  $D_{pop}$  coordinates is mapped to a SAIL and raw iGRC score
5. **Section 2.6** describes how the iGRC, based on nominal Critical Area values, needed to be adjusted to reflect the influence that obstacles have and how this is used to produce the final iGRC Table 2 with Critical Area values replaced by Wingspan and Velocity.

## 2.2 iGRC Design Considerations

A key aspiration for the design of the iGRC table was the ease of use without compromising safety. The table should be able to be used by applicants and authorities and use data and information that is easy to find for most systems. This ethos was immediately challenged by the requirement to determine accurate values for  $A_C$ .

For any UAS ground impact, there are a number of performance and dimensional characteristics to be considered, including speed, wingspan, impact dynamics, friction of the surface at impact, impact angle, and even potential obstacles. Section 2.3 provides a summary of how these variables contribute to  $A_C$ , whilst the more complex elements are deferred to Appendix A. While the examination of critical area contributed to the goal of safety, validation of the mathematical calculations outlined in Appendix A is not easy for the public. To reduce the complexity and support the standardization of the process for operators and regulatory authorities, ***routinely available or easily determined aircraft parameters were selected to act as a conservative proxy for  $A_C$ .***

Intuitively, the parameter(s) selected to act as a proxy should conservatively predict the real value for  $A_C$  for most UAS concept of operations, ultimately as assurance that the predictor does not allow grossly unsafe operations to proceed. In SORA V2.0, the chosen proxy was wingspan, with guidance also given for Kinetic Energy ranges. However, it was established that wingspan and velocity were generally more accurate predictors for  $A_C$ .

The substitution of velocity for kinetic energy means operators are less likely to be placed in an inappropriate risk class, either reducing unwarranted compliance costs when this placement is higher than it should be or reducing the safety implications when it is lower.

## 2.3 Basics of Critical Area Determination

The Critical Area ( $A_C$ ) variable used in this Annex and ultimately SORA, is defined as the sum of all areas on the ground where a person standing would be expected to be impacted by the UA system during or after a loss of control of the operation event, and thus the area where a fatality is expected to occur if a person were within it. The total critical area  $A_C$  composed as

$$A_C = A_{C\text{-inert}} + A_{C\text{-explosion}} \quad (10)$$

where

- $A_{C\text{-inert}}$  is the critical area from inert (non-explosive) debris.
- $A_{C\text{-explosion}}$  is the critical area due to either explosion (shock wave) or deflagration (thermal radiation).

### 2.3.1 Models

A diverse array of studies were considered before settling on this basic formulation, but it was observed there was significant consensus around the general approach. These studies included:

- RCC model [3, p. D-4]
- RTI model [4, p. 3-11, 53]
- FAA model [5, p. 99-103]
- NAWCAD model [6, p. 11-47]
- Deflagration model [7, p. 84–89]

The relevant merits of each of the models considered in the literature review were used to inform the development of the JARUS Critical Area model, which was, in turn, used in the calculations for the iGRC table. In essence, the JARUS model is a combination of components from the RTI [4] and the NAWCAD[6] models. It uses the basic glide and slide areas as well as the coefficient of restitution from the RTI model and employs the concept of reduced slide distance from the NAWCAD model. Figure 6 consolidates many of these concepts, illustrating how they contribute to the overall  $A_C$ . A summary of the key variables/concepts contributing to  $A_C$  is provided to support understanding:

- The glide critical area is the area covered by the path of the aircraft at an altitude equal to or below the height of an average standing person (1.8 m) but before it contacts the ground. For a steep dive, such as the end of a ballistic descent, this area can be very small, while for a shallow glide, this area may have a significant size.
- The slide occurs right after impact and until the aircraft is at rest. The slide may be short for a near-ballistic descent and long for a shallow impact on a slippery surface (such as wet grass). The slide distance depends on the horizontal speed of the aircraft after impact and the friction between the aircraft and the ground. Slide does not include tumbling, bouncing, and break-up of the aircraft. It is represented by the long blue arrow as well as the dotted blue box of the same length as the arrow.
- Bounce or Ricochet - Aircraft becomes ballistically airborne again after impact.
- Splatter or Cratering - Aircraft experiences structural disintegration on impact and transfers its energy into ground deformation.
- Secondary Effects - Debris from the initial impact spreading over an area.
- Blade Throw - Rotor blades leaving a rotorcraft when the rotor is spinning.
- Explosion and deflagration - The rapid combustion of fuel and its effects. The fuel onboard the aircraft may ignite and cause an explosion. The explosion may occur at any location along the slide path but is depicted here at the end for figure clarity.

Each concept has dependencies on other concepts; it is not expected an aircraft will be able to do each of the above actions to their maximum extent in the same incident, as there is only a given amount of initial energy to convert into each action.

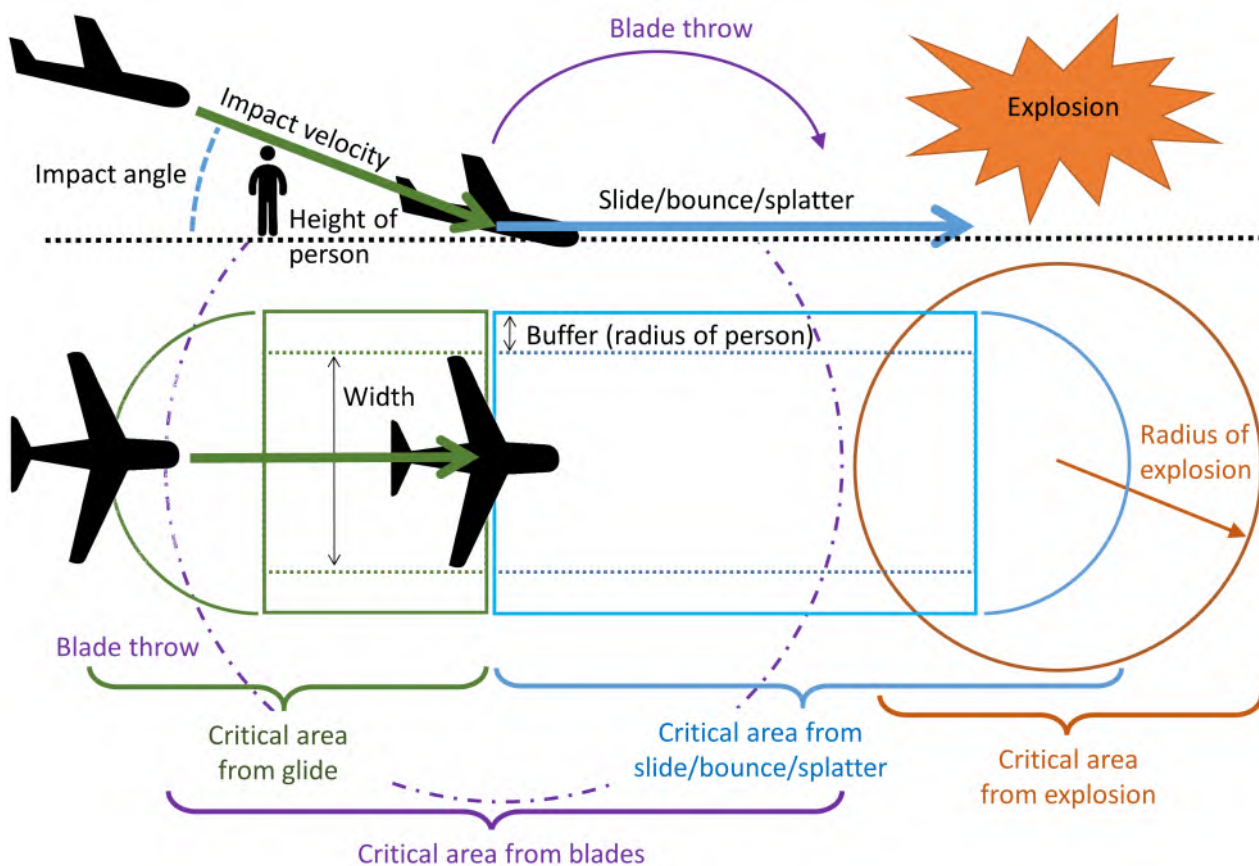


Figure 6: General depiction of the critical area. The area  $A_{C-expllosion}$  resulting from explosion and deflagration is in orange, while the inert area  $A_{C-inert}$  is composed of the blue and, green, and purple areas. The  $A_C$  used in this Annex is the area defined by the solid blue and green rectangles plus the half circles at each end. For more details, see section 2.3.2.

It is highlighted that:

- The width of the dashed box is equal to the wing span of the aircraft, while the length is computed in various ways depending on the applied model (see below).
- Typically, a buffer is added all around the glide plus slide area that represents the size of a person as seen from above, resulting in the solid blue box.
- Aircraft impacting the ground do not typically conserve all of their impact energy, and so the subsequent slide/bounce/splatter has a reduced velocity component. This is captured via the Coefficient of Restitution, which has a value between 0 and 1.
- Note that while Figure 6 depicts a fixed-wing aircraft, the same model approach applies to other types of aircraft, including rotorcraft.

Details, including equations for the JARUS model, are provided in Appendix B, while an implementation of the model is available through the CasEx software package as described in Appendix E.

### 2.3.2 Critical area used in Annex F

The total critical area resulting from all the contributing factors listed above can be quite complex to determine. In an effort to keep it relatively simple, the following simplifications have been made in

this Annex. First, in considering whether to incorporate weighted combinations of slide, bounce, and splatter to calculate  $A_C$ , we note that in [4], it was determined that choosing any one, or combination of them, produces roughly the same result. Accordingly, slide, which has a greater body of evidence and simpler computation, was selected. Second, explosions resulting from a crashing unmanned aircraft seem generally somewhat unlikely, given that fuel very rarely explodes. Deflagration may occur, although typically fuel would result "only" in escalating effects, but not in fatalities due to thermal radiation. In addition, a deflagration would often largely overlap the slide area. Third, blade throw is disregarded due to its relatively small contribution and high complexity. Finally, the effect of rotating parts during impact will happen inside the slide area, meaning that its effect on lethality has already been included (due to the assumption that the entire slide area is considered lethal). In summary, the following effects are excluded from the JARUS model:

- Bounce and splatter/cratering
- Explosion
- Deflagration
- Blade Throw
- High-energy rotating parts
- Secondary effects of ground collision, such as debris scattering

As a result, the critical  $A_C$  used in the remainder of this Annex is composed of the glide and slide effects only, including the buffer, as shown by the solid line blue and green rectangles plus half-circles in Figure 6. Appendix B contains details on how these areas and effects are defined, including a mathematically rigorous definition of the  $A_C$  from the JARUS model.

If an operator or regulator believes that a different approach is warranted, the appropriate literature and models should be applied to calculate  $A_C$ . Note that there are models for deflagration and explosion available in the CasEx package.

## 2.4 Initial Threshold Selections for Population and Wingspan Bands

In Section 1.5, it was highlighted that Annex F incorporates more iGRC cells compared to V2.0 of SORA, alongside replacing the qualitative population bands with quantitative variants. These changes necessitated a decision on where to situate the band thresholds for not just the old variables (population and wingspan) but also critical area and velocity.

A key requirement for the iGRC table is that movement horizontally or vertically to another cell should produce an order of magnitude change in the product of  $A_C$  and  $D_{pop}$ . In parallel, it was decided to maintain the legacy thresholds for wingspan. This constraint impacts significantly on the available choices for both  $A_C$  and  $D_{pop}$ , because of:

- wingspan and the corresponding assessed limit on velocity impact on the resultant critical area for each column
- Equation (8) embeds an inverse proportionality requirement between  $A_C$  and  $D_{pop}$ , which then limits the range of population bands that can be used to maintain the required order of magnitude scaling.

Our initial choice of values for the critical area used magnitude increments around 2 (i.e., 20, 200, 2,000, 20,000, and 200,000 m<sup>2</sup>), paired with an array of population values increasing from 0.05 in

orders of magnitude (i.e., 0.05, 0.5, 5, 50, etc.). This choice of values supported the need for an order of magnitude changes when moving laterally and vertically through the table.

We term these initially selected bands described in Item 1 as the *Nominal Bands* for  $A_C$  and  $D_{pop}$  and maintain these values in Tables 4 through 7 to facilitate an easy explanation of the relationship between Equation (3), Table 1, SAIL, and  $\lambda_{GI}$  values.

However, it is emphasized that this nominal choice differs from the ultimate values deployed in the final iGRC table (Table 2) for reasons to be explained.

## 2.5 Step-by-step Progression in the development of the nominal iGRC Table

### 2.5.1 Unmitigated Casualty Expectation given Nominal $D_{pop}$ and $A_C$ Values

Table 4 provides the unmitigated casualty expectations for the nominal doublet of  $D_{pop}$  and  $A_C$  values, applied in accordance with Equation (4). The number in each cell is the average number of casualties for one event.

Table 4: Casualty expectations for combinations of  $D_{pop}$  and  $A_C$  for unmitigated crash

Unmitigated Casualty Expectation (persons killed per loss of control of the operation event)						
		Critical area $A_C$ [m <sup>2</sup> ]				
		20	200	2,000	20,000	200,000
Population density $D_{pop}$ [ppl/km <sup>2</sup> ]	0.05*	0.000001	0.00001	0.0001	0.001	0.01
	0.5	0.00001	0.0001	0.001	0.01	0.1
	5	0.0001	0.001	0.01	0.1	1
	50	0.001	0.01	0.1	1	10
	500	0.01	0.1	1	10	100
	5,000	0.1	1	10	100	1,000
	50,000	1	10	100	1,000	10,000
	500,000	10	Not part of SORA			

\* The use of 0.05 in lieu of the controlled area (which is technically zero) is simply to avoid divide by zero errors. Attributed iGRC scores for the controlled area were determined via consultation with Subject Matter experts from both regulatory bodies and Industry

In perusing Table 4 readers should note:

- The inclusion of the row with a population density of 0.05 people per square kilometer (rather than zero) is to not have a division by zero. The term “controlled” ground area will be substituted for this value in subsequent tables.
- Since  $A_C$  is measured in m<sup>2</sup>, the unit for calculating  $D_{pop}$  in Equation (6) through (8) is ppl/m<sup>2</sup>. For practical use, the population density in the table is converted to, and displayed in, ppl/km<sup>2</sup>

## 2.5.2 Maximum Allowable loss of control of the operation rate ( $\lambda_{GI}$ ) for nominal $D_{pop}$ and $A_C$ Values

The values provided in each cell of Table 5 are the calculated values for  $\lambda_{GI}$  values described earlier for Equation (8), required to maintain TLOS at  $10^{-6}$ .

Table 5: The maximum allowable loss of control of the operation rate to comply with TLOS.

Maximum allowable aircraft failure rate $\lambda_{GI}$						
		Critical area $A_C$ [m <sup>2</sup> ]				
		20	200	2,000	20,000	200,000
Population density $D_{pop}$ [ppl/km <sup>2</sup> ]	0.05	$10^0$	$10^{-1}$	$10^{-2}$	$10^{-3}$	$10^{-4}$
	0.5	$10^{-1}$	$10^{-2}$	$10^{-3}$	$10^{-4}$	$10^{-5}$
	5	$10^{-2}$	$10^{-3}$	$10^{-4}$	$10^{-5}$	$10^{-6}$
	50	$10^{-3}$	$10^{-4}$	$10^{-5}$	$10^{-6}$	$10^{-7}$
	500	$10^{-4}$	$10^{-5}$	$10^{-6}$	$10^{-7}$	$10^{-8}$
	5,000	$10^{-5}$	$10^{-6}$	$10^{-7}$	$10^{-8}$	$10^{-9}$
	50,000	$10^{-6}$	$10^{-7}$	$10^{-8}$	$10^{-9}$	$10^{-10}$
	500,000	$10^{-7}$	Not part of SORA			

\* The population value assumed for a Controlled Areas was arbitrary (it is technically zero). Its use was to avoid divide by zero errors in calculations.

It is emphasized here that the complementary Nominal Bands produce results for  $\lambda_{GI}$  in multiples of ten and do not require rounding.

## 2.5.3 Mapping from SAIL to iGRC values

By taking advantage of the mapping between  $\lambda_{GI}$  and SAIL provided in Table 1, the indices in the cell entries can be mapped easily to unmitigated SAIL scores as

$$SAIL = -\log_{10}(\lambda_{GI}) . \quad (11)$$

Readers should note that the SAIL values depicted in Table 6 are prior to the application of any mitigation and before considering the air risk. They are not representative of any true SAIL score and are provided purely to support understanding.

## 2.5.4 Intrinsic Ground Risk Class for nominal $D_{pop}$ and $A_C$ Values

Excluding the influence of air risk, the relationship between the SAIL scores shown in Table 6 is described according to the simple relationship

$$\text{Intrinsic Ground Risk Class (iGRC)} = SAIL + 1 . \quad (12)$$

Applying this simple formulation to the values in Table 6 supports the derivation of Table 7.

Table 6: Unmitigated SAIL Score associated with loss of control of the operation rate shown in Table 5

SAIL Value						
		Critical area [m <sup>2</sup> ]				
		20	200	2,000	20,000	200,000
Population density [ppl/km <sup>2</sup> ]	0.05	0*	I**	II**	III**	IV**
	0.5	I	II	III	VI	V
	5	II	III	IV	V	VI
	50	III	IV	V	VI	VII*
	500	IV	V	VI	VII*	VIII*
	5,000	V	VI	VII*	VIII*	IX*
	50,000	VI	VII*	VIII*	IX*	X*
	500,000	VII*	Not part of SORA			

\* SAIL levels go from I to VI, so these SAIL scores exceeding SAIL VI are representative only.

\*\* The ultimate values for Controlled Areas in the Final iGRC table do not align with the SAIL values shown, because of the controlled area population used

Table 7: Intrinsic ground risk class based on critical area using (5)

Intrinsic Ground Class Value						
		Max critical area [m <sup>2</sup> ]				
		< 20	< 200	< 2,000	< 20k	< 200k
Max population density [ppl/km <sup>2</sup> ]	Controlled	1	2	3	4	5
	< 0.5	2	3	4	5	6
	< 5	3	4	5	6	7
	< 50	4	5	6	7	8
	< 500	5	6	7	8	9
	< 5,000	6	7	8	9	10
	< 50,000	7	8	9	10	11*
	< 500,000	8	Not part of SORA			

\* The final iGRC table does not include an iGRC score of 11

### 2.5.5 Raw iGRC Formulation

It is important to note that the nominal population and critical area values in Table 6 produced integer iGRC values purely because when multiplied, they produce multiples of 10. However, there are many other real-world combinations that lead to non-integer RAW iGRC scores. This is an important consideration as the population density can vary widely, as can critical area. Notably, our analysis to identify suitable critical areas given wingspan, velocity, and many other variables, resulted in very different values to those provided in Table 7 (see also Appendix A for more details).

This analysis effort establishing realistic values for the critical area motivated the development of

a general formulation for calculating the “raw” iGRC, complementing the rounded version outlined previously in (5). The formulation is based on a manipulation of (8), (11), and (12) and is as follows:

A more general form is

$$\text{“raw” iGRC} = 1 - \log_{10}\left(\frac{10^{-6}}{D_{\text{pop}} \cdot A_C}\right), \quad (13)$$

which can be further simplified to

$$\text{“raw” iGRC} = 7 + \log_{10}\left(D_{\text{pop}} \cdot A_C\right). \quad (14)$$

Note that, as also explained above,  $D_{\text{pop}}$  and  $A_C$  should be in the same units.

### 2.5.6 Rounding Policy

Figure 7 uses Equation 14 to establish raw iso-iGRC bands as population density and critical area vary. In a similar manner to that described previously with Figure 2, cell boundaries for population and critical area are shown in white, with the values used in the derivation of the critical area also shown.

Each right-hand bottom corner of each of the cells reveals the maximum iGRC score in the cell is actually 1 integer larger than the allocated values in Table 2.

For example, for the iGRC-4 quanta in the second column, it can be seen that a portion of the iGRC-5 exists in that corner.

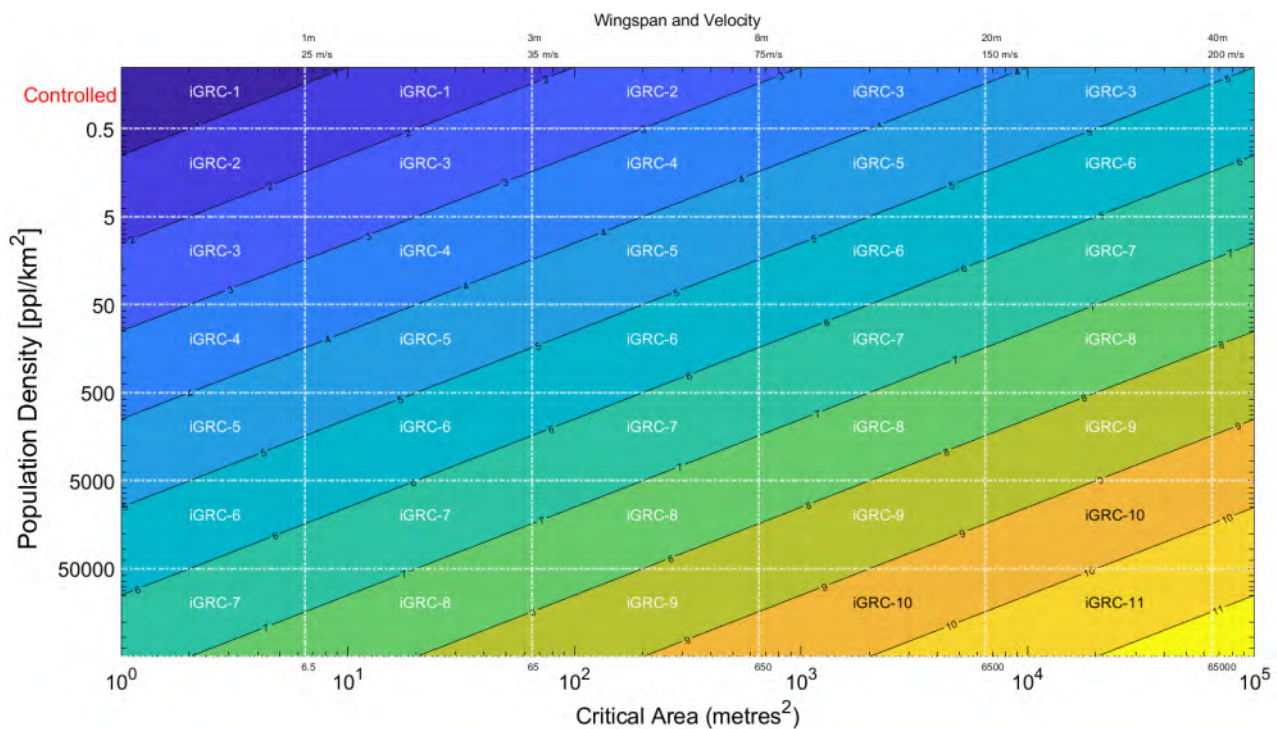


Figure 7: Iso-parametric iGRC bands with No iGRC Score Rounding Applied

While a simple “rounding up all raw scores” policy would maximize safety, this is considered overly conservative, as the right-hand bottom corner represents a relatively small percentage of operating scenarios, and an increase by one integer iGRC value coincides with an order of magnitude difference. Accordingly, a simple and balanced policy is to accept that the product of population density and critical area can be up to 3 times larger than the nominally allowable values producing integer iGRCs. Since iGRC scores are measured in log space, this factor of 3 becomes an addend of 0.5

(since  $\log_{10}(3) = 0.5$ ). Consequently, for example, if the raw iGRC score is less than 4.5, it would be rounded down to 4, but if it is greater than 4.5 it would be rounded up to 5. Therefore, the relation between the “raw” iGRC and applied iGRC is

$$\text{iGRC} = \lceil \text{“raw” iGRC} - 0.5 \rceil . \quad (15)$$

## 2.6 Progression from $A_C$ to Wingspan and Velocity in the final iGRC Table

As flagged, Table 7 is a highly idealized and overly conservative model for the iGRC table. The development of the final iGRC (Table 2) required numerous iterations exploring viable values in population and critical area to develop a safe and practical set of bands. More detail on this effort is provided in Appendix including:

- The use of wingspan and velocity as a proxy for critical area, based on investigations conducted using the JARUS critical area model, is detailed in Appendix A.
- The modification of the critical areas/wingspan and velocity combinations in the first (see Appendix A.5.1) and fifth (see Appendix A.4.2) columns of Table 7 using more appropriate assumptions for the physical model at these extremes.
- The inclusion of an obstacle model that serves to reduce the observed critical area, thereby allowing higher population or velocity/wingspan combinations, is described in Appendix A.5.2.

## 3 Determination of Population to Support iGRC

### 3.1 Introduction

Fundamental to the determination of iGRC, is that the population estimate is sufficiently accurate. This requires that the user employs an appropriate resource for reflecting the true population density.

Ideally, the methods and quality of mapping products presented to support  $D_{pop}$  determination would be harmonized across nations based on agreed methods and data quality, the outcome being a harmonized, spatially, and temporally accurate depiction of population density at high resolution. Obviously, this would alleviate many concerns from operators and competent authorities. Unfortunately, there is considerable variation in both the data and methodologies employed across nations, and this situation is likely to persist for some time.

To support better harmonization across jurisdictions that employ SORA, this section outlines key information that is relevant to the accurate determination of population density for the purposes of the SORA iGRC assessment. This section is broken down into 7 subsections:

- Subsection 3.2 is the Bottom Line Up Front (BLUF) for population density measurement. The section outlines how mapping products should be used within Step #2 of SORA, and references subsequent subsections in Annex F that can assist.
- Subsection 3.3 outlines the different ways population density can be measured from the perspective of the aircraft, and how these different measures effect the risk to overflowed populations. It then determines the appropriate measure for the purposes of the SORA iGRC assessment.
- Subsection 3.4 introduces the processes used to take point data for where persons are and convert them into area based mapping products, covering
  - the modifiable unit area problem, a fundamental characteristic of any point dataset converted into an area based dataset. The information presented includes an overview of the way mapping products are produced, including the methods and data used and how these impact the accuracy.
  - contemporary methods and data used to develop global population density maps around the world, such as spatial interpolation, areal interpolation, pycnophylactic interpolation, dasymmetric interpolation, and other smart interpolation techniques, highlighting the impact these varying approaches can have on accuracy.
- Section 3.5 introduces temporal considerations that affect the accuracy of population maps, including mobile phone data usage and knowledge of human movement over time.
- Section 3.6 discusses the Degree of Urbanisation Method (DEGURBA) process, a common method to identify smooth clusters of urbanization. This subsection provides further detail on the issues that arise when using a map developed using this technique
- Subsection 3.7 elicits practical considerations for both authorities and applicants, such that they can ensure they understand the rationale and purpose behind a mapping product, and how this may affect the suitability of such a product for use in an iGRC assessment.
- Subsection 3.8 lists global mapping products that are commonly used to visualise population density, their underlying methods and data.
- Subsection 3.9 provides the mathematical basis for the grid resolution table in the SORA main body, based off the concept of the dispersion area.

- Subsection 3.10 discusses the creation of hybrid mapping products by an applicant, should they wish to present to the authority an alternative map to the one designated by the authority.

## 3.2 Step by Step Process to iGRC Map Selection and Modification

For both the authority and applicant to agree on an iGRC in Step #2 of SORA, they both must agree that the underlying population density is accurate enough for an approval to be given. It is typically expected that the authority will designate an appropriate mapping source (i.e. either provide or point to appropriate data sources), if available. In the case where the authority is not willing or able to designate a map, the applicant may provide one, or they may utilise qualitative descriptors for the population density, as per Table 8.

Given this, the authority should review available mapping products for the given nation, utilise the information available about the mapping product, and along with Section 3.7 to come to a decision if the mapping product is appropriate for calculating the iGRC. Particular attention should be paid to any underlying assumptions used as part of the map development process.

If there is a designated map available the applicant should:

1. for the designated mapping product, use an available population density map that has grid square size approximately the same size as the dispersion area, using Table 11 as a guide.
2. for population density maps with grid cells of a smaller size (grid length  $l_{grid}$ ) than the dispersion area (grid length  $l_{disp}$ ), use a smoothing algorithm that uses adjacent grid cells to inform the value of the grid cell of interest. The number of adjacent cells used should ensure the area of interest (mask) is approximately the size of the dispersion area.
3. for population density maps with grid squares of a larger size than the dispersion area, utilise the map with the closest grid square size to that of the dispersion area. There will be an underestimate of the risk, but as long as this is understood and accepted, the iGRC can still be calculated.
4. if there is no available mapping products, or the mapping product available is considered not appropriate, then the qualitative descriptors in Table 8 can be utilised as a proxy for the population density. An operational area can be broken up into multiple qualitatively described areas.

For more information, please see Section 3.9. If any of the previous options are utilised, the applicant and authority now have a baseline map (or qualitative baseline) from which to undertake an iGRC assessment.

Operational demand will see operators present evidence that designated maps are overstating the density. Pragmatically, there will be areas where the maps understate the density as well. For applicants that wish to generate their own maps and present them to the authority, further guidance on considerations for applicant-generated mapping solutions is provided in Section 3.10

### 3.2.1 Dealing with erroneous static data in designated population density maps

Regardless of mapping product designated by the authority, there will inevitably be errors in the data due to the process used to develop the map. For static mapping errors (i.e. a train tunnel in the middle of the countryside being classified as populated because the concrete was inferred to mean human habitation), it should be possible for an applicant to undertake simple, justifiable processes that demonstrates the error in the designated map. These may include (not exhaustive):

Table 8: Qualitative Descriptors for Population Density Estimate

Quantitative $D_{pop}$ (ppl/km <sup>2</sup> )	Qualitative Descriptors	Area Description
Controlled Ground Area	Controlled Ground / Extremely Remote	<p>Areas that are controlled where unauthorized people are not allowed to enter.</p> <p>Hard to reach areas (mountains, remote deserts, etc), large bodies of water away from expected boat traffic.</p>
< 5	Remote	<p>Areas where people may be, such as forests, deserts, large farm parcels, etc.</p> <p>Areas where there is approximately 1 small building every 1km<sup>2</sup>.</p>
< 50	Lightly populated	<p>Areas of small farms.</p> <p>Residential areas with very large lots (approx. 4 acres or 16,000m<sup>2</sup>).</p>
< 500	Suburban / Residential lightly populated	<p>Areas comprised of homes and small businesses with large lot sizes (approx. 1 acre or 4,000m<sup>2</sup>).</p>
< 5,000	Low density metropolitan	<p>Areas single family homes on small lots, apartment complexes, commercial buildings, etc.</p> <p>Can contain multistory buildings, but generally most should be below 3-4 stories.</p>
< 50,000	High density metropolitan	<p>Areas of mostly large multistory buildings.</p> <p>The downtown area of most cities.</p> <p>Areas of dense skyscrapers.</p>
≥ 50,000	Assemblies of people	<p>The densest areas in the largest cities.</p> <p>Large gatherings of people such as professional sporting events, large concerts, etc.</p>

- using other static mapping products,
- up-to-date satellite imagery,
- on-site inspections,
- authoritative local knowledge of the area

This process should occur in Step #2 of SORA, otherwise the combination of both correcting errors, and undertaking deliberate temporal based mitigations through M1(B) could be artificially inflated in terms of robustness requirements.

For example, a designated map error may cause an increase in the iGRC by 1 level compared to the true iGRC value. Furthermore, an applicant that wants to take credit of a -1 in iGRC using dynamic, temporal population data. The credit for both would equate to a -2 in robustness, which in M1(B) would be considered a high robustness, despite the fact that the actual mitigation (from the true iGRC) is only a -1 (the one coming from correcting the erroneous data)

### 3.3 Selecting which Population Density to use in the iGRC footprint

Determining the population density to calculate the iGRC during Step #2 of SORA requires determination of the iGRC footprint for the intended flight path alongside the most accurate assessment available for the density of the population underneath that footprint. The semantic model shown in Figure 8, illustrates the components which make up the iGRC footprint

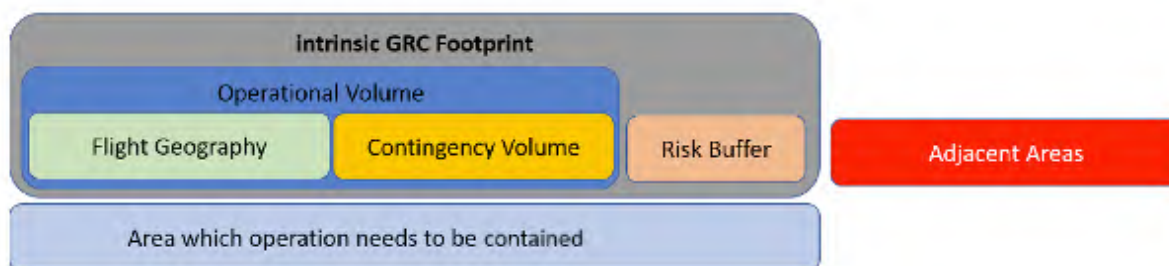


Figure 8: iGRC Component of the SORA Semantic Model

It can be seen that the iGRC footprint contains the Operational Volume (OV) and the Risk Buffer (GRB), with the sub-elements of the OV including the Flight Geography (FG) and the Contingency Volume (CV). Applicants are expected to:

- Conduct necessary flight planning to determine appropriate flight geography between desired departure and destination points, taking into account relevant mission objectives. A key factor influencing this appropriateness will be the population density overflowed by the preferred Flight Geography and the approval basis for the RPAS. This may necessitate flying over lower population density areas.
- Trigger contingency procedures upon entering the CV, with the intent to return to the Flight Geography (examples may include a return home mode or via manual control) or perform a safe contingency landing,
- Leaving the Operational Volume is considered a loss of control of the operation<sup>9</sup> with an expectation to immediately land within the bounds of the GRB, which might be supported by the

<sup>9</sup>Readers should note that Appendix C.1 provides an overview of the failure modes and key outcomes for loss of control of the operation against the backdrop of the iGRC framework, including a Fault Tree and Event Tree

use of a Flight Termination System.

While Step #2 requires the determination of an iGRC footprint, this may be reliant on information that doesn't emerge until subsequent Steps in the SORA process are completed. This includes:

1. A key element for determining the iGRC footprint in Step #2 is determining the size of the Ground Risk Buffer, with a default expectation to use a 1-1 ratio. However, applicants may prefer to shrink the GRB buffer using a more capable containment system when the population within the GRB or adjacent area is several population bands higher than the population directly underneath the Operational Volume.
2. SORA Step #3 allows applicants to reduce their initial iGRC via a suite of mitigations described in Annex B.
3. SORA Step 8 places technical design and operational requirements on the RPAS to ensure containment within the iGRC footprint (including the RB), where the extent of the requirements is commensurate with the population of both the iGRC footprint and the adjacent area(s). The are also increased computation requirements for the size of the GRC buffer.

It can be seen that the population ( $D_{pop}$ ) required in Step #2 requires knowledge of the OV, CV, and GRB, but these are not often finalized until Step #3 and Step #8 are completed. This is because applicants might subsequently choose to vary their route (and hence iGRC footprint) if their risk buffer intercepts a highly populated area or if the corresponding containment expectations for the adjacent area are similarly unpalatable. The dependencies between information gleaned across Steps #2, #3, and #8 during iGRC footprint and population determination necessitate a holistic and iterative approach from applicants and competent authorities rather than sequential.

It was observed that these dependencies could introduce confusion and the potential for mistakes or double counting when calculating M1 reductions under SORA 2.0 or the M1(B) reductions in the updated SORA 2.5. Consequently, the approach has been simplified across the SORA Main Body and in Annex B. In Section 4.2, it will be highlighted that demonstrating static map errors within the baseline map in Step #2 will be contained within Step #2 of SORA. Strategic operational restrictions that demonstrate a reduction in population density by spatio-temporal means (i.e. flying over a factory when it is closed) are contained within M1(B) of SORA v2.5.

Some CAAs may use other qualitative terminology that cannot be easily converted. JARUS recommends that CAAs that continue to use qualitative terms also publish quantitative equivalents so that those equivalents can be compared with the population density breakpoints in Annex F.

### 3.3.1 Determining the Population Density for Flight over Heterogeneous iGRC Footprints

It is expected that for many flight operations, the iGRC footprint will overfly several segments where the population density varies or is "*heterogeneous*". The key question is then: "*what approach should be used to calculate the population band when the population varies?*" Historically, approaches submitted by applicants have included arguments based on:

- **Approach 1:** Expected Casualties per Mission per flight hour, where the derived value is restricted to the single mission, but where each segment with a different population density weights the average based on the proportion of time overflown.
- **Approach 2:** Expected Casualties per flight hour, using all instances of all flights flown by the operator across all missions.

- **Approach 3:** Expected Casualties are established by considering iGRC volume for the individual flight and isolating the segment with the maximum population density.

Many applicants have historically sought to employ the averaging effect embedded within Approaches 1 and 2, employing arguments drawn from Appendix 3 of FAA AC 23-1309 [8] drawing on its use of “average probability per flight hour” as the reinforcing basis for their safety argument. The key distinction is in manned aviation, the biggest risk is to people on board, and they are continually exposed to the risk, which means these metrics for determining failure rates for equipment (failure per flight hour) are appropriate for manned aircraft.

For UAS, the key risk is to third parties on the ground, and where the risk varies proportional to the population density overflow. This means averaging approaches like Approach 1 and 2 may underestimate the risk to certain segments of the RPAS operation, especially when applied for the iGRC.

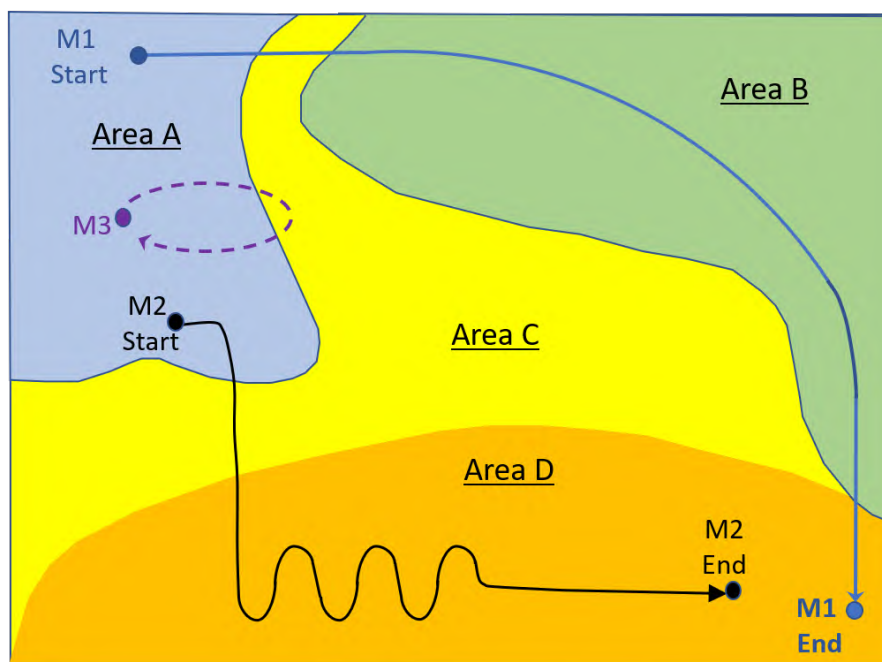


Figure 9: Multiple Overflow Areas

To illustrate, consider the 4 distinct segments of population density (Areas A, B, C, and D) shown in Figure 9, where the progression of population increase occurs as the segments progress through the color sequence blue, green, yellow and orange. Three mission profiles are also overlaid and annotated M1, M2, and M3.

Figure 10 provides a timeline for each mission, decomposing the proportional flight time for each population segment overflow, where  $t_{i,j}$  represents the  $i^{\text{th}}$  time segment of mission  $j$ .

Most applicants intuitively understand that Area D is the appropriate population density band for Mission 2 since the flight is overflying the highest population density for a significant portion of the overall flight time. In turn, they expect the same principle to hold for Mission 1, where the dominant portion is Area B, which has a lower population density and would result in a lower iGRC. Accordingly, many applicants argue along the lines of Approach 1, asserting that Area B should be the band selected. However, in many cases, this under-represents the risks for third parties in Areas C and D (with higher population densities).

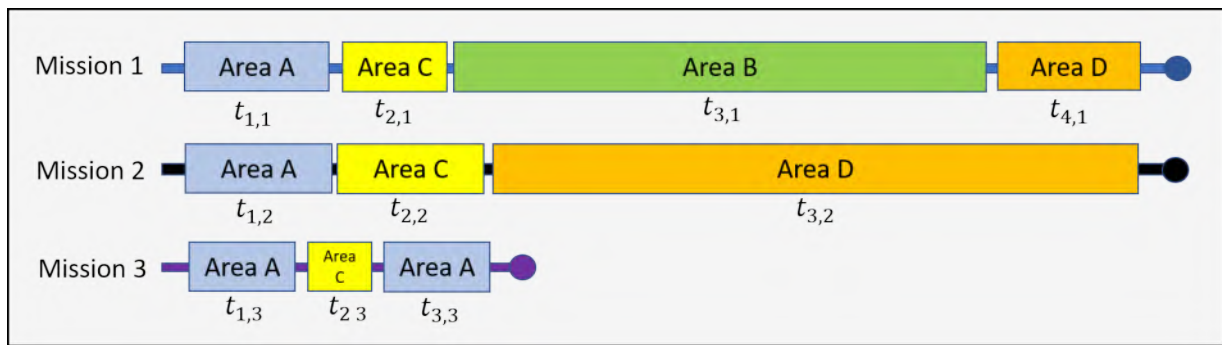


Figure 10: Overflight Timelines for each population segment of Missions 1, 2 and 3

### 3.3.2 Short Exposure Flight Over Higher Population Segments

Mission 3 is included to highlight the approval conundrum for competent authorities when a flight has a particular mission segment of higher density, but it represents a very small portion of the overall flight time, with a safety argument this small portion should not be included in the determination of the value for  $D_{pop}$  to be used in the iGRC table.

As a general rule, when using the SORA, the TLOS should be met for all the population densities overflown. This means that the segment with the highest population density should be used when determining the iGRC. Note that **how** the highest population density is calculated is critical to ensuring this value is a true representation of risk. Subsection 3.8 covers issues around grid resolution and smoothing issues.

This Annex acknowledges the competent authority may choose to allow small portions of a mission over flight segments with higher population density underfoot, cognisant that the expected TLOS for that segment is not met.

In permitting this concession, authorities should recognize the coinciding SAIL loss of control rate leads to a TLOS value greater than  $10^{-6}$ , irrespective of whether this is a longer flight time or repeated short-time flights for these flight segments, exposing third parties on the ground to greater than acceptable levels of risk.

Competent authorities are advised to closely scrutinize how often an operator intends to perform repetitive missions that include overflight of high population density areas without commensurate mitigations. A single flight may have negligible implications, but repetitive flights that accumulate one hour per year (or more) of unmitigated high-risk population exposure may jeopardize adherence to the prescribed target level of safety. Key considerations for authorities when considering approvals that include overflight of this higher population density environment should be:

- How long an individual flight intends to operate in that environment,
- The repetitiveness of this overflight,
- The density of other traffic also contributes to accumulating risk incurred by third parties.

### 3.3.3 Higher Population Densities in the Ground Risk Buffer

Competent authorities may receive applications where

- The population density within the ground risk buffer is heterogeneous,

- The ratio of higher population segments within the buffer is small and/or
- The higher population segments are on the outer boundary of the risk buffer and would, therefore, be at the extreme end of the glide ratio buffer and, thus, less likely to be impacted on the assumption that the appropriate flight termination capabilities were triggered upon leaving the Operational Volume.

Impacting those more densely populated segments may be reliant on multiple failures or, in rare edge case events, which means an already low likelihood event will be diminished further if the more dense segments only make up a small percentage of the heterogeneous elements with the buffer. As always, approval is at the discretion of the competent authority. However, any approval should pay particular attention to the percentage of higher populated segments within the buffer, how much greater the population within those segments is in comparison to the approved band within the operational volume, and the robustness of any containment system.

### 3.4 Common Methods Used to Create Population Density Maps

This section overviews both:

- the underlying population count data and the modifiable area unit problem, effectively a bias that is introduced when mapping point like data (positions of humans) to area based metrics (people per square km).
- spatial interpolation techniques, used to generate finer resolutions than available in an original mapping source.

#### 3.4.1 Census Data and the Modifiable Areal Unit Problem (MAUP)

A foundational element for developing a population density map is census data. At the highest level, aggregation and dis-aggregation approaches have historically been deployed to take census data and process it for use in population density maps, as follows:

1. In some countries, data is first collected for individual households and then **aggregated**<sup>10</sup> into higher order polygons to protect privacy. The size of the polygon is typically quite large, often variable, and often lacking the resolution needed for population density maps used for iGRC. Higher resolution maps are subsequently produced using a suite of **disaggregation**<sup>11</sup> methods typically supported by ancillary data to take the data in the aggregated units and distribute within the desired target cell (often gridded) as close as possible to reality.
2. In other countries, data is acquired via the conduct of micro censuses and is not always available everywhere in the country. To expand beyond the coverage of the micro-census requires a different approach, where available data is used to interpolate what the population might be in other locations. This interpolation is often informed by ancillary data such as satellite imagery with land coverage information embedded, and where prior knowledge about how the population is distributed around these features is subsequently used to provide estimates where no census data is available. Significant improvements in the accuracy of this approach have been achieved via organizations like WorldPop/CEISIN [10], [11] and Facebook HDX [12]

<sup>10</sup>Aggregation, also known as upscaling, involves transferring information from a smaller (detailed) scale to a larger (coarser) scale

<sup>11</sup>Disaggregation, or downscaling, the variation of a variable at a small (detailed) scale is reconstructed, given the value at a larger (coarse) scale

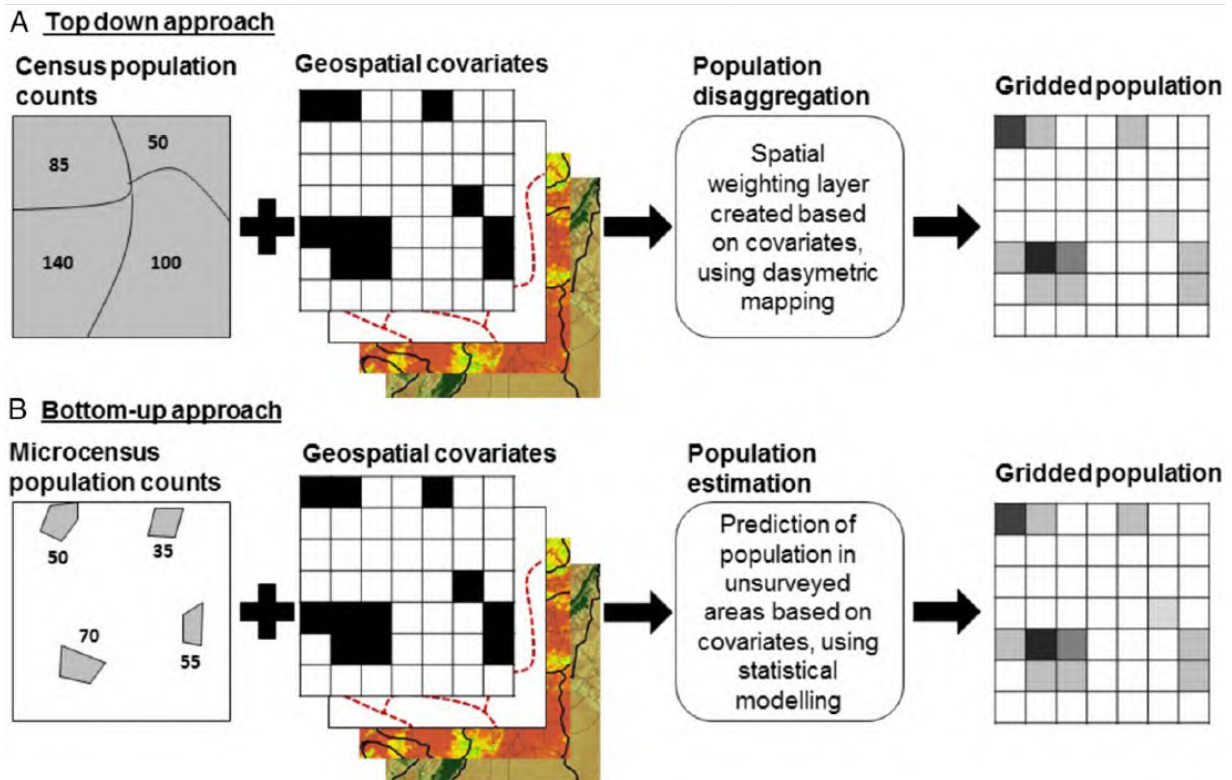


Figure 11: Illustration of top-down and bottom-up mapping approaches for Population Density Maps [9].

Figure 11 illustrates the top-down dis-aggregation component of the process described in Item 1, alongside the bottom-up aggregation for Item 2.

The aggregation process for Item 1 deserves further elaboration, as the combined effects of varying polygon size and orientation followed by the quality of dis-aggregation methods can significantly impact the overall accuracy of the map. For example, in Australia, household data is first aggregated into Mesh Blocks (30-60 dwellings), which are not publicly available<sup>12</sup>. Mesh blocks are then aggregated into Statistical Area Level 1 (SA-1) areas, for which data is made publicly available. SA-1 areas are then nested within SA-2 areas, which typically coincide with suburbs, that are again aggregated into SA-3 regions that contain between 30,000 and 130,000 people. These are then further aggregated into state and territory areas. Similar hierarchies of census units can be found across the world in Europe, the United States, the United Kingdom, and New Zealand.

SA-1 areas have a population of between 200 and 800 people, with an average population of approximately 400 people. Figure 12 contrasts the shape and size of both Mesh Blocks (red) and SA1 Units (blue) for a portion of Sydney, Australia.

Scrutinizing Figure 12 it can be seen that both the Mesh Block and SA-1 boundaries vary considerably in size and spatial arrangements, and whilst there are some constraints on the number of houses in each unit, aggregation into parent units is not always of equal area.

The phenomenon is called the Modifiable Areal Unit Problem (MAUP), which has two permutations, both have relevance to the accuracy of population density maps<sup>13</sup>[13],[13]:

- **Scaling Effect:** used to describe the situation where the initial areal data is aggregated into

<sup>12</sup>This first level aggregation is commonly referred to as an Enumeration block in other jurisdictions around the world

<sup>13</sup>This problem was first noticed by Taylor and Openshaw in 1970, who found that correlations in Iowa between Republican voting and percentage of old people could vary by  $\pm 1\%$  subject to how counties were aggregated

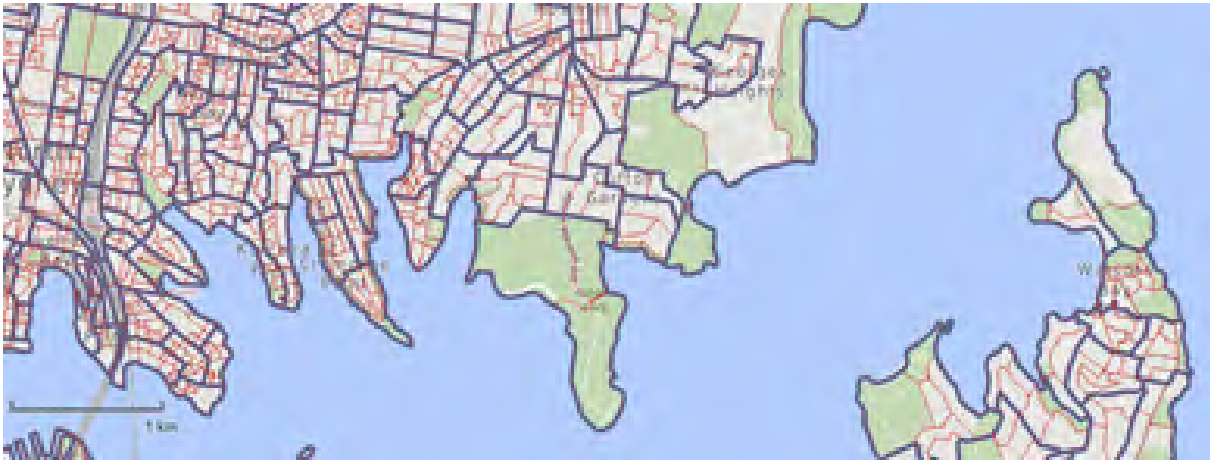


Figure 12: Mesh Blocks and SA-1 Units for Australian Census Data

sets of larger areal units with different spatial resolutions, with each combination producing different data values for the population density.

- **Zoning Effect:** also known as the aggregation effect, refers to the situation where the initial areal units are recombined into zones that are of the same size but oriented or located differently, and this again produces variation in values for the population density

In many cases, the selection of boundaries is motivated by political or economic forces rather than the pursuit of population density estimates to suit UAS operations. Ultimately, these aggregation-related problems in enumerating data are not eliminated and instead are propagated into a different data structure, which is a combination of the hierarchy from the census unit to the reporting units that are then mapped back into gridded cells.

Figure 13<sup>[14]</sup> illustrates the varying results that occur when the same census data is aggregated into two distinctly different boundary systems. Reviewing Figure 13a it can be seen the area on the right of the diagram has a low population count, but in contrast, that same area, when grouped differently, is deemed to be highly populated in 13b. Information has been lost at the completion of the aggregation stage, and dis-aggregation methodologies cannot recover it.

Practically, if an applicant seeks to operate over a suburb, then using maps with grid cells of 150 m or 250 m might appear reasonable. It would be if the input data to the mapping process were at the census(mesh) block or even tract (SA-1) level. If, however, the input data was disaggregated from large administrative units (e.g., district or region), the accuracy of the estimates could be questionable.

Competent authorities and applicants will have limited ability to influence maps produced, let alone the selection of the fundamental aggregation unit (Mesh Blocks for Australia) and the subsequently publicly released aggregation blocks.

When the aggregated Administrative Unit is larger in size or with significant variation in shape compared to the collection units (e.g., mesh or enumeration units) the population value is likely to underestimate the real value. To mitigate this risk, competent authorities may choose to consult with national census bodies to better understand the impact of MAUP and the acceptability of the maps presented by applicants or the nationally available map. Section 3.4 will highlight how the key methods used impact accuracy.

In cases where the maps overstate the population, there is likely to be increased instances of applicants presenting with supplemental information, such as satellite imagery, to support a lowering

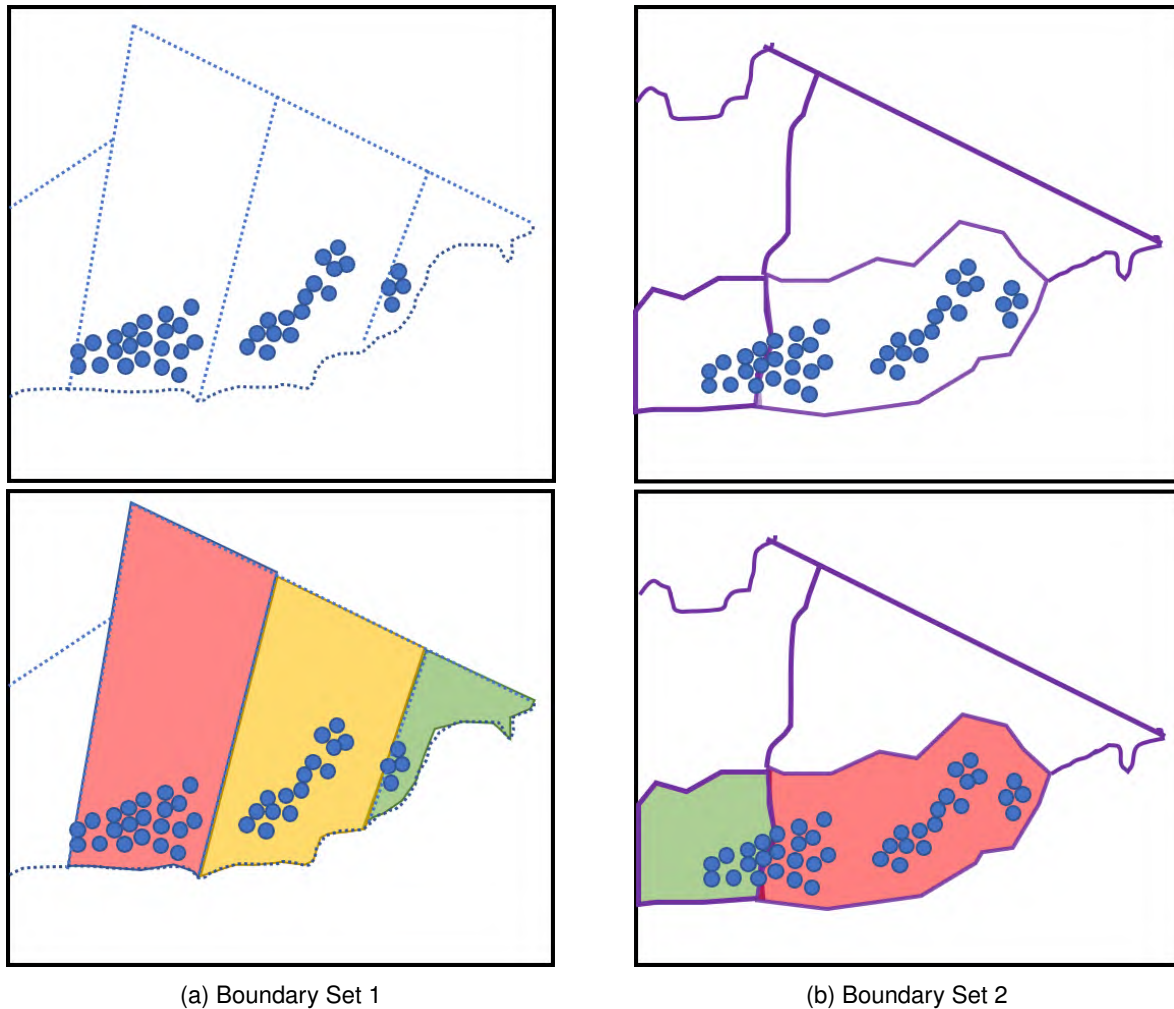


Figure 13: Illustration of Modifiable Areal Unit Problem

of the population estimate. Some third-party vendors may choose to post-process publicly released data, but these maps may not have been verified for accuracy.

### 3.4.2 Spatial Interpolation

Spatial Interpolation is a technique that uses sample values of known geographical points (or area units) to predict values at other unknown points (or area units) and can generate estimates of values at finer resolutions than the original data. This is useful when the fine-scale data is unavailable or has been restricted and/or aggregated for privacy reasons. Both aggregation and dis-aggregation are reliant on spatial interpolation. Spatial Interpolation can be achieved via the following sub-ordinate methods:

1. **Areal interpolation:** transfers attribute information from source zones with known values to other, usually smaller but not always, target zones with unknown values. Source zones completely cover the study area, but their resolution is insufficiently fine for a particular analysis.

(a) Without Ancillary Information:

- Areal Weighting
- Pycnophylactic Interpolation
- Area to Point Interpolation

- (b) With Ancillary Information:
    - Dasymetric Mapping
    - Street Weighting Method
    - Point-Based Approaches: using point data as ancillary data.
2. **Point Interpolation:** Makes the assumption that data within the source zone varies continuously and makes predictions for locations without data using other sample points where data is available. The methods for achieving this include:
- (a) **Exact Methods:** inverse distance weighting, kriging, natural neighbor and minimum curvature
  - (b) **Approximate Methods:** trend surface analysis

Expanded detail for Areal Weighting, Pycnophylactic Interpolation, Dasymetric Mapping, and Street Weighting is provided in the remainder of this section, as these methods are predominantly used in the creation of population maps.

### 3.4.3 Areal Interpolation

The most basic form of areal interpolation is “areal weighting,” in which the population in the source area is spatially apportioned into the target areas based on how much of each source area falls within each target area.

Area weighting is inherently volume preserving: this means that the cumulative total of all the counts allocated to the target grids matches the overall area in the source data. Figure 14 provides an illustration of how basic areal weighting is performed. Figure 14a represents a simplified census count

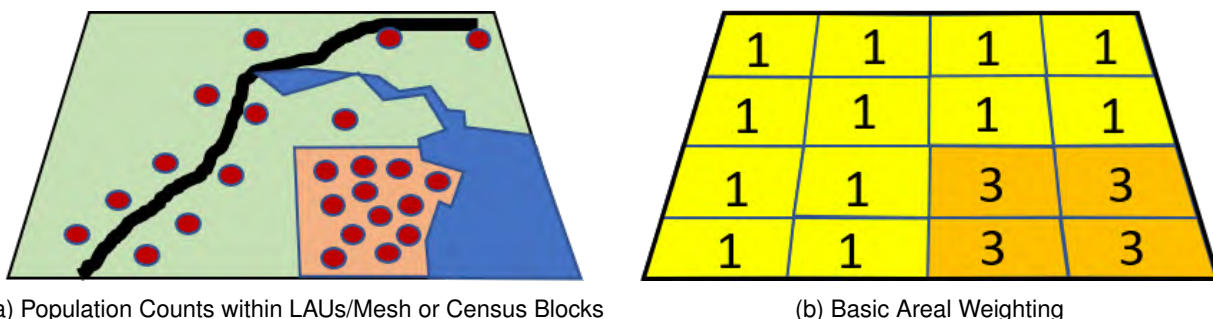


Figure 14: Illustration of Areal Weighting

(in red) across two separate collection boundaries (Local Admin Units (LAUs), Mesh Blocks, or Census Tracts), which are shown in pink and green. Also embedded in the diagram are a lake (in blue) and a road (in black). These features will be used in later sections to highlight the improvements in accuracy achieved in dasymetric mapping. Areal mapping takes the count within the green and pink areas and pro-rata apports the counts in the target grids that overlap. There is an inherent assumption that the distribution of data in the source zone is homogeneous, which produces the following noticeable inaccuracies:

- Several of the grid cells in the target area, associated with the green LAU, have population attributed even though the source LAU indicates there was no population present in that grid square (top left-hand corner)
- In arbitrarily allocating the population from the pink LAU, the population was allocated to cells where a lake was present, leading to a situation where the population for the land element is underestimated.

Methods to overcome this shortfall will be detailed in Section 3.4.5 and 3.4.6

The Global Population of the World (GPW) [15] density maps employ areal interpolation. Table 9 provides details on the mapping product alongside a variety of contemporary products using different approaches. In addition to its use in GPW, this method is incorporated into most GIS software packages, and it is quite possible these population density maps may be presented to competent authorities in support of iGRC calculations.

In the absence of other ancillary data that can support improved allocations, it remains a reasonable solution. However, the disadvantage of areal weighting is obvious: in pro-rata allocation of population counts to the target zone based on area, an assumption is made that the source zone is spatially homogeneous. This is rarely true in practice, particularly in more densely populated areas or when the source zone area is large. This means there is a significant probability that any area taken from the source zone actually has a different population density than the average.

Aside from raw census counts, this method is the least desirable.

### 3.4.4 Pycnophylactic Interpolation

Pycnophylactic interpolation [16] seeks to iteratively generate a smooth surface and minimize discontinuities in the target zone. It supports the production of density or contour maps when only area data statistics are available. The method is most easily explained with Figure 15, sourced from [17] based on work originally provided by the U.S. National Center for Geographic Information and Analysis at the University of California Santa Barbara, based on work originally published by Tobler [16].

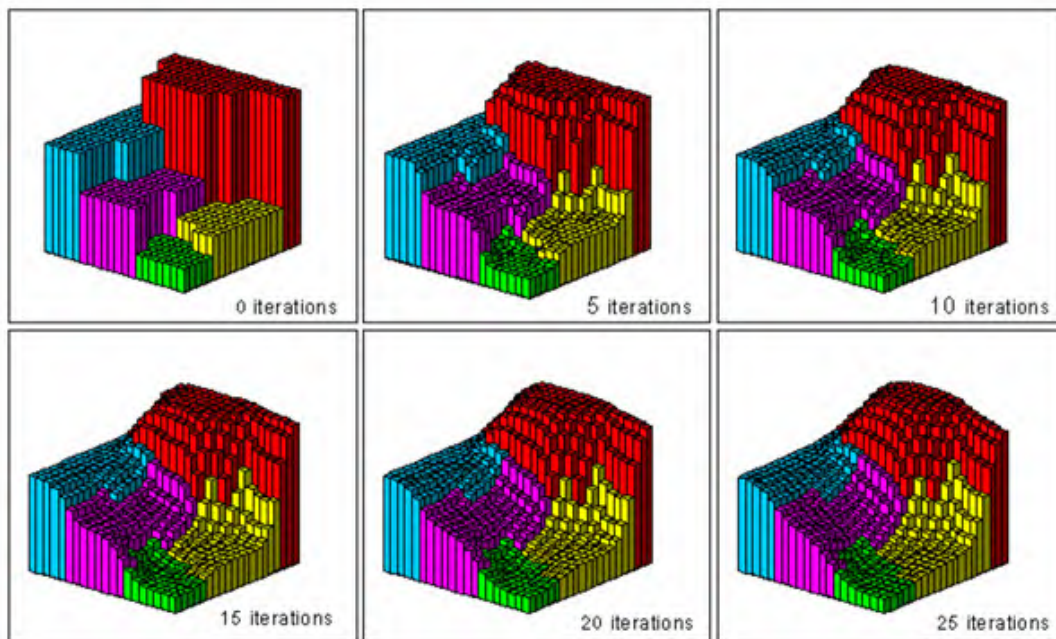


Figure 15: The Smoothing Process of Pycnophylactic interpolation over multiple iterations: Source U.S National Center for Geographic Information and Analysis

In Figure 15, it can be seen there are 5 colored subordinate target zones. Areal weighting would uniformly allocate population density in each of these colored target zones. In fact, the first iteration of Pycnophylactic interpolation applies areal weighting, as illustrated in the top left of Figure 15. The method iteratively works through each of the cells (shown as a 3D polygon), adjusting the count by considering a weighted combination of the neighboring cells values[18].

Pycnophylactic interpolation is also mass or volume preserving, which means that the overall population count in the source data, is maintained in the target zone, even after the smoothing process. Key variables that impact the quality of the product include the number of iterations conducted and the number of sub-ordinate cells in the target zone, which subsequently impacts the degree of smoothing that can be achieved by the algorithm [19].

The disadvantage of the method is that it assumes no sharp discontinuities exist in the data, which is not true in many cases, including water bodies, government/military land, or railway lines. The key advantage is that it removes the assumption of homogeneity in areal weighting and dasymetric methods. When pycnophylactic interpolation is hybridized with these approaches, it can produce superior results.

Maps produced using Pycnophylactic interpolation are generally preferred to those using basic areal weighting but are generally inferior to dasymetric mapping unless hybridized with other methods.

### 3.4.5 Dasymetric Mapping

Dasymetric mapping seeks to improve on areal weighting by establishing a relationship between the underlying source data and information from ancillary data, such that original source population counts in the larger source unit are redistributed to finer spatial units but with higher accuracy than basic areal weighting.

The ancillary data is typically land cover data captured via satellite (e.g. LandScan [20], Corine [21], Global Human Settlement Layer (GHSL)[22]) containing information on the land cover such as lakes, rivers, whether an area is forested, urban, or where road and building infrastructure is located. Basic information on Landscan and Corrine Ancillary data is provided in Table 10.

The basic process consists of an overlay between population data in the form of polygons and land cover data, which produces dasymetric zones nested within both the population polygons and the land cover data. The population is subsequently spatially apportioned from the population polygons to the dasymetric zones based on the relationship between land cover and population density. As with areal mapping, there is an assumption that the population density within each dasymetric zone is uniform. However, these zones are typically much smaller than the source areas and more accurate than basic areal weighting without ancillary data.

There is a wide array of implementations for dasymetric mapping, and this variation can significantly impact the accuracy of the population density. The simplest approach is the application of a binary mask that identifies areas known to be uninhabited, such as bodies of water and government-owned land, where these areas are cropped from the original source map, with the original population subsequently redistributed to the inhabited areas. Figure 16b illustrates this effect. In comparison to Figure 14, which employed basic areal mapping, it can be seen that the binary mask improves the accuracy by reallocating the population from the water mass to the land mass in the pink LAU.

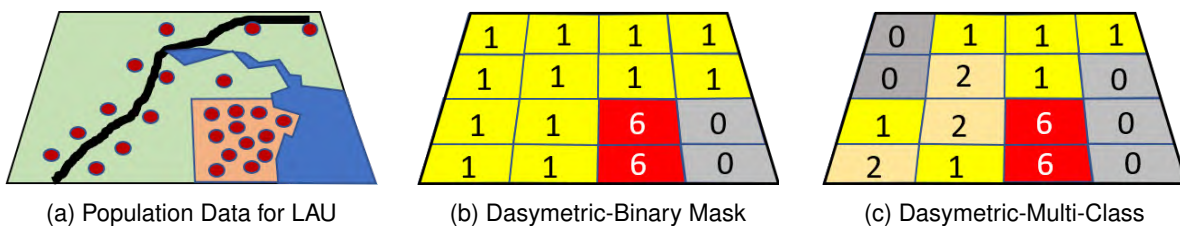


Figure 16: Comparison of Different Population Interpolation Schema

When more detailed ancillary data, such as land cover, is available, a multi-class system can be implemented. Typically, land cover data has improved resolution compared to the census data. By

making population density estimates for each land cover type, these weightings can be used in the redistribution of original source zone population counts.

A further advancement is the use of street network data, with the simplest implementation using the street network from the source data and distributing the population uniformly along the street segments. Figure 16c illustrates this effect, providing a more appropriate allocation of the population in the green LAU.

Whilst dasymetric mapping provides a more spatially informed interpolation, they require the capture of both census and ancillary data, with the latter requiring expert processing of the ancillary data with the choice of weights having a particular influence on overall accuracy.<sup>14</sup> The reliance on census data means this approach can still be influenced by the MAUP problem mentioned in Section 3.4.1. The lack of good-quality census data means that these products may be less accurate. Population Density data sources that employ Dasymetric Mapping include WorldPop [10], WPE [23], GHS-POP [24] and Oakridge Landsan [20].

### 3.4.6 Smart Interpolation

As summarized in [25], dasymetric mapping employs ancillary data to assist in the distribution of the original census data. Smart Interpolation techniques can employ multiple ancillary data sources. For example, LandScan process distributes the sub-national level census counts using multiple ancillary data sets generally with much finer resolution, including land cover, roads, slopes, urban areas, village locations, and night-time lighting. The population distribution model then calculates a “likelihood” coefficient for each cell and applies the coefficients to the census counts, which allocates the population to each cell proportionally based on the calculated population coefficient.

## 3.5 Temporal Accuracy

Capturing census data is time-consuming and costly, and as a byproduct, it’s done infrequently. Ancillary data, particularly those captured via satellite, are similarly expensive, and most epoch updates are done every four years. This means the temporal accuracy of some population mapping products can be poor, especially in rapidly growing areas. This section outlines some basic considerations that impact on the temporal accuracy of mapping products.

### 3.5.1 Human movement: Residential and Business Properties

Whilst some multi-national population maps employ nighttime lighting to better model where people live, understanding their movement over a 24-hour period will be important for catering for the large variation in people’s movement and its impact on the population at risk for UAS operations.

As a general rule, residential properties have fewer people in them during the day because a large portion of people are at work, and these people have migrated to office buildings and commercial properties, often in business districts but also interspersed in residential areas. Limiting the assessment to the census data depicting residential distribution will significantly underestimate the number of people around business parks, shopping centers, or other business-heavy districts during business hours and overestimate the risk of residential areas.

Satellite data can be used to create a binary mask for subsequent areal mapping of population counts as described in Section 3.4.5. This data and approach will also be important when establish-

<sup>14</sup>The accuracy of these maps cannot be any greater than the spatial unit from the ancillary data, with the assumption that each of these units is homogeneous

ing the effect and boundaries of sheltering used as part of Mitigation 1, to be discussed in Section 4. However, this still leads to an underestimation of population density in business districts, as office buildings generally have higher densities of people per unit area when compared to residential buildings. If data is available on the breakdown of residential and business premises, a more accurate hybrid dasymetric/smart interpolation could be produced to adjust for this effect.

### **3.5.2 Human Movement: Temporary changes due to events**

Another consideration for human movement are those movements that humans undertake for leisure activities, particularly those that result in short term high changes to population density. Examples include:

- sporting events,
- concerts,
- fairs or community events, or
- political events

Competent Authorities should also note that population distributions can also vary by significant amounts for longer durations. This variation could be seasonal, for example at tourist destinations, including:

- camping sites,
- small towns or villages near known tourist sites, or
- areas of known human congregation, such as:
  - beaches,
  - malls or markets, or
  - transport hubs

Local authorities will generally have information or knowledge of these events/movements, and can assist applicants with obtaining more accurate population estimates outside of using purely census data.

### **3.5.3 Mobile Phone Data for Use in Population Maps**

The shortcoming in temporal accuracy has seen the emergence of many studies using mobile phone data to produce better representations of human movement [26], [27], [28]. As time progresses, it's increasingly likely that UAS regulatory authorities will be presented with safety cases supported by population maps derived from mobile phone data rather than traditional methods. A strong argument will be that the mobile data represents a more accurate temporal representation that could be tailored to better reflect movements in different seasons, days of the week, and even times of the day, and in the limit, provide dynamically updated assessments of where people are located in real-time. These merits mean that authorities should start planning for that eventuality to better describe what assurance mechanism they would expect for the quality of the process given the risk of the operation. For the moment, we note the following:

- The status of the data from a privacy perspective will require similar scrutiny to census data,

- A likely method might be to employ the mobile data as ancillary input supporting dasymetric mapping, where the distribution of people according to the mobile data is used as a mask that is used to weight the original census data. The accuracy of this process is likely to need assessment for accuracy, variability, and consistency across different demographics, taking into consideration
  - that mobile phone data may not be available for areas without coverage, even if populated,
  - Access to MNO data around the customers might not be freely available,
  - knowledge of the ratio of the population carrying and connecting to a mobile might not be known and could vary.

## 3.6 Settlement Maps and Density Smoothing

### 3.6.1 Background

In some countries, the resolution embedded in available population density maps may not align with the bands shown in Table 2. An interim approach may be to consolidate bands from Table 2 and seek out products with less quanta, such as settlement maps rather than population density maps.

These maps offer improved harmonization in both the definition around thresholds between population classes in addition to consistency in the process used to go from raw census data to population categories and in many cases, greater spatial accuracy. These benefits are important, as inconsistency in both the thresholds and methodology impacts the portability of both products and services across nations. This means that harmonization is a common goal for operators, manufacturers, and authorities. Notably, a report which looked at harmonized definitions for cities and rural areas [29] and the application of Degree of Urbanisation (DEGURBA) model[30] was tabled by the European Commission in 2014 to ensure more consistent outcomes.

Whilst the benefits of harmonization and consistency offer up attraction for many nations, some care needs to be taken in the use of these maps in lieu of population density maps. The remainder of this section helps to illuminate the strengths and limitations of settlement maps and their use in UAS-related operations.

### 3.6.2 Establishing Consensus over Definitions and Methodology

As mentioned, nations with less accurate mapping products may choose to consolidate the bands in Table 2 and then use settlement maps rather than population density maps because of harmonization and consistency. For example, settlement maps often present information that delineates between rural and urban areas and cities, and these could, for example, be mapped back to the quantitative classes in Table 2.

Historically, consensus on definitions for rural, urban, and city environments varies significantly across nations, as does the methodology producing the mapping products. This meant settlement maps were not particularly useful for supporting iGRC determination.

For example, in a study done in 2020, [30], Dijkstra established that in the USA, 82% of their population resides in nationally defined urban areas which would average at least 222 residents per km<sup>2</sup>. In contrast, India deems that only 33% of its population is urban, which would mean a density threshold of 17,000 residents per square km, 75 times higher than the density threshold of 222 in the USA. Similar differences include:

- Australia defines urban areas as population clusters of 1000 or more, with a density of at least 200 people per square kilometer.
- Japan defines urban as clusters of 4,000 people per square kilometer.
- U.S. Census Bureau identifies two types of urban areas:
  - Urbanized Areas of 50,000 or more people; &
  - Urban Clusters of between 2,500 and 50,000 people.
- US Science and Research Panel defines an urban area as containing an average population of 193 people per square kilometer.

This variation led to the United Nations Statistical Commission endorsing a harmonization in methodology called the Degree of Urbanisation (DEGURBA) model[30] [29]. DEGURBA serves to reduce the extent of distortion in real density values, which occurs because of MAUP-related factors (Section 3.4.1). This method was implemented by all European national statistical institutes in 2012. Furthermore, conversations around wide-scale implementation are also underway with the USA, Australia, Brazil, Korea, India, Pakistan, South Africa, Turkey, Ethiopia, Uganda, and Malaysia. Status fact sheets for most countries can be found at [31].

Certainly, the harmonization benefits of the DEGURBA approach are attractive; however, there are some shortcomings in the approach that warrant emphasis.

### 3.6.3 DEGURBA Incorporation in GHS-SMOD

A key example of a settlement mapping product employing DEGURBA is the Global Human Settlement Model (GHSL-SMOD). This is a fusion of the more detailed population data found in GHS-POP and the greater spatial accuracy provided in GHS-Built, with the DEGURBA process applied. Expanded detail is provided in Table 10.

The GHS Settlement Model classifies each country's territory into 1km<sup>2</sup> grid-squares annotated as one of the following three classes:

- Cities - have the majority of their population in urban centers.
- Towns and Semi-Dense Areas - have the majority of their populations in urban clusters but are not cities.
- Rural Areas - have the majority of their population in rural grid cells.

Urban area is the term used to collectively capture cities, towns, and semi-dense areas or suburbs. The basis for determining whether an area is an urban center, urban cluster, or rural grid cell is informed by a combination of population density, contiguity, and population size thresholds according to:

1. **Urban centre:** Also known as high-density cluster and consist of contiguous grid cells with a density of at least 1,500 inhabitants per km<sup>2</sup> and has at least a total population of 50,000; gaps in this center are filled, and the edges are smoothed with an iterative application of the majority rule (if five out of the eight surrounding cells are part of an urban center, this cell is added to the center).
2. **Urban cluster** (also known as moderate density cluster) consists of contiguous grid cells with a density of at least 300 inhabitants per km<sup>2</sup> and at least a total population of 5,000; and

- Rural grid cells** (also known as thinly populated or low-density cells): grid cells outside urban clusters.

A simple visualization of the difference in classes can be found at [32], with expanded detail available at [30], [29]. Tools supporting the application of the DEGURBA methodology to national data can be found at [33].

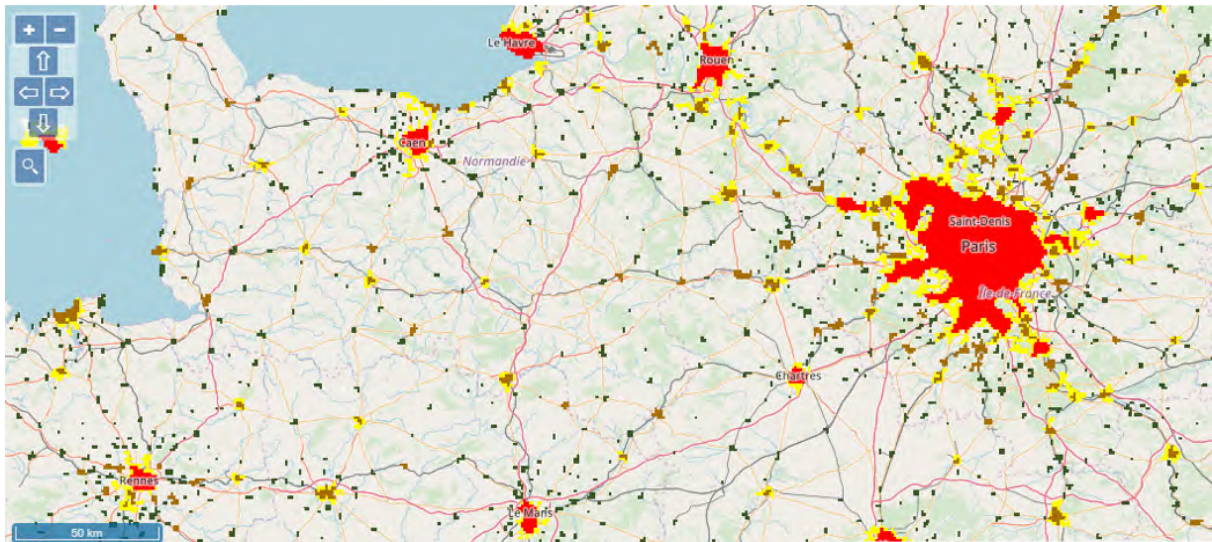


Figure 17: Global Human Settlement Model Grid- DEGURBA Implementation around Paris-Widescale view

Figure 17 provides an example of the DEGURBA model applied as part of GHS-SMOD for sections of France. This snapshot is taken with a wide-scale zoom, whereas Figure 18 provides a higher-level resolution instance focused on Paris.

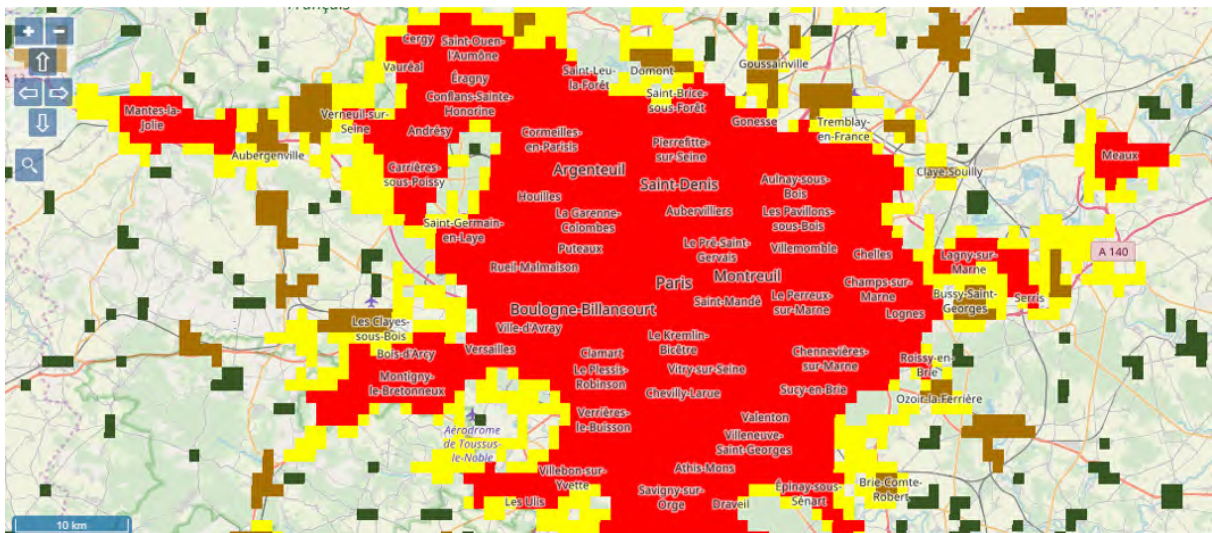


Figure 18: Global Human Settlement Model Grid- DEGURBA Implementation around Paris-Finer Resolution

It can be seen in reviewing Figure 17, that the settlement model and DEGURBA implementation might have utility for authorities in their initial efforts to segregate low and medium risk flight areas, and delineate them spatially from more highly populated cities and urban centres.

However, the process to assess contiguity (defined in detail at [30]) acts as an aggressive smoothing

filter on the true population data. In cities, this smoothing process acts to reclassify any 1 km grid squares with low population density when the number of grid squares sitting in a higher population cohort exceeds it by a certain number.

The outcome of this process is evident in Figure 18, where many grid squares within the Paris region have low population levels, which would normally require lower SAIL levels, yet have been smoothed. Ultimately, this will lead to increased instances of operators in city environments presenting with alternate mapping products, which illustrate this disconnect, and this may subsequently increase the burden on regulatory authorities in processing applications.

### 3.7 Understanding the Original Intent of a Map Generation

As can be seen, there are a variety of methods used to compile these products, with many having resolution limited to population per square kilometer. It is expected governments of many nations may provide higher-resolution maps. However, competent authorities should consider the various issues discussed in Section 3.4.1 and 3.4 to understand the map compilation process and ensure these maps are fit-for-purpose for UAS-related operations under SORA. In assessing suitability, the following general rules may assist:

- More sophisticated methods such as intelligent dasymetric mapping &/or smart interpolation. (GeoStat1B/ESRI/GHS-POP/WorldPop/LandScan) that employ multiple layers of supporting ancillary data are preferred to more lightly modeled variants such as GPW4, GRUMP, and HSRL.
- Higher resolution maps are preferred to minimize the homogeneous assumption effects.
- Maps using census and ancillary data with more recent epochs are preferred.
- Density Maps are preferred over Settlement Layer maps (HSRL/GHSL-SMOD).
- Some maps may have quanta that do not align with the population bands used in SORA or may have an insufficient range (e.g., GRUMP), and this may necessitate the use of multiple maps by authorities.
- Preference should be given to maps produced by organizations providing detail on the methodology used for their map production, in addition to detail on validation efforts on accuracy.

The remainder of this subsection ties together information presented on map creation methods and issues and provides guidance on areas of practical concern based on feedback from applicants and authorities in their use of the SORA process. These areas include:

- The underlying intent of the mapping product.
- The underlying data and methodology used to obtain the population count.
- The assumptions made to correlate ancillary data with population density.
- The grid resolution and shape.
- The temporal accuracy of the map.
- The Applicants intended Flight Level/s and its implication for Map Resolution.
- Hybrid Mapping products created by the applicant.

### 3.7.1 Underlying Intent of the Mapping Product

Maps are generally produced to support a specific purpose (i.e., to accurately portray geography, to support the allocation of funding, to delineate voting boundaries, or to differentiate between urban and non-urban areas using DEURBA [34]). This means that many of the available maps were not produced with the specific context of assessing safety for UAS operations or aligning with the SORA, where the critical need is spatial, numerical, and temporal accuracy. Accordingly, both applicants and competent authorities should consider the assumptions underlying the provided map to ensure they are consistent with the safety needs of the SORA process.

### 3.7.2 Population Counts: Underlying Data and Methodology

As described in Section 3.4.1, the method used to gather population counts greatly affects the accuracy of the population density map. In general, the approach of using micro-census and a mix of interpolation and ancillary data inherently has less information and will be less accurate than the approach that has a complete census which is aggregated up and then subsequently dis-aggregated into grids top-down approach<sup>15</sup>. Some maps may not utilize a census count and require substantial evidence to demonstrate the relationship between the ancillary data and population density estimate.

### 3.7.3 Ancillary Data Assumptions

It is likely that any population density map provided by an applicant will have utilized ancillary data to refine and distribute the raw population counts for the reporting unit. This process is reliant on the correlation between the ancillary data features and population density. In some cases, the prediction accuracy for that feature is very high (e.g., low or zero population on a body of water), but in others, it has less accuracy. This becomes more subjective when multiple ancillary data features and sources are weighted but without coinciding validation over the choice of weights or the accuracy of each source as a predictor.

Particularly for data sources that are not generated by government-endorsed organizations, including applicant-generated mapping sources, justification for any correlations drawn from ancillary data should be sought. For example, if satellite data is used to establish the boundaries of building and habitat footprints for a particular region, it is important to understand how the population mass in the original map was disaggregated across the building footprints and open areas. This is likely to vary in different nationalities. It is the applicant's responsibility to provide appropriate justification for any correlation claims.

## 3.8 Common Mapping Products

Table 9 and 10 provide details for a selection of population density maps and ancillary data sources provided by various governmental organizations or high-integrity commercial providers. The maps provide coverage either globally or with significant continental coverage in areas that have historically had fewer resources to conduct regular census activities. The tables also include details on map resolution, methods used (See Section 3.4 for descriptions), and the quanta in which the population is banded. An excellent map-viewing product that allows readers to contrast some of the datasets in Table 9 is provided by the NASA SocioEconomic Data and Applications Center (SEDAC) at [35].

---

<sup>15</sup>The allocation of the term bottom up and top down can be confusing, as most top-down methods actually start by aggregating up the original, albeit complete population counts.

Table 9: Multinational Population Density Products and their Characteristics

Database	Coverage	Resolution	Methods Used	Quanta Used	Reference URLs
Global Population of the World (GPW)	Global	1km	Areal Weighting	[<1],[1-5],[5-25],[25-250],[250-1000],[>1000]	[15]
Global Rural Urban Mapping Project (GRUMP)	Global	1km	Disaggregation of national census data, smooth pycnophylactic interpolation	[0],[1-5],[6-25],[26-250],[251-1000],[>1000]	[36]
Global Human Settlement Population(GHS-POP)	Global	250m & 1km	Hybrid Areal Weigthing & Dasymetric Mapping: GPWv4 is broken into 250m cells and population is dis-aggregated proportionate to the built up area informed by GHS-BUILT. 250m cells are produced in Mollweide	[0-20], [20-100],[100-500],[500-1000],[1000-1500],[1500-2000],[2000-4000],[4k-10M]	[37],[24],[38]
GHSL Settlement Model (GHSL-SMOD)	Global	1km	Combines GHS-BUILT settlement areas & GHS-POP population data to create classes (urban center, urban, cluster, & rural). Degurba model[13] used to smooth clusters	Urban Centres:[1500 ppl/km <sup>2</sup> & cluster size of 50k] Urban Clusters[300 ppl/km <sup>2</sup> & cluster size of 5k] Rural Clusters [300 ppl/km <sup>2</sup> & cluster size of 500] Low Density Rural [≤ 50 ppl/km <sup>2</sup> ]	[39, 38, 40, 38]
Geostat 1B	Europe	1km	Bottom-up aggregation for most countries; intelligent dasymetric mapping for others	[0], [1-4], [5-19], [20-199], [200-499], [500-5000], [>5000], [Data no Avail ]	[41], [42], [43],
OakRidge National Laboratories LandScan	Global	1km	Provides average day/night population distribution. Census data a several layers are used to inform a Dasymetric Mapping/Smart Interpolation based approach which derives a relative likelihood of population in cells due to road proximity, slope, land cover and night-time lights	People counts per grid. Each Grid approx 1 km, [0],[1-50],[51-100],[101-200],[201-400],[401-600],[601-1200], [1201-1600],[1601-2861],[2861-4120],[4121-5380], [5381-8320], [8321-11260], [11261-24900]	[20][25]
ESRI World Population Estimate (WPE)-Commercial Product	Global	150m	Ancillary data including land cover, roads, and place-names derived from LandSat8 produces a probability surface which is then calibrated using census data	100 ppl/km <sup>2</sup> , 400 ppl/km <sup>2</sup> , 1,500 ppl/km <sup>2</sup> , 2,500 ppl/km <sup>2</sup> , 16,979 ppl/km <sup>2</sup> , 29k ppl/km <sup>2</sup> or more	[23]
World Pop	Global	100m (Population Counts) & 1km (Population Density)	Weighted Dasymetric based Random Forests or Landcover. Also used bottom up approaches where census data is unreliable or outdated. Ancillary data includes settlement locations, extents, landcover, roads, building maps, satellite nightlights, vegetation and topography	Not Found in published data	[10], [11],[12]

Table 10: Ancillary Data Sources and their Characteristics

Database	Coverage	Resolution	Methods Used	Quanta Used	Reference URLs
GHS-Built	Global	38m	Synthetic Aperture Radar from Sentinel 1 &2 and 4 epochs of LandSat data are processed using a deep learning to capture proportion of building footprint area in each 30m grid square, <b>regardless of admin boundaries</b>	no data, water surface, land no built-up, built-up	[44],[45]
Coordination of information on the environment (CORINE) Land Cover (CLC)	38 countries	minimum mapping unit (25 hectares) and minimum width for linear elements (100 metres), geometric accuracy j 25m	computer assisted photo-interpretation of the Landsat ETM (Enhanced Thematic Mapper) satellite which has 10m resolution	44 land cover classes based on 5 main groups spanning artificial surfaces, agricultural areas, forests and semi natural areas, wetland and water bodies	[21], [46]
European Settlement Map	Europe	2.5m, 10m and 100m	uses machine learning techniques in order to understand systematic relations between morphological and textural (pantex) features, extracted from the multispectral and panchromatic (if available) bands, describing the human settlement.	Morphological built-up, Green in morphological built-up, Open spaces (in built-up areas), Green in open spaces, Not green in open spaces	[47], [48], [49]
High Resolution Settlement Layer(HRSL)	Various parts of African Continent, Mexico, Argentina, Indonesia, Thailand, Cambodia, Phillipines	30m	Binary Dasymetric- Settlement extant data is derived via computer vision techniques using DigitalGlobe satellite ancillary data. Sub-national census data is then proportionally allocated to the settlement extents. Population estimates are from the GPW data collection.	Not Found in published data	[50], [51], [52]

### 3.9 Appropriate grid resolution to accurately measure population density

Intuitively, the bigger the grid cell (or the lower the resolution) used for measuring population density, the more likely the population distribution in that area is not homogeneous and that there are areas within that individual cell where the population density varies significantly from the value attributed to the whole cell. This increases the chance that the operation could be flying over a higher population density than is allowable by an applicant's SORA based operational authorisation. As the resolution increases (i.e. the grid cell gets smaller), the likelihood that this occurs diminishes. This is true up to the point the aircraft's dispersion area begins to impact the requirements for grid resolution.

Going back to first principles, the fully expanded equation for expected casualty for the  $i$ th population density is:

$$E_C(i) = \lambda_{GI}(t) \times P_{impact}(i) \times D_{pop}(i) \times F_{exp}(i) \times A_C \times P(Fatality|impact) \quad (16)$$

Where the key variables for this discussion are  $P_{impact}(i)$  and  $D_{pop}(i)$ , which describe the probability that the aircraft will impact the  $i$ th population density and the value of the  $i$ th population density.

The probability of impact at a given location is driven by the:

- location, speed, bearing (and many other characteristics) of the aircraft when it has a loss of control of the operation event.
- the type of failure mode that causes the loss of control of the operation event.
- the external environment (wind at altitude(s), density of air etc.)
- level of shelter at each location

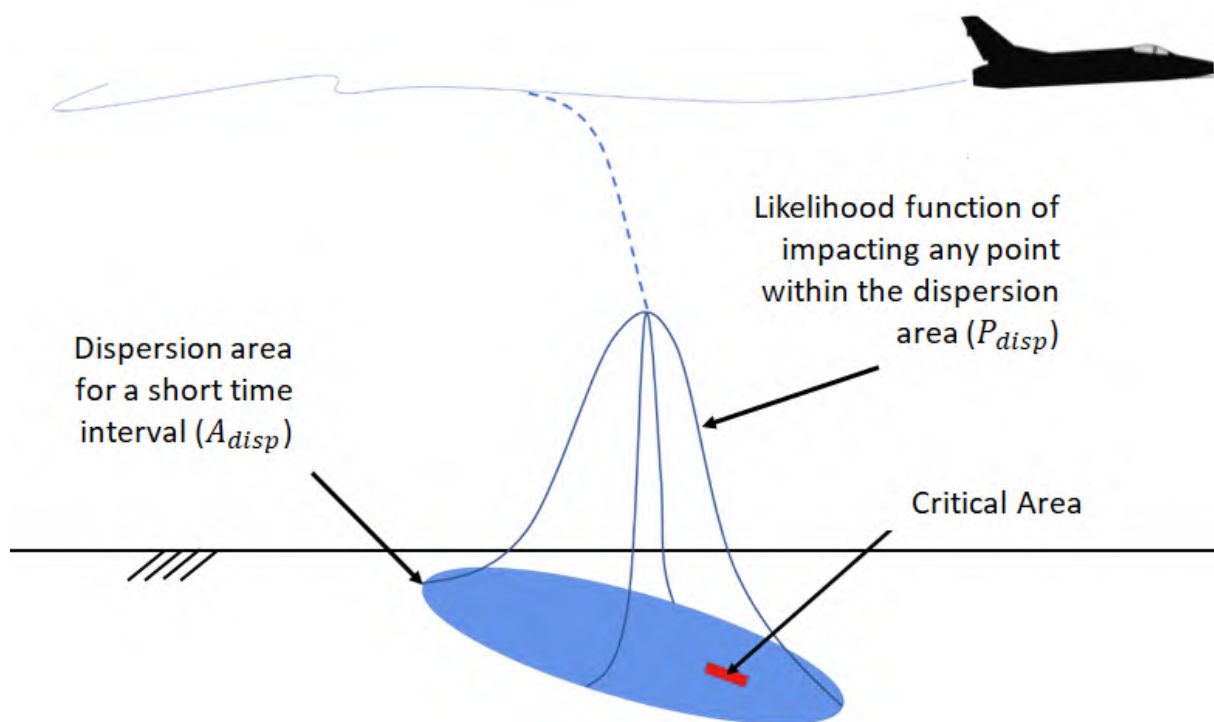


Figure 19: Dispersion Area Diagram

The inherent variance across all these parameters leads to uncertainty of the exact position the aircraft may end up at, given it has a loss of control of the operation event at some point. We

represent this uncertainty using the dispersion area. We define the dispersion area as an area on the surface of the Earth that describes the likelihood of the UA critical area intersecting with a specific location on the ground, given that an aircraft has an event that leads to it impacting the ground at a given point in flight. We can visualise this in Figure 19.

It needs to be noted that in reality the dispersion area is not a constant shape. It changes depending on all the variables mentioned above. For the purposes of this analysis, we will assume the dispersion area is constant for any loss of control of the operation event, centred on the location of the event.

Additionally, the true population density also changes within this dispersion area. To truly calculate the expected casualty at a point in the operation, we need to modify equation 16 as follows:

$$E_C(a, b) = \lambda_{GI}(t) \times F_{exp} \times A_C \times P(Fatality|impact) \iint_{A_{disp}} d_{pop}(x, y) \times P_{impact}(x - a, y - b) dx dy$$

The variables under the integral effectively describe the "weighted population density", a value that represents an equivalent uniform population density at risk by the operation at that point.

$$E[D_{pop,weighted}](a, b) = \iint_{A_{disp}} d_{pop}(x, y) \times P_{impact}(x - a, y - b) dx dy$$

If a population density is less likely to be impacted, its effect on the overall expected casualty is weighted less than one is more likely to be hit.

As an example we create a contrived, simplistic case. Let's say that a single dispersion area exists on a 4 by 4 grid, with probability density function and population density as within the red dotted line in Figure 20:

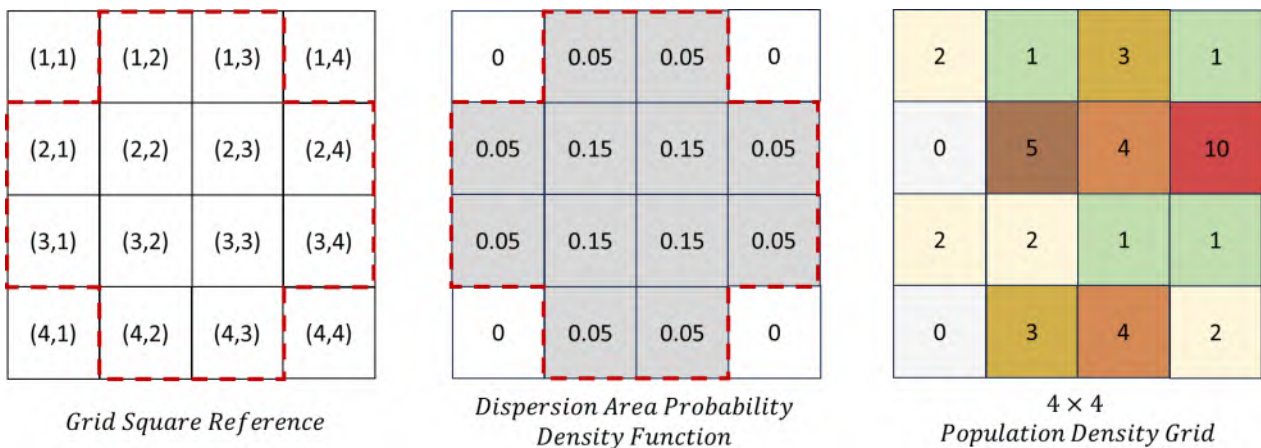


Figure 20: Simple population grid sizing example

Assuming that the population density grid is a truly accurate measurement, we can calculate the weighted average population density using the following discrete version of the equation 3.9:

$$E_C = \lambda_{GI} \times A_C \times F_{exp} \times P(fatality|impact) \sum_{\forall i \in A_{Disp}} P_{impact}(i) \times D_{pop}(i) \quad (17)$$

For the contrived example, the weighted population density is **3 people per unit squared**.

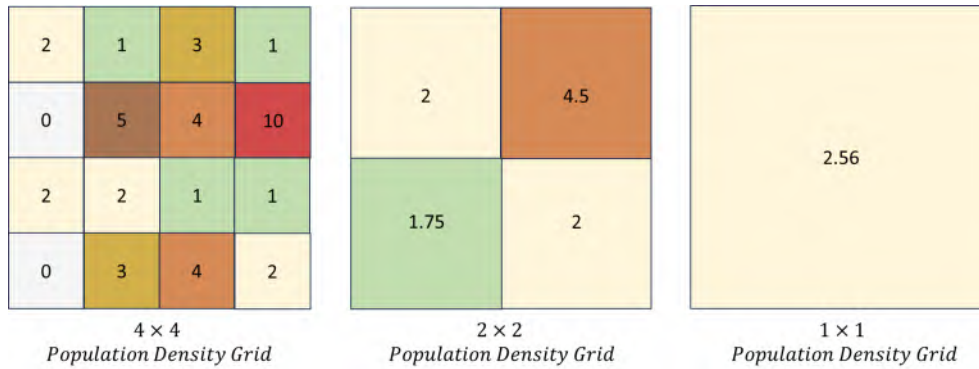


Figure 21: Increasing grid size effect on the maximum population density

$$E[D_{pop,weighted}] = 0.05 \times 1 + 0.05 \times 3 + 0.05 \times 0 + 0.15 \times 5 + 0.15 \times 4 + 0.05 \times 10 + 0.05 \times 2 + 0.15 \times 2 + 0.15 \times 1 + 0.05 \times 1 + 0.05 \times 3 + 0.05 \times 4 \quad (18)$$

$$E[D_{pop,weighted}] = 3$$

The way the SORA iGRC is calculated is by using the "maximum" iGRC in the operational volume (as discussed in Section 3.3.3. If the entire operational volume is a single population density (and hence **any** dispersion area is also in a single population density, then the weighted average is **just** the population density).

In our example, we can now contrast the "maximum" iGRC in the dispersion area, given the 4 by 4 population density grid ( $10ppl/unit^2$ ), and the "true" weighted population density ( $3ppl/unit^2$ ), which better reflects the true number of people at risk. This is over three times as high as the value should be.

We can see how this contrast changes as the grid square size increases. In Figure 21, a two more grid square sizes are shown. One that is half the size of the dispersion diameter (i.e. 4 grid squares in a  $2 \times 2$  arrangement) and one that is the same size as the dispersion diameter (i.e. 1 grid square).

In the  $2 \times 2$  grid example, the maximum population density is 4.5, or 150% larger than the true weighted population density. When the grid square is slightly larger than the dispersion area, the maximum population density is 2.56, which is 15% lower than the true risk value. This is because the dispersion area is actually smaller than the grid square in this particular example.

There are a few caveats to note in this analysis:

- the heterogeneity of the underlying population data has a significant effect on the amount of variation between the true expected casualty value, and the maximum iGRC value. In the two most severe cases, a completely uniform population density in the operational volume would have no change between the iGRC used in Step #2 and the true iGRC based on the weighted average population density. On the other hand, if the population density is all consolidated at a single point, the max population density is infinite, and the true weighted population will be a much smaller, finite value.
- the probability density function of the dispersion area (in terms of both shape and distribution of probability) can also have a large effect on the outcome of the weighted average. In our example we have used a completely contrived example.
- the position of each grid cell has an effect on the population density in each cell. This is the MAUP characteristic, however, this exists regardless of the cell resolution.

As the population density grid size decreases in size relative to the dispersion area, the maximum population density cell within the dispersion area will always be at best equal to the weighted population density (if homogeneous). However, it is expected that most likely will be significantly higher than that, which reflects the true risk.

The converse is also true, as the population grid size increases, the maximum population density cell will be at best equal to, but more likely be significantly less than the weighted population density (unless there are some very unusual population density functions, which can result in a higher population density estimate).

The result of this phenomenon is that without a true knowledge of the underlying homogeneity of the data within any population density map, in order to be accurate to the true risk of an operation, the grid size should be equivalent in size to the dispersion area (this is the same result as the guidance set out in the Flight Safety Analysis Handbook [5]):

$$A_{grid} \approx A_{disp} \quad (19)$$

Another consideration is the shape of the smallest grid unit employed. Consistency in grid cell shape is not necessarily required; however, for some countries, irregularities in the size and shape differentials between the original collection unit and subsequent public reporting unit may be an indicator that the map creation process may be more heavily influenced by economic or political requirements, such as gerrymandering. This rest of this analysis will assume a square grid is employed. Any unique grid shapes would require a more complicated analysis of the appropriate grid sizing. We can then write:

$$A_{grid} = x_{grid} \times y_{grid} = l_{grid}^2 \quad (20)$$

### 3.9.1 Map resolution as a function of intended operating altitude

An often repeated query is the relationship between the operating altitude (AGL) of an operation and the required resolution of the population density map. In essence, the higher the operating altitude, the larger the dispersion area and consequently the lower the resolution of the map required. This section derives some acceptable criteria for grid size as a function of altitude.

We start by generating a series of assumptions about the dispersion area that should almost always give a relatively sized (if not slightly undersized) grid resolution as a function of altitude. We will assume the following:

- An aircraft's dispersion area can be represented as a circle, the radius of which is proportional to the altitude, using a simple trigonometric calculation.
- The probability density function within the aircraft's dispersion area can be accurately represented by a uniform distribution within the dispersion area.
- Any underlying population density grid will use a square-based grid with side lengths  $l_{grid}$  (i.e.,  $x_{grid} = y_{grid} = l_{grid}$ ).
- In order to ensure accurate sampling, the maximum length size of a grid square must be  $\frac{1}{2}$  the radius of the dispersion area circle.

Fitting a square to a circle is somewhat difficult, we achieve this by ensuring the sizing is between a square that fully encapsulates a circle, and one that is full encapsulated by that circle. These two configurations are shown in Figure 22:

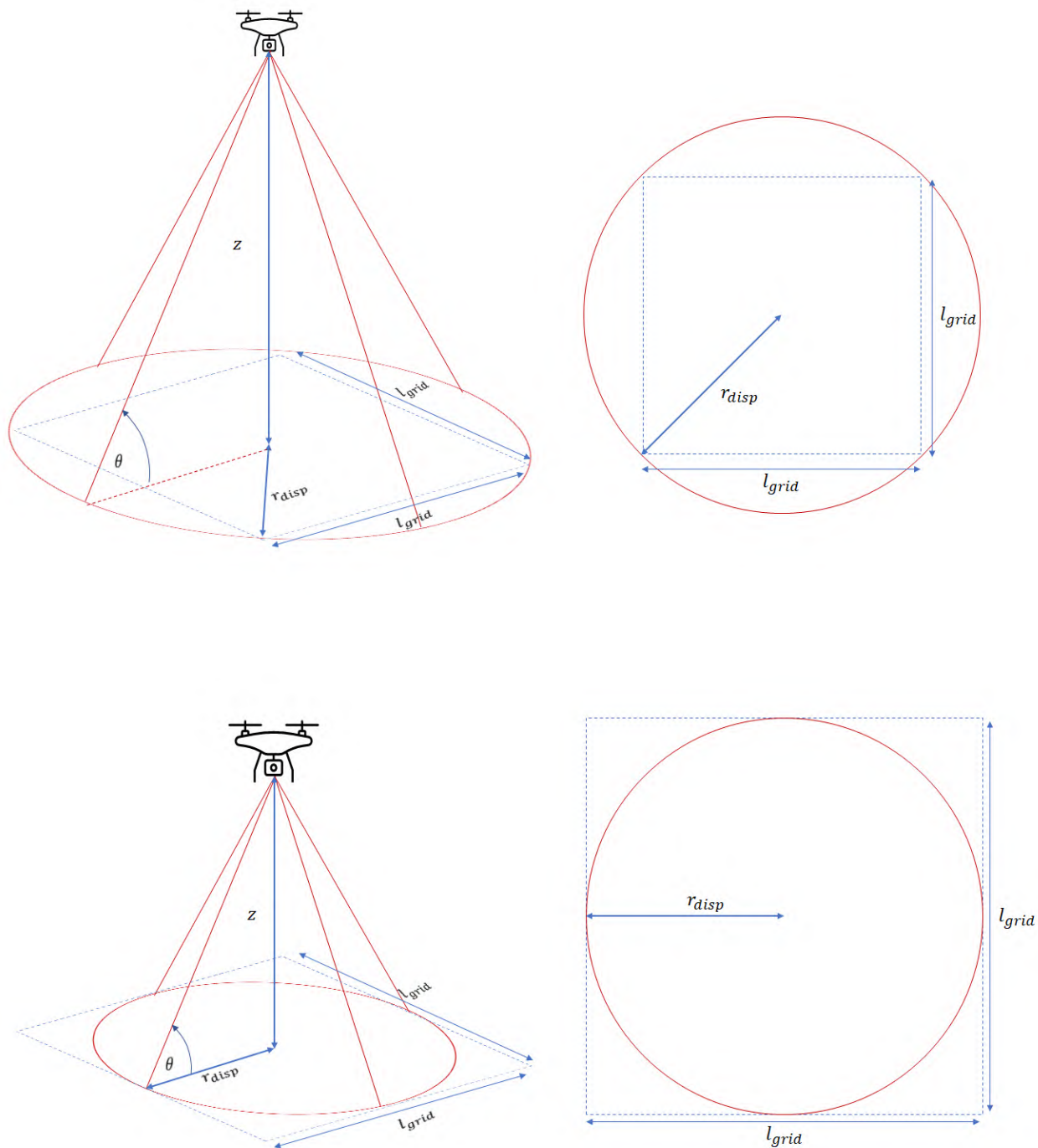


Figure 22: Grid Sizing

where:

- $z$  is the altitude of the operation under normal operating conditions
- $r_{disp}$  is the radius of the dispersion area
- $\theta$  is the angle of inclination, measured from the ground up to the aircraft. This angle is the equivalent of the angle of depression measured from the aircraft.
- $l_{grid}$  is the maximum grid cell height and width (assuming a square grid cell)

The angle of inclination is a complex value to ascertain in general, as it requires knowledge of the

types of failure modes, their prevalence, and the combination of the two to derive an expected angle of inclination.

For the purposes of the dispersion area, we can refer to other angles SORA has used; in the definition of the ground risk buffer, and in the definition of the angle of glide inclination. In the first case, the angle will be much shallower than the 45 degree angle used in a Low Robustness (1:1) ground risk buffer. This is because the 1:1 buffer assumes the operator is trying to end the flight quickly, causing the aircraft to impact at a relatively high angle, whereas the dispersion area should include all kinds of impacts, which will include shallow angle impacts as well as high angle impacts.

Conversely, the critical area model uses a 10 degree impact angle, which assumes a particular, glide in impact angle. This is also only a specific impact case and would not be appropriate to use for the overall dispersion area, which should include the other likely failure modes.

Given these two limits, it is assumed that a 30 degree angle of impact will best approximate the angle of inclination associated with the dispersion area.

To meet our stated goals, the value of  $l_{grid}$  at a given altitude should be between

$$\frac{\sqrt{2}z}{\tan \theta} \leq l_{grid} \leq \frac{2z}{\tan \theta} \quad (21)$$

We can tabularise common altitudes for flying to define some form of acceptable grid sizing. Because of the variation in altitudes between each band, we use the minimum grid size value from the lower band, and the maximum from the higher band, to try and intuit a suggested optimal grid sizing:

Table 11: Suggested Optimal Grid Size

Max. $z$ (ft)	Max. $z$ (m)	$l_{grid,min}(\theta = 30^\circ)$	$l_{grid,max}(\theta = 30^\circ)$	Suggested Optimal Size (m×m)
500	152.4	Critical Area	527.9	$\geq 200 \times 200^*$
1000	304.8	373.3	1056	$\geq 500 \times 500$
2500	914.4	746.6	2640	$\geq 1000 \times 1000$
5000	1524	1867	5279	$\geq 2000 \times 2000$
10000	3048	3733	10559	$\geq 4000 \times 4000$
20000	6096	7466	21117	$\geq 5000 \times 5000$
60000	18288	14392	63351	$\geq 10000 \times 10000^{**}$

\*For operations below 200ft AGL, the recommended grid size tends towards the critical area dimensions. The QM group rationalised that for the most part, map resolutions better than  $200m \times 200m$  are likely to be scarce, so we have limited our recommendation to this value.

\*\*10km by 10km is considered the upper limit to ensure that the heterogeneity of the dataset is not corrupted by extremely large grid squares, and is left as the maximum value for grid resolution.

### 3.10 Hybrid Mapping products created by the Applicant

As indicated earlier, mapping products with 1km resolution may be inadequate for many low-level operations because the assumption that the population is homogeneous is invalid. This means applicants are likely to present with their own population density data sources, perhaps a combination of highly reputable data sources like those detailed in Table 9, or one produced nationally, supplemented with higher resolution satellite imagery or other ancillary data, with the intent to lower the population density or demonstrate that the area is sheltered. For these circumstances, the following should be considered:

- To avoid the re-introduction of MAUP-like artifacts, the grid squares superimposed on the combined product should not differ from the original population source.
- The ratio of people indoors compared to outdoors should pay attention to proximate areas, which might alter that ratio. For example, seaside locations or those areas with parks may have more people outside.
- The date of collection for the ancillary data will be important.
- The primary mapping source used by the applicant should be the one with the highest resolution available and a level of acceptability to the authority because of its quality.
- For ancillary data focused on providing greater temporal accuracy, authorities will need to consider the following:
  - How much of the market share the telecommunication company has, including the demographic breakdown, such that any conclusions drawn on daily or hourly movement are representative of the real population.
  - Whether privacy provisions have been appropriate in the collection and commercial use of this data.

## 4 Mitigations

### 4.1 Overview of Available Mitigations

As detailed in Section 1, the basis for the intrinsic ground risk process is Equation 3, with the following conservative assumptions made:

- Contact between the unmanned aircraft at any point and a person is fatal (i.e.  $P(\text{fatality}|\text{collision, GI}) = 1$ )).
- The critical area is based on generic, conservative assumptions related to an inert aircraft gliding and sliding with no credit given to the design of the aircraft to reduce the impact speed or energy or increase the impact angle.
- The percentage of exposed people is 100% (i.e.  $F_{\text{exp}} = 1$ ).

The mitigation process in Step #3 of the SORA allows an applicant to demonstrate why these assumptions are not applicable to their aircraft or operation. The iGRC can be reduced using one of four mitigation types, creating a final GRC Value. These mitigations are:

- M1(A) - Sheltering: This mitigation aims to reduce the number of people at risk because they are protected from harm by some form of shelter.
- M1(B) - Operational restrictions: This mitigation applies operational restrictions (by time and location) that reduces the number of people at risk compared to the iGRC score found in Step #2.
- M1(C) - Ground Observation - Reducing the risk of an impact with a person tactically by observing the ground area at risk and adapting the flight path based on people observed.
- M2: Reducing the effect of ground impact such that it can be shown to be less lethal and/or reduce the impact area.

Each integer reduction in the GRC represents approximately an order of magnitude change in casualty expectation. For example, a decrease from a GRC score of 5 to 4 corresponds to a decrease in expected casualties on the ground by a factor of 10, or an order of magnitude. The odds of single mitigation resulting in neat factors of 10 reductions in risk is likely to be rare. Noting that iGRC calculations have some embedded conservative assumptions, and the importance of incentivising positive safety behaviour/features, the competent authority may consider:

- If the application cannot demonstrate the full factor of 10, credit may be considered when the applicant is close. For example, a competent authority may recognise a minus 2 reduction (2 orders of magnitude) if an applicant can only show 95% rather than 99%.
- If the applicant has several elements that collectively contribute to demonstrating the order of magnitude reduction. In considering this, its important that the competent authority understand the potential risk accepted by treating a partial order of magnitude as a full order of magnitude change in risk. It is always advisable to assess a risk assessment holistically to realize that the requirements are in balance as a total. This way partial mitigation's can be assessed against the necessity of achieving a full order of magnitude or if less is enough to achieve TLOS.

Mitigations have requirements for integrity and assurance (see Annex B) which are jointly intended to achieve the required robustness to ensure that the mitigations can deliver the claimed reduction

in risk. Integrity is the intended effectiveness of a mitigation and should provide matching strength to the different levels from Low to High and the GRC reduction value associated with it. It is understood that claiming the higher integrity level is lucrative to applicants, but the higher integrity level must be proven with more/better data and potentially competent third party validation (in high robustness cases) of the effectiveness of the mitigation.

## 4.2 M1(A) - Strategic Mitigations for Ground Risk - Sheltering

M1(A) mitigation is determined and applied before an operation commences and is thus termed a strategic mitigation. The use of M1(A) to reduce the iGRC and fatality rate is best illustrated by reference to Equation (3), which is restated for convenience:

$$\lambda_{\text{fatality}} = \lambda_{\text{GI}} \cdot D_{\text{pop}} \cdot \underbrace{F_{\text{exp}}}_{\text{Mitigation 1(A) reduces this term}} \cdot A_C \cdot P(\text{fatality}|\text{collision, GI}) . \quad (22)$$

A reduction in iGRC can be achieved via sheltering because it acts to reduce the exposure variable ( $F_{exp}$ ) in 22. If a person is considered sheltered, then they are effectively removed from the population density from the perspective of the descending aircraft under the SORA process, and thus cannot be impacted. Further guidance on how sheltering and obstacles applied is provided in Appendix A.

If the applicant claims a reduction, due to a sheltered operational environment, the applicant must:

- use a drone that is expected to be stopped by structures sufficiently to protect people underneath or within,
- fly in an area where it is reasonable to consider that most of the uninvolved participants will be located under a structure.
- not fly over assemblies of people.

Its expected that claiming this mitigation should include a general assessment of the sheltering effectiveness. However, the extent of this assessment should note that UA's with MTOM below 25 kg are not expected to sufficiently compromise even light construction materials, to the extent that people inside the structure are likely to be harmed.

Larger aircraft may penetrate shelters only partially (e.g. only a part of the nose), but still be evaluated to be stopped by the structure to provide sufficient protection from shelter. The second point can be shown via a number of studies which supplement the basic census population data, for example time-exposure studies show that the vast majority of time people are indoors or inside vehicles. As a general rule, sheltering can be expected to deliver a reduction of minus 1 to the GRC, by reducing the people exposed to 1/10 of the original population value (i.e. a 90% reduction in risk). Further reductions are possible, but require sufficiently strong evidence supporting the claim that approximately 99 percent of the local population are adequately sheltered.

Sheltering is an effect that is applied to a bulk population in an area. To that end, in general an operation that occurs at any random time over a population can expect that on average the sheltering factor will apply. However, if an operation is conducted over an open air assembly, this averaging effect no longer holds and sheltering does not provide any substantial reduction in risk.

Note: it is assumed that mapping products used in Step #2 **do not** include any sheltering effects. If they do, then this mitigation should be considered very carefully to prevent double counting of the sheltering factor.

### 4.3 M1(B) - Strategic Mitigations for Ground Risk - Operational Restriction

Mitigation M1(B) involves planning a flight for a location at a particular time to avoid higher population densities, and is hence considered a strategic mitigation. Equation 24 shows the variable this mitigation affects:

$$\lambda_{\text{fatality}} = \lambda_{\text{GI}} \cdot \underbrace{D_{\text{pop}}}_{\text{Mitigation 1(B) reduces this term}} \cdot F_{\text{exp}} \cdot A_C \cdot P(\text{fatality}|\text{collision, GI}) . \quad (23)$$

Mitigation 1(B) reduces this term

Note: Showing a difference in population density with a different static map is not a M1(B) mitigation and should be performed in Step #2, where mapping products are assumed to be static (i.e. maps with average estimate of population distribution during the day with no temporal variations included). These do not capture the changes from movements of people throughout the day or throughout seasonal variation. Use of best available static maps is encouraged in Step #2.

M1(B) mitigations always include a time restriction which reduces the population at risk for the specific area and time.

Acceptable mechanisms for lowering the population ( $D_{\text{pop}}$ ) in the iGRC to obtain an M1(B) reduction include:

- Applicant conducts an appraisals/on-site inspections of the iGRC region and demonstrates that the assessed population is lower than that indicated in available population density maps. This might occur in residential areas during daytime (where the population migrates to work), or industrial areas at night (where the reverse occurs)
- The applicant makes use of temporal density data relevant for the proposed area and restricts time of operation to substantiate a lower density of population at risk. This can incorporate real time or historical data.

The opposite effect can also happen. Population assessments may show the population density exceeds the mapping product used for Step #2 requiring an adjustment in the iGRC to ensure accuracy of risk assessment. Special considerations should be given to areas that will usually attract people, but are not covered by census data mapping products:

- Areas which frequently feature assemblies of people. (known tourist sites, busy open transport hubs, specific city streets during carnivals, etc)
- Areas where known human recreation will occur at times of high use (theme parks, sporting grounds, concert arenas etc.)

Note: this does not mean any of the above mentioned areas cannot be overflowed, but they should be assessed for activity to ensure no assemblies of people are overflowed.

### 4.4 Achievable iGRC Reductions using strategic mitigations

It is important to note that each reduction in risk is equivalent to showing that the number of people at risk has been reduced by approximately an order of magnitude because this is equal to the GRC reduction being claimed. That is, claiming a -1 should reduce the number of people at risk by approximately a factor 10, which is equivalent to a reduction by 90%. Similarly, -2 represents a reduction by approximately a factor 100, which is equivalent to a reduction by 99%.

Annex B outlines expectations for integrity and assurance requirements associated with demonstrating a reduced population density or using shelter.

## 4.5 M1(C)- Tactical Mitigations - ground observation

It is recognized that if the operator has the ability to observe the immediate operating area of the aircraft throughout the flight, the operator can take advantage of this to potentially take actions to alter the aircraft trajectory to reduce the number of people exposed to the risk.

There are many ways this can be implemented, and with success reliant on the skill of the pilot or capabilities of the aircraft system. This makes weighting the value of each approach difficult to quantify. Accordingly, it is determined that reduction in risk due to ground observation should be limited to a maximum of -1 due to the low assurance level. Below are inherent aspects of ground observation which the operator may implement to satisfy the authority:

1. The operator has clear sight of the flight area where the aircraft might crash in the event of a failure.
2. The operator has the ability to identify less populated areas and can command the aircraft to fly over these areas.

## 4.6 M2 - Effects of ground impact are reduced

$$\lambda_{\text{fatality}} = \lambda_{\text{GI}} \cdot D_{\text{pop}} \cdot F_{\text{exp}} \cdot \underbrace{A_C \cdot P(\text{fatality}|\text{collision, GI})}_{\text{Mitigation 2 reduces one (or both) of these terms}} \cdot \quad (24)$$

M2 is meant to be a general category where an applicant can show a method of reducing the effects of an impact by reducing the critical impact area and/or limiting energy transfer dynamics reducing the lethality of an impact with a person.

Any M2 mitigation should not induce potential new failures to the aircraft which would affect overall system safety adversely. An M2 safety case utilising a mechanism with potential failures should include an appropriate demonstration that the overall safety has not deteriorated as a consequence of these potential new failures. For example, whilst a parachute certainly reduces impact energy, if it activates inadvertently ten times more often than the aircraft would fail, it may actually increase the overall risk of the operation. Additionally, if a parachute were to deploy in a windy environment and cannot be strategically and/or mechanically contained within a predetermined flight path, the ground risk buffer may not have been adequately defined to cater for the performance of aircraft during a parachute deployment.

If the applicant wants to use a velocity lower than the maximum cruise speed as an M2 mitigation, they need to demonstrate that the failure modes associated with exceeding the proposed new speed are mitigated appropriately.

### 4.6.1 Criterion 1 - Technical Design

There should be substantiation that the design of the mitigation mechanism(s) to reduce the critical area and/or reduce the impact lethality with the iGRC reduction sought. Additional to this, the mechanism will need to be robustly designed to function as intended during expected credible failure modes and environmental conditions when the mitigation is employed.

For both the medium and high level of robustness, the operator may combine various mitigation means to achieve the factor 10 or factor 100 in the fatality rate. For instance, to achieve a factor 10 reduction, a factor 5 could be achieved by a parachute that reduces the critical area enough to justify the reduction by a factor of 5 (i.e reduced to 20% of the critical area). Additionally, lets say

that the lethality of the aircraft is reduced by a factor of 2 (i.e. 50%) when the aircraft is descending in a parachute. These in combination achieve the 90% reduction in risk (50% of 20% is 10%, or 90% reduced).

If applicants wants to claim the high level of integrity, the level of assurance can support 2 or 3 orders of magnitude of reduction of risk. To achieve a -2 to the iGRC the integrity of the mitigation must demonstrate a 99% reduction to the combination of critical area and/or lethality. To achieve a -3 to the iGRC, the integrity of the mitigation must demonstrate a 99.9% reduction in the critical area and/or lethality.

Note that any discussion about a reduction in iGRC must consider the expected outcome of the system. This means that the reliability of the mitigation must be considered as part of the calculation for the overall mitigation effectiveness.

The following qualitative requirements should be considered to ensure proper functionality of the mitigation mechanism(s) used to achieve a high robustness:

- If the mitigation is not passive. An automated activation method is required; this does not reduce the fatality rate, but it increases the probability of activation such that the argued reduction is more probable.
- Compliance with industry standard, when applicable.
- Consideration of adverse consequences in case of malfunction of the mitigating mechanism (such as unintended deployment of parachute or unintended ballistic descent). The probability of any such malfunction must be appropriately included in the arguments for how to achieve the iGRC reduction.

If the mitigation is based on a passive setup, such as a fragile design or inherently very slow aircraft (perhaps made of polystyrene and with very large drag), the operator must clearly describe the mechanism by which the aircraft achieves reduction in fatality rate.

If the mitigation is based on a smaller critical area resulting from ballistic descent, the operator must clear argue how this descent condition is achieved (e.g., stopping the motor(s) on a rotorcraft or intentional flat spin inducement of a fixed-wing). If the ballistic descent is either initiated at relatively high altitude or at relatively low velocity, the operator may assume a higher-than-normal impact angle. More detail on this scenario is given in section [A.3.7](#). The Python tool CasEx can also be used for estimating the actual impact angle for a given scenario. In almost all cases, it will be possible to achieve a factor 2 reduction in the critical area. For this reason, it is generally acceptable to assume a factor 2 reduction for a ballistic descent without any additional calculations. Note that a reduction factor of 3 to 6 is achievable under certain conditions.

#### **4.6.2 Criterion 2 - Procedures (if applicable)**

To maximize the chances of proper deployment of the M2 mitigation and for the applicant to get credit, where applicable, they must provide evidence that any installation, operating, and maintenance procedures are done in accordance with manufacturer's instructions.

#### **4.6.3 Criterion 3 - Training (if applicable)**

For the applicant to get credit for M2, where applicable, they must provide evidence that any installation, operating, and maintenance procedures are identified and personnel responsible for these (internal or external) are qualified for the task.

## 4.7 Summary of Mitigation Reductions

Table 12 details the reductions to the iGRC which are available for using M1(A), M1(B) and M2.

Table 12: Mitigation reductions

iGRC Reduction Methods	Low	Medium	High
M1(A)- Sheltering	-1	-2	N/A
M1(B)- Operational Restrictions	N/A	-1	-2
M1(C)- Ground Observation	-1	N/A	N/A
M2 - Effects of ground impact are reduced	N/A	-1	-2

## 4.8 Optional JARUS Model Trade-offs

The quantisation in the iGRC table arbitrarily limits several combinations in wingspan, velocity and population, which means that iGRC scores in Table 2 can be disconnected from the real iGRC that Equation (9) would determine. Some measures have already been incorporated to reduce the iGRC values to more realistic values. This includes acknowledging that 1m platforms have limited kinetic energy and size during slide, and that obstacles in suburban areas can reduce the average critical area.

Applicants are free to apply the basic elements of Equation (9), and the detailed methods for calculation of Critical Area and impact of obstacles in Appendix A and B. However this process does require some skill in math and a good understanding of the concepts described throughout those Appendices. As an intermediate step, some of the properties of JARUS model and the iGRC derivation can be used to make some relatively simple trade-offs that may be of use to some operators. Table 13 gives six trade-offs, which hold for any combination of population density, aircraft size, and maximum speed.

Table 13: Six trade-offs applicable to the iGRC table (Table 2).

Operational reduction	Operational gain
Reduce maximum population density by 50%	T1: Increase maximum velocity by 40% OR T2: Increase maximum size by 100%
Reduce maximum size by 50%	T3: Increase maximum population density by 100% OR T4: Increase maximum velocity by 40%
Reduce maximum velocity by 25%	T5: Increase maximum population density by 70% OR T6: Increase maximum size by 70%

While these trade-offs do not produce exactly the raw iGRC values as the original iGRC table, they come close. The largest differences in raw iGRC are +0.2 and -0.4, where plus means higher iGRC in the trade-off table. As such, these six possible alternatives are almost identical to the original iGRC in terms of fatality rate.

Note also that all six tables and their deviation from the original iGRC table can be produced by running example 4 from the CasEx package.

Table 14: An alternative to the iGRC table generated using trade-off T4 in Table 13. Note that the iGRC values are unchanged, but the characteristic dimension and max speed are changed.

<b>Alternative Intrinsic Ground Class Value</b>						
<b>Max UAS Characteristic Dimension</b>	<b>0.5 m</b>	<b>1.5 m</b>	<b>4 m</b>	<b>10 m</b>	<b>20 m</b>	
	<b>Maximum Speed</b>	<b>35 m/s</b>	<b>49 m/s</b>	<b>105 m/s</b>	<b>168 m/s</b>	<b>280 m/s</b>
<b>Max population density [ppl/km<sup>2</sup>]</b>	<b>Controlled</b>	1	1	2	3	3
	< 5	2	3	4	5	6
	< 50	3	4	5	6	7
	< 500	4	5	6	7	8
	< 5000	5	6	7	8	9
	< 50,000	6	7	8	9	10
	> 50,000	7	8	Not part of SORA		

These trade-offs are used in the following way. For every cell in Table 2, there is a maximum population density, maximum size, and maximum speed. By using either of the trade-offs, the operator is allowed to change these maximum values in the table and thus obtain an alternative iGRC table that might be better suited for the operator. As an example, we can use the T4 trade-off to reduce the maximum size of the aircraft by 50% and increase the maximum velocity by 40%. Table 14 incorporates these principles to capture an alternate regime of population and  $A_C$  bands within an iGRC table.

## 5 Adjacent Areas and Containment

This section has been added to Annex F from the externally consulted explanatory note to the SORA Main Body v2.5. This section is composed of the following sections:

- Section 5.1, which provides a justification for the size of the adjacent area used in the SORA main body, along with the relevant assumptions and simplifications made.
- Section 5.2, which provides the mathematical basis for containment from a ground risk perspective, and identifies the quantitative functional performance for containment systems. The tables generated are used to ensure Step #8 of SORA ensures an acceptable level of safety.
- Section 5.3, which provides an alternate means to determine containment requirements. This model is the one that was provided in the external consultation version of the SORA Main Body v2.5.

### 5.1 Adjacent Area Ground Risk Assumptions

#### 5.1.1 Adjacent Area Ground Risk Assumptions and sizing

The reasonably probable flyaway area for an unmanned aircraft will be different for each aircraft design, so a single easy-to-define size is not expected to accurately model each system. The 3 minutes of cruise speed was selected because this definition would generally fit all the newly proposed iGRC table aircraft categories within the 5 - 35km minimum and maximum definitions while adjusting the size somewhat to reflect the aircraft differences.

Therefore, the definition tries to achieve values that will not underestimate the risk to the adjacent area, but that is still able to reliably detect surrounding areas/airspace with higher population densities or airspace densities (which is not relevant in Annex F but more broadly in SORA). The measurement process is designed not to cause excessive analysis of the surrounding areas. The size definition was therefore derived more from external limitations such as smoothing effects with population density measurement.

#### 5.1.2 Adjacent Area Size Justifications

The following examples show an empirical approach of trying different size adjacent area (ground area) definitions being used in combination with quantitative population density maps. These empirical tests were used to show that there is an upper limit to the size of an adjacent (ground) area after which the measured average population density will always be reduced due to smoothing effects. Also, the examples show how the proposed minimum 1km distance works for the evaluation of gatherings of people.

The definitions and methods are intended to be fairly straightforward while still offering a conservative, but credible approach to estimating risk from surrounding adjacent areas.

#### 5.1.3 Maximum Size of Adjacent Area

Because city sizes do not seem to exceed 35 km in radius practically anywhere in the world, adjacent area definitions larger than 35 km will lead to a reduction in the measured average population density and not increased conservatism as might be the first intuition. The following examples show how

the smoothing effects in practice reduce the measured population density with very large adjacent area definitions

Table 15: Maximum Sizes of Cities

City	Diameter	Radius
Brisbane	32 km	16 km
London	38 km	19 km
Los Angeles	70 km	35 km

In the table below are adjacent area buffer sizes calculated with different time values using the iGRC table speeds for different sizes of UAS. Highlighted in green are distances that are starting to exceed the size of even the largest cities on earth and therefore will certainly be counterproductive definitions. If the area measured is larger than a city then the measured population density will start to always lower and not be useful in distinguishing between high and low population density areas. Potentially smaller time definitions could be used, but at least the maximum time limit for using this sizing method is found.

Table 16: Adjacent Area Buffer Sizes for Different UAS Class Ranges

UAS Class Range	1m (25/m/s)	3m (35/m/s)	8m (75/m/s)	20m(120/m/s)	40m(25/m/s)
1 min	1.5 km	2.1 km	4.5 km	7.2 km	12 km
2.5 min	3.75 km	5.25 km	11.25 km	18 km	30 km
3 min	4.5 km	6.3 km	13.5 km	21.6 km	36 km
5 min	7.5 km	10.5 km	22.5 km	36 km	60 km
10 min	15 km	21 km	45 km	72 km	120 km

The worst possible areas from a containment perspective are donut or U-shaped cities with no population in the middle where an operation takes place. The farm on the outskirts of Lisbon is exactly this type of worst-case location. It can be seen that with a 2.5 minutes of cruise speed definition the measured average population density keeps rising even until 30 km distance, but with the 5 min definition the density starts immediately to lower after this distance is reached showing that the 2.5 min cruise definition was actually more conservative than a longer time buffer.

**Example #1:**

The adjacent areas of 22.5km and 30km show in this example the largest average population density measurements. However, these distances would realistically be only achievable with larger UAS and so the sizing method excludes smaller UAS from these distances and densities.

With the longer time definition, the largest average population density measured is for the 22.5 km size adjacent area. Any larger definitions start to reduce the population density measurement and stop being a conservative definition to distinguish areas of more risk around an operation.

**Example #2:** the next example considers the hypothetical extreme where a UAS operation takes place in the English Channel, so that we could potentially find a case where average population density increases with very large adjacent area definitions. The largest definitions even extend to the area of multiple countries, which already points to one major practical problem of trying to use very large adjacent area definitions.

With this extreme example it can be seen that the very large adjacent area definitions do produce the largest average population density number. However, this largest measured population density is only 268.7 ppl/km<sup>2</sup>, which does not trigger any major concerns over UAS containment.

**Example #3:** To see if very large adjacent area definitions behave the same way as in Example #2 also when located on land the case studying an operation in a forest south of Paris is assessed.



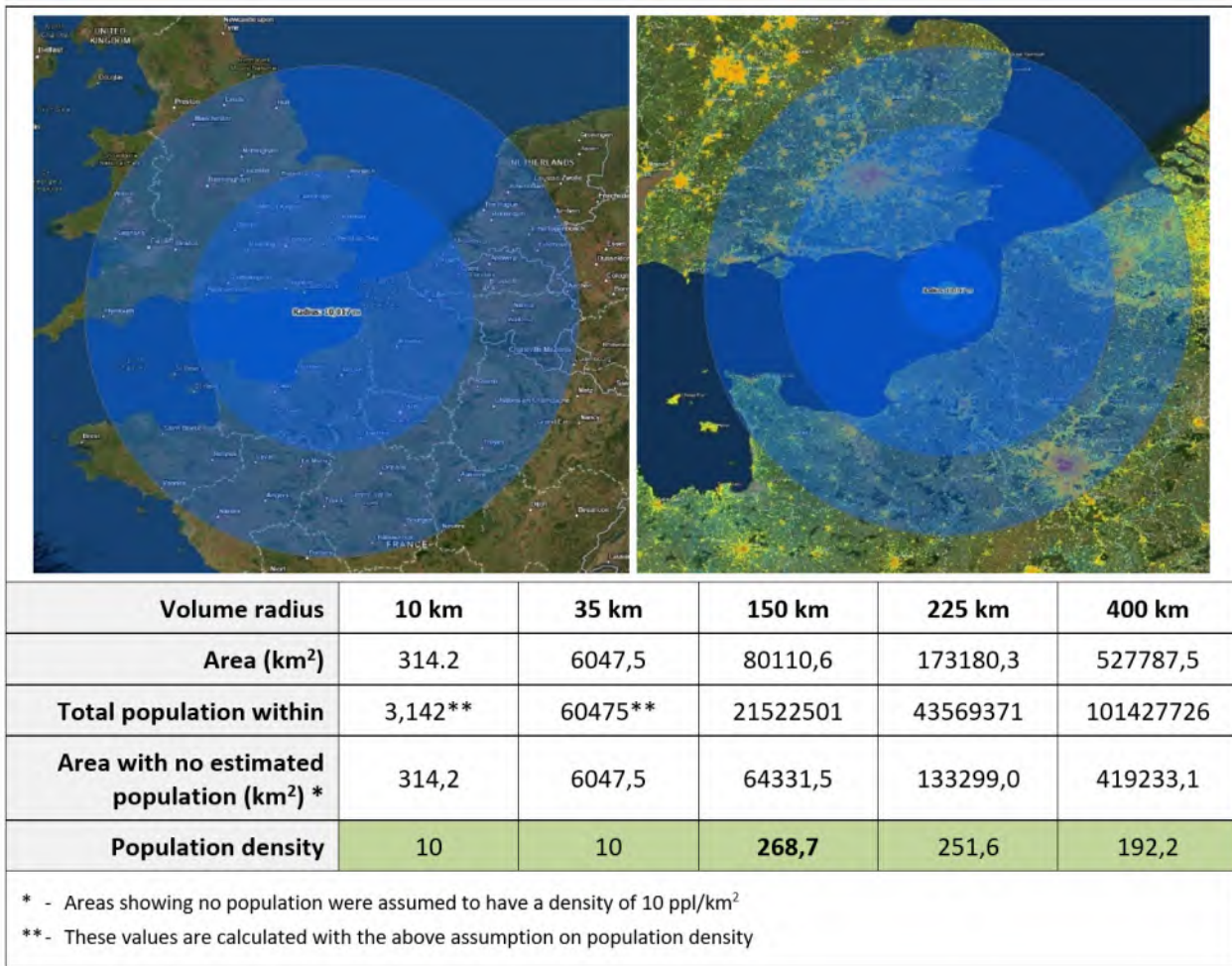
Table 18: Lisbon Nearby Farm (300 seconds at Cruise Speed)



UAS class	1 m (25 m/s)	3 m (35 m/s)	8 m (75 m/s)	20 m (150 m/s)	40 m (200 m/s)
Volume radius	7,5 km	10,5 km	22,5 km	45 km	60 km
<b>Lisbon Farm 5 min definition</b>					
10	167,1	153,3	600,7	2874,7	3621,9
100	9,24	7,28	94,7	149,2	413,9
1500	0,42	5,82	298,6	1250,8	854,5
15K	0	3,27	250,1	496,6	57,7
100K	0	0	0	0	0
Average POP_D sector	18,2	353,9	3388,0	1963,6	449,6
Average POP_D tot ADJ	18,2	182,7	<b>2689,9</b>	2145,2	1403,4

Here the largest measured population density is found with a 150 km size adjacent area definition, but the measured density is again very small, only 169 ppl/km<sup>2</sup>. Therefore, it can be fairly definitely said that a very large adjacent area definition is not useful for detecting increased risk areas close to an operation.

Table 19: Operation in English Channel (Operational Volume and GRB of 10km + Adjacent Area of 35km, 150km, 225km, 400km)



**Example #4:** To see if the placement of the operation closer to a city makes any difference a park in the centre of Paris is studied. Here the measured average population densities are very high and the largest density is found with a 3.6 km adjacent area definition. The second largest population density is found with a 12 km size definition.

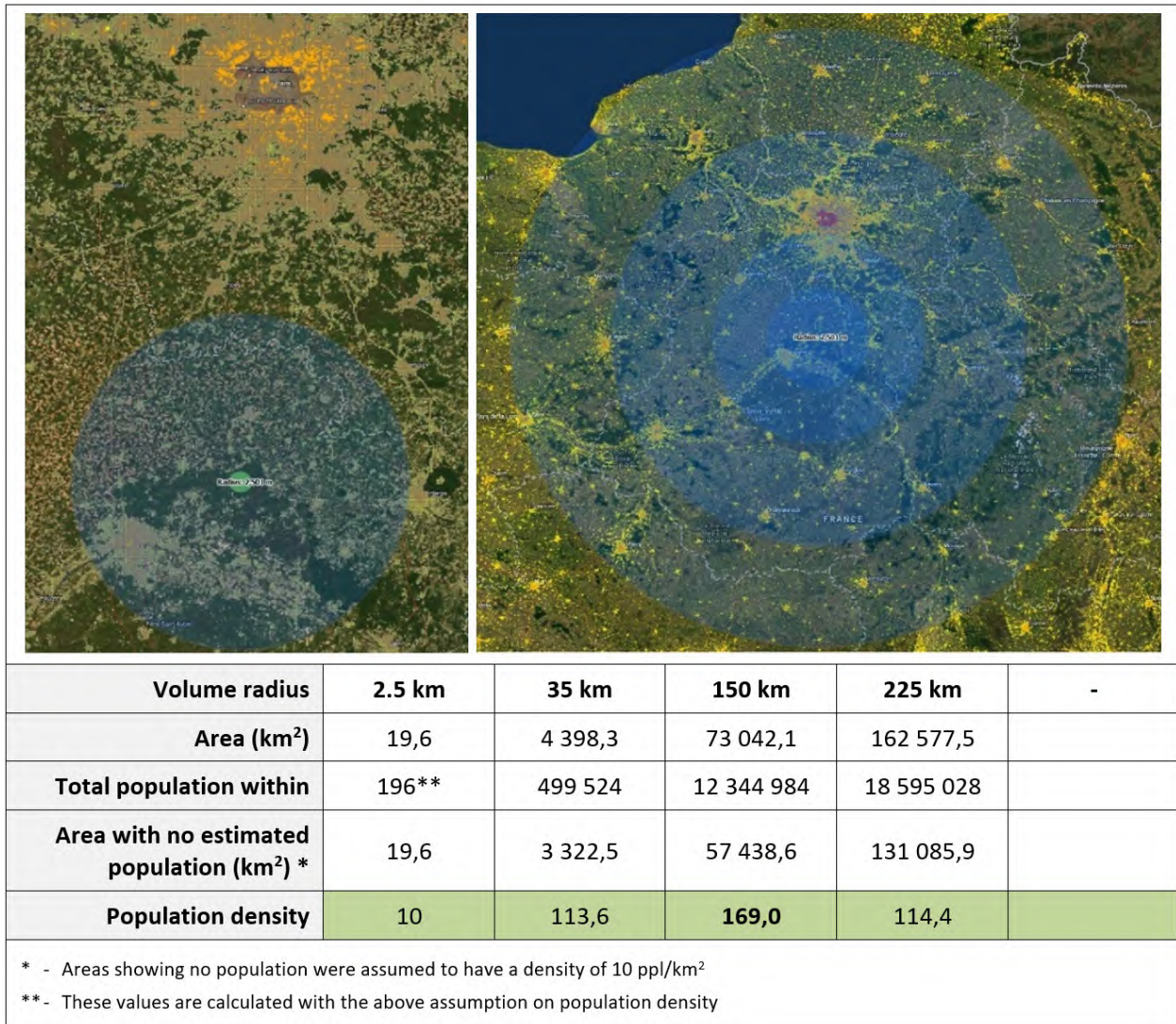
**Example #5:** To see if the size of a city makes a big difference to this trend a smaller city in France, Tours was assessed. Here also the 3.6 km adjacent area definition measured the largest average population density. In Tours the measured population densities were much smaller than in Paris, but had a similar pattern as in Paris when it comes to the used size definition.

#### 5.1.4 Evaluating Gathering of People in the Adjacent Areas

The purpose of the proposed 1 km distance from the outer edge of the operational volume is to assess if gatherings of people are adjacent. This means that any gatherings further than 1km distance would not be considered by the Competent Authority as adjacent to the operation and can be ignored in the analysis made by the UAS operator. Furthermore, the maximum dimensions of gatherings of people are rarely multiple kilometers in size, so as to not present a probable target further away than 1km distance.

The following worst-case ground risk containment scenarios show examples of using a proposed 1km distance to evaluate quantitatively surrounding gatherings of people and populated areas.

Table 20: Operation in South of Paris Forest (Operational Volume and GRB of 2.5km + Adjacent Area of 35km, 150km, 225km)

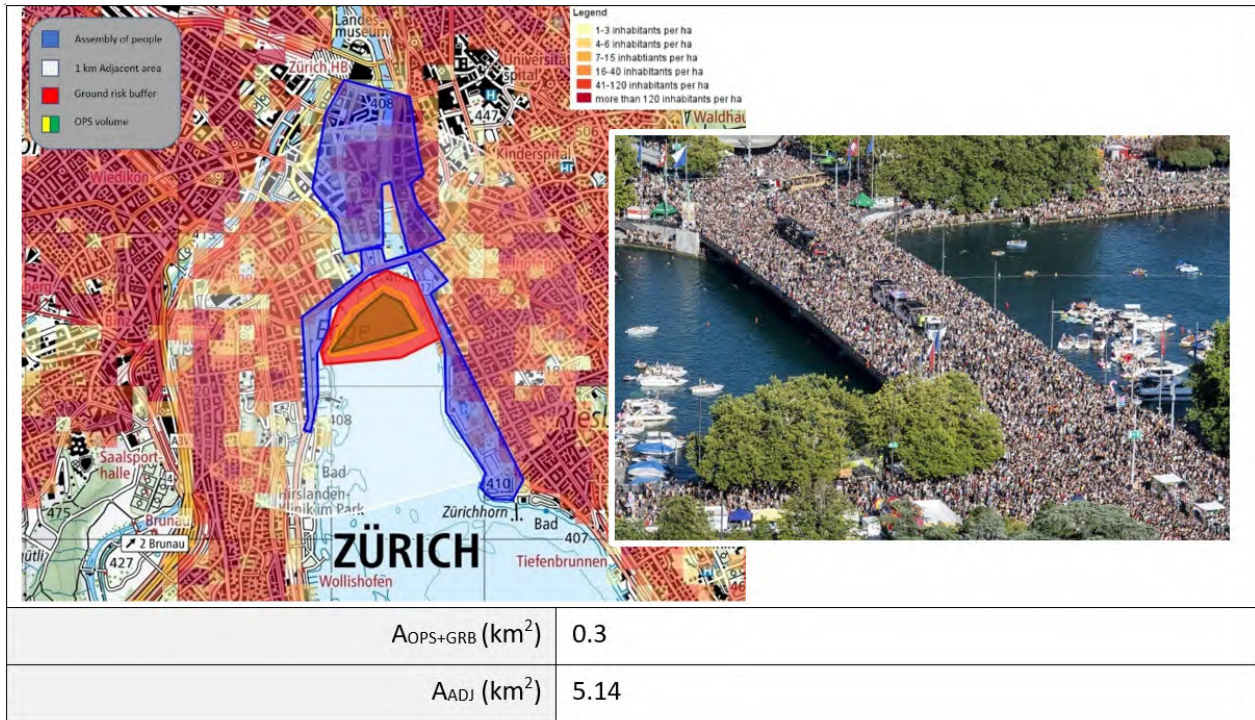


**Example #1:** The street parade is an annual event drawing people from multiple countries and causing major road closures and changes to public transport routes. This type of an event is very easy to predict and detect by a UAS operator.

The Street parade example shows that there is a minimum increase in population density of factor 10 or a factor 100 measured within 1km of the operational volume from the average base population density (#3). The difference could also be much more if the operational area is a controlled ground area. The triggers in this example are the gatherings of people in the normal shopping centre area and the larger gathering of people in the street parade. So, in this case the more limiting gathering of people around 400,000 people would require the UAS operator to choose >50,000 ppl/km<sup>2</sup> as the average population density used for picking the adjacent area GRC.

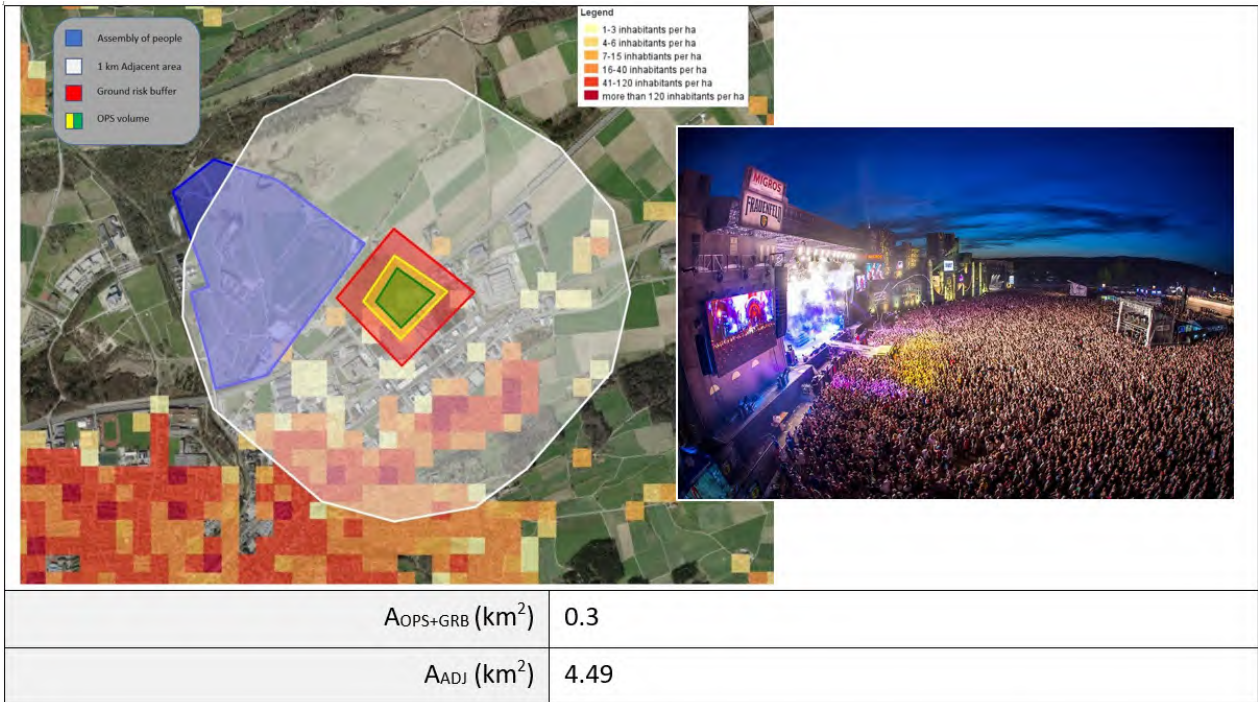
**Example #2:** The OpenAir Frauenfeld example also shows that there is a minimum increase in population density of factor 10 or a factor 100 measured within 1km of the operational volume from the average base population density. The difference could also be much more if the operational area is a controlled ground area.

The trigger in this example is the gatherings of people in the festival. The competent authority has to estimate in this case if the 150,000 people is closer to 400,000 than 40,000 and which corresponding



#	Description	Area (km <sup>2</sup> )	Density (ppl/km <sup>2</sup> )	Population (people)	% of A <sub>ADJ</sub> 1km
1	Assembly shopping centre (blue area in North)	0.6	50 000	30 000	11.67 %
2	Assembly street parade (blue area near shore)	0.4	500 000	200 000	7.78 %
3	Average base population in 1km A <sub>ADJ</sub>	5.14	4 936	25 370	
4	All together	5.14	49 683	255 370	

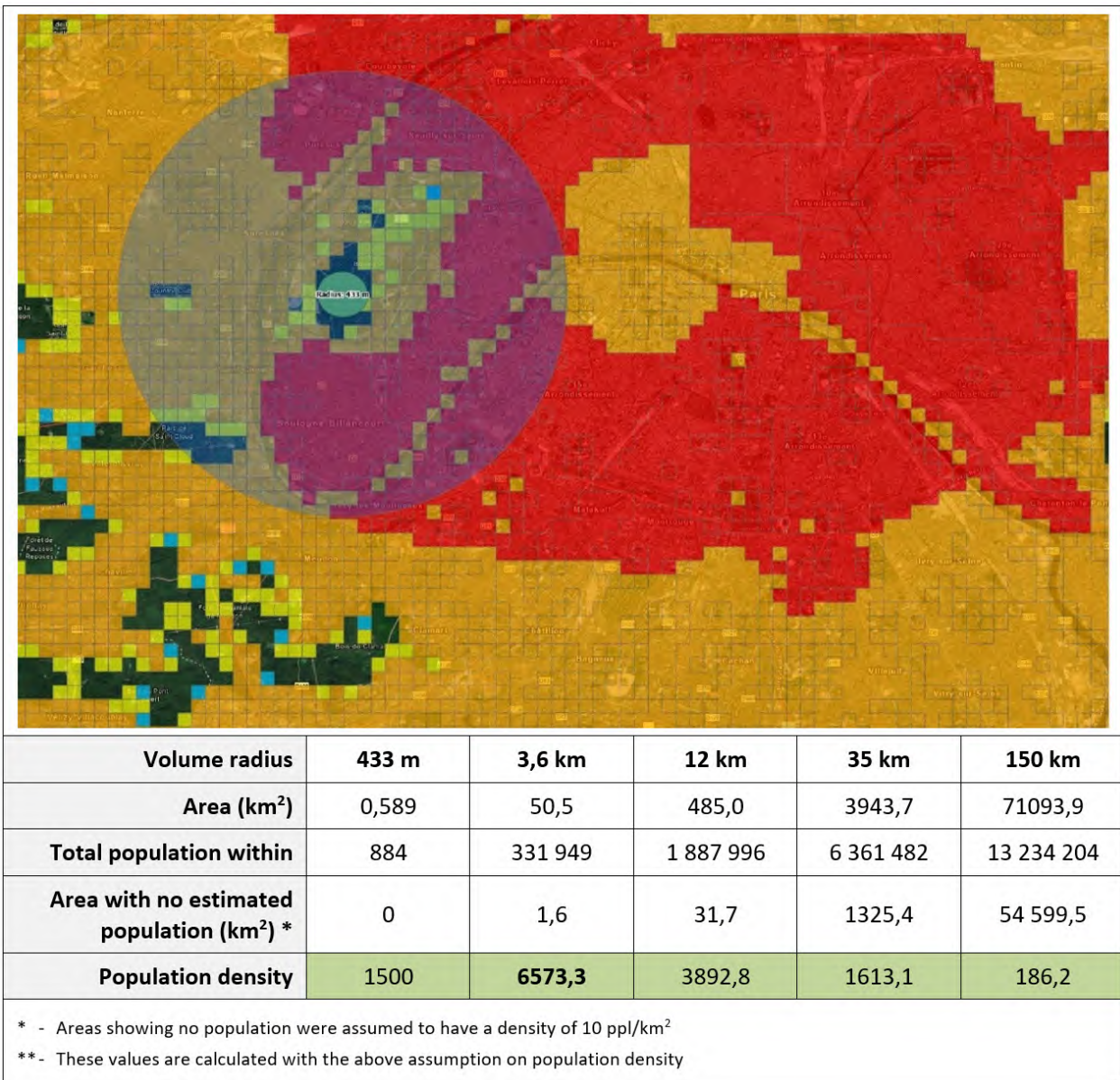
Figure 23: Street Parade in Zurich with around 200,000 people



#	Description	Area (km <sup>2</sup> )	Density (ppl/km <sup>2</sup> )	Population (people)	% of $A_{ADJ}$ 1km
1	Assembly at "Openair Frauenfeld" (Blue area)	0.81	185 185	150 000	18.04%
2	Average base population in 1km $A_{ADJ}$	4.49	1 073	4 820	
3	All together	4.49	34 481	154 820	

Figure 24: Open Air Event in Frauenfeld with around 150,000 people

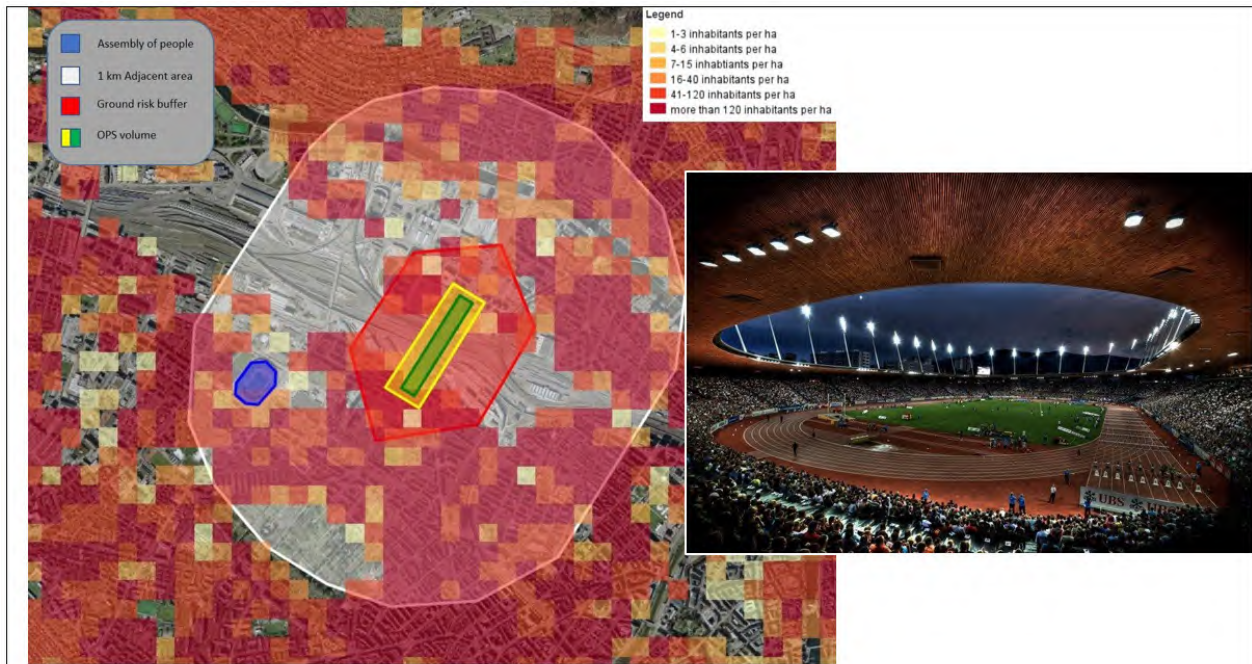
Table 21: Operation in Park Near Paris Centre (Operational Volume of 433m + Adjacent Area of 3.6km, 12km, 35km, 150km)



density to choose for the assessment. In this case the conservative estimate would be the 400,000 people, but it is also conceivable that if only a small part of the gathering would be within the 1km adjacent area the smaller density value may also be argued for. However, in this case the density of >50,000 is used for the adjacent area GRC evaluation.

**Example #3:** The Stadium example shows that a 30,000 ppl gathering inside an already densely populated area does not significantly increase the population density measured within 1km of the operational volume. However, as with the previous examples the difference could also be much more if the operational area is a controlled ground area.

The trigger in this example is the gatherings of people in the sports event at the stadium. The gathering is around 30,000 people and so the competent authority must decide whether this is closer to the 400,000 or 40,000 definition of gatherings of people. Arguably the 40,000 people definition is much closer and so the selected population density for the adjacent area GRC evaluation is <50,000.

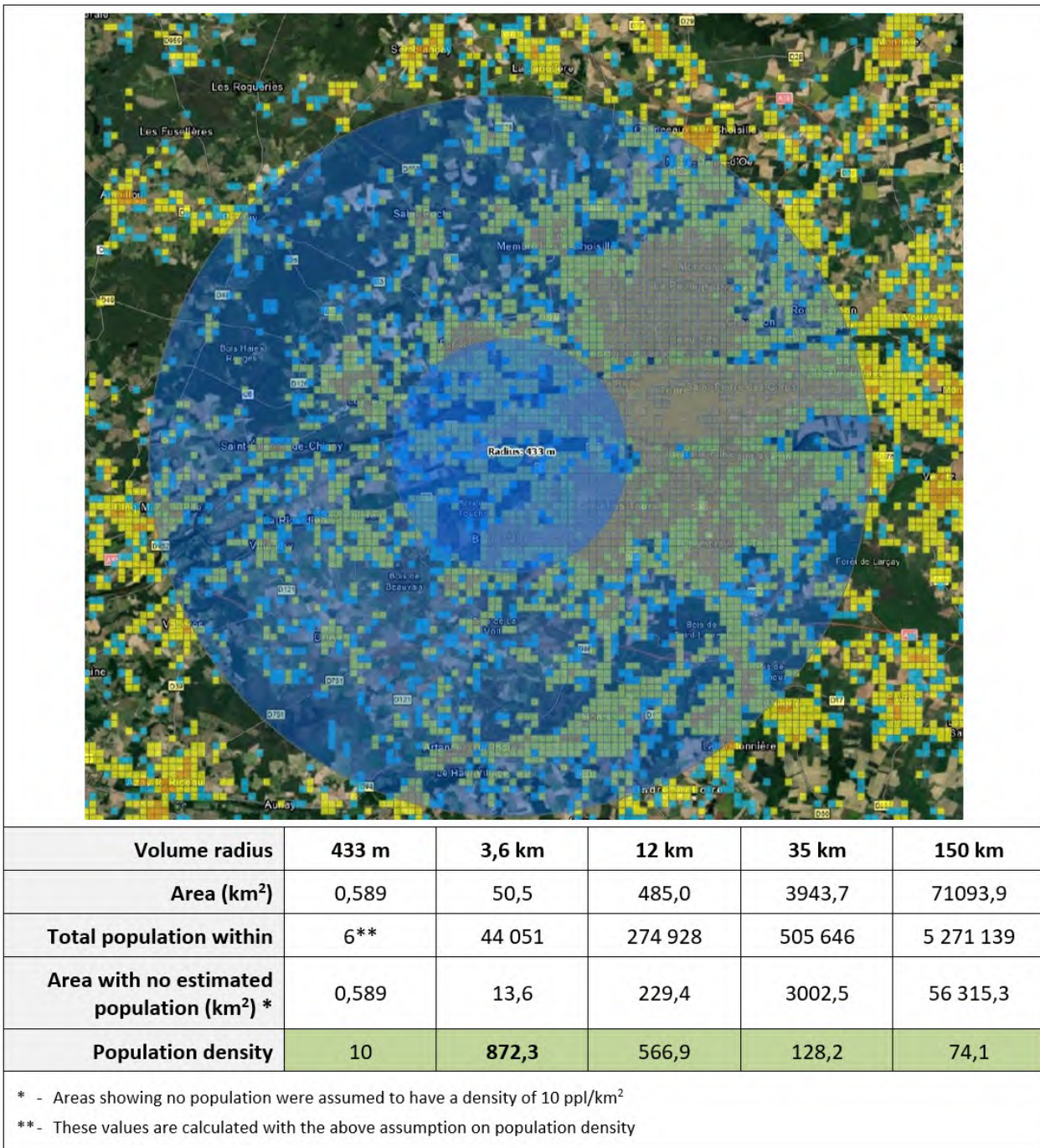


$A_{OPS+GRB}$ (km <sup>2</sup> )	0.69
$A_{ADJ}$ (km <sup>2</sup> )	4.58

#	Description	Area (km <sup>2</sup> )	Density (ppl/km <sup>2</sup> )	Population (people)	% of $A_{ADJ}$ 1km
1	Assembly Stadium Letzigrund (Blue area)	0.81	37 037	30 000	17.69%
2	Average 1km $A_{ADJ}$ base population	4.58	9 031	41 360	
3	All together	4.58	15 893	71 360	

Figure 25: Stadium Letzigrund with Around 30,000 people

Table 22: Operation in Field Near Tours Centre(Operational Volume and GRB of 433m + Adjacent Area of 3.6km, 12km, 35km, 150km)



## 5.2 Expected Ground Risk Casualty Rate Model in the Adjacent Area

We describe the risk to persons on the ground in the adjacent area using a similar concept for the risk to persons in the operational volume and buffers, the Expected Casualty Rate. The following events must occur for a UAS that begins operation within the operational volume to fatally injure a person in the adjacent area:

- the aircraft must exit the operational volume (at this point, a loss of control of the operation event has occurred), and
- then the aircraft must pass outside the ground risk buffer into the adjacent area, and

- then the aircraft needs to have an event that causes it to impact the ground in the adjacent area, and
- during this ground impact event, the aircraft must then impact and fatally injure a person (we will assume that an impact with a person will cause a fatality to simplify - ground Risk Mitigations M1 and M2 are only effective at reducing the number of people at risk and critical area/probability of fatality, if they are still functioning in the adjacent area)

We can write this in probabilistic form:

$$E_{C,adj} = P(ADJ) \times P(GI|ADJ) \times D_{popavg,adj} \times A_{C,unmit} \times 10^{M_{1,adj}+M_{2,adj}} \quad (25)$$

where:

- $E_{C,adj}$  is the expected casualty rate in the adjacent area.
- $D_{popavg,adj}$  is the average population density in the adjacent area.
- $A_{C,unmit}$  is the critical area absent any effect of Mitigation 2.
- $M_{1,adj}$  is effect of all M1 mitigations (M1(A), M1(B), M1(C) in the adjacent area.
- $M_{2,adj}$  is the effect of Mitigation 2 in the adjacent area.
- $P(ADJ)$  is the probability that the aircraft ends up in the adjacent area due to any means.
- $P(GI|ADJ)$  is the probability of a ground impact event occurring within the adjacent area, resulting in an impact with the ground. As a conservative assumption, it is assumed that the aircraft will impact the ground in the adjacent area at some point (i.e.  $P(GI|ADJ)$ ).

## 5.2.1 Containment Requirements as a Function of Final GRC in the Adjacent Area

If we set the allowable expected casualty rate to the SORA Target Level of Safety (1 fatality per million hours), we can rearrange the equation to solve for the maximum allowable probability that the aircraft enters the adjacent area ( $P(ADJ)$ ):

$$E_{C,adj} \leq TLOS \quad (26)$$

$$P(ADJ) \leq \frac{TLOS}{D_{popavg,adj} \times A_{C,unmit} \times 10^{M_{1,adj}+M_{2,adj}}} \quad (27)$$

We can replace the right-hand side by understanding that the expression for  $P(ADJ)$  is effectively the final GRC in the adjacent area:

$$SAIL = fGRC_{adj} - 1 \quad (28)$$

$$10^{-SAIL} = \frac{TLOS}{D_{popavg,adj} \times A_{C,unmit} \times 10^{M_{1,adj}+M_{2,adj}}} \quad (29)$$

$$\frac{1}{10^{fGRC-1}} = \frac{TLOS}{D_{popavg,adj} \times A_{C,unmit} \times 10^{M_{1,adj}+M_{2,adj}}} \quad (30)$$

We can then restate the right-hand side of this equation in terms of the “final GRC” of the adjacent area:

$$P(ADJ) \leq \frac{1}{10^{fGRC-1}} \quad (31)$$

This probability is the **absolute containment requirement**, needed to be satisfied in order to meet the Target Level of Safety.

We can further split up into the following two events:

$$P(ADJ) = P(\neg OV) \times P(ADJ|\neg OV) \quad (32)$$

Where  $P(\neg OV)$  is the probability aircraft exits the operational volume, and  $P(ADJ|\neg OV)$  is the probability of entering the adjacent area (or alternatively stated, the probability of exiting the ground risk buffer), given that the aircraft has exited the operational volume.

These two probabilities come in two flavours, *inherent*  $P_{in}(ADJ)$ , i.e. the probability absent any specific mitigations to prevent this from happening, and *mitigated*, i.e. when functions are deliberately put in place to reduce the probability of these events from happening compared to the inherent cases. The mitigated probability of entering the adjacent area ( $P_{mit}(ADJ)$ ), can be broken down into the following components:

- $P_{mit}(\neg OV)$ , the mitigated probability of exiting the operational volume, implemented by some function that is intended to prevent the aircraft from leaving the operational volume.
- $P_{mit}(ADJ|\neg OV)$ , the mitigated probability of exiting the ground risk buffer on the condition that the aircraft has breached the operational volume, implemented by some function that strives to ensure the aircraft does not escape the ground risk buffer.

## 5.2.2 Inherent Probability of Entering the Adjacent Area

We define the inherent probability of leaving the operational volume as such:

$$P_{in}(\neg OV) = 10^{-SAIL} \quad (33)$$

i.e. inherently there is a 1/10 probability that a loss of control event leads to the aircraft leaving the operational volume, absent any mitigations to reduce this probability. This is a conservative assumption based on expert judgement from the current loss of control events experienced by UAS operations.

We further define the inherent probability of entering the adjacent area, given the operational volume has been breached as:

$$P_{in}(ADJ|\neg OV) = 1 \quad (34)$$

This means that absent any mitigations if the aircraft leaves the operational volume, there is a 100% probability that the aircraft will also leave the ground risk buffer. This is due to the lack of requirements to prevent this occurrence happening. We can simplify the inherent probability of entering the adjacent area with this information:

$$P_{in}(ADJ) = P_{in}(\neg OV) = 10^{-SAIL-1} \quad (35)$$

### 5.2.3 Mitigated Probability of Entering the Adjacent Area

Now we can discuss the mitigated probability of leaving the operational volume ( $P_{mit}(\neg OV)$ ), and of exiting the ground risk buffer ( $P_{mit}(ADJ|\neg OV)$ ) attained by the use of a containment function. This containment function has two sub-functions:

- F1 - To decrease the probability of leaving the operational volume (i.e., by ensuring that the aircraft remains within the operational volume) and
- F2 - Upon exiting the operational volume, to prevent the aircraft from leaving the ground risk buffer (usually via the termination of flight).

### 5.2.4 Low, Medium, and High Robustness Containment Objectives

We now define the following three levels of containment robustness as shown in the requirements table in section A, Low, Medium, and High, with the following robustness objectives (note that criterion for containment in Annex E #1 deals with  $P_{mit}(\neg OV)$ , while criteria #2, and #3 deal with  $P_{mit}(ADJ|\neg OV)$ ).

### 5.2.5 Low Robustness Containment Assumptions

Low containment has low-level integrity requirements to deliver robustness against both  $P_{mit}(\neg OV)$  and  $P_{mit}(ADJ|\neg OV)$ . The safety objectives for  $P_{mit}(\neg OV)$  require the applicant to demonstrate that no probable failure leads to exit of the operational volume. Using JARUS AMC 1309 Issue 2 guidance [2], this means that at most, the probability of exiting the volume due to the single  $i$ th ( $FC = i$ ) failure condition ( $P_{Low,FC=i}(\neg OV)$ ) will be equivalent to a worst-case remote failure occurring:

$$P_{Low,FC=i}(\neg OV) = 10^{-4} \quad (36)$$

Assuming that there are around 10 failure conditions that could lead to this event, we arrive at a probability of exiting the operational volume for Low Robustness containment ( $P_{Low}(\neg OV)$ ) of:

$$P_{Low}(\neg OV) = 10^{-3} \quad (37)$$

This constant figure exceeds or equals the capability of the inherent containment for SAILs I and II. For SAILs III and higher, the inherent containment exceeds this requirement, and will be used instead for Low Robustness containment:

$$P_{Low}(\neg OV) = \begin{cases} 10^{-3}, & \forall SAIL \leq II \\ 10^{-SAIL-1} & \forall SAIL \geq III \end{cases} \quad (38)$$

In other words, the higher the SAIL, the lower the probability of a loss of containment. As a loss of containment event is considered a loss of control of the operation event, the higher the SAIL, the higher is the inherent protection from the event of leaving the operational volume.

The probability of exiting the ground risk buffer, on the condition the aircraft has left the operational volume, with a Low Robustness containment system is conservatively set to 1 in 10 ( $10^{-1}$ ):

$$P_{Low}(ADJ|\neg OV) = 10^{-1} \quad (39)$$

This results in an overall effect of Low Robustness containment on the probability of entering the adjacent area ( $P_{Low}(ADJ)$ ) of:

$$P_{Low}(ADJ) = P_{Low}(\neg OV) \times P_{Low}(ADJ|\neg OV) \begin{cases} 10^{-4}, & \forall SAIL \leq II \\ 10^{-SAIL-2} & \forall SAIL \geq III \end{cases} \quad (40)$$

## 5.2.6 Medium Robustness Containment Assumptions

Medium robustness containment provides the same probability of exiting the Operational Volume as the low robustness containment, but provides a better (lower) probability of exiting the ground risk buffer(i.e.  $P_{Med}(\neg OV) = P_{Low}(\neg OV)$ ):

$$P_{Med}(\neg OV) = \begin{cases} 10^{-3}, & \forall SAIL \leq II \\ 10^{-SAIL-1} & \forall SAIL \geq III \end{cases} \quad (41)$$

This increased integrity and assurance requirement for  $P_{Med}(ADJ|\neg OV)$  provides one order of magnitude more capability to the second containment function (F2), compared to the Low Robustness containment objectives:

$$P_{Med}(ADJ|\neg OV) = 10^{-2} \quad (42)$$

We can summarise the effect of Medium Robustness containment below:

$$P_{Med}(ADJ) = P_{Med}(\neg OV) \times P_{Med}(ADJ|\neg OV) \begin{cases} 10^{-5}, & \forall SAIL \leq II \\ 10^{-SAIL-3} & \forall SAIL \geq III \end{cases} \quad (43)$$

## 5.2.7 High Robustness Containment Assumptions

High Robustness containment, in contrast to Medium Robustness containment, focuses on increasing the capability of the system to prevent the aircraft from exiting the operational volume ( $P_{High}(\neg OV)$ ) in the first place. The requirement changes from **no probable** failure for Low and Medium Robustness containment to **no remote** failure for High Robustness containment. Using a similar analysis to the one provided for Low Robustness containment, this gives a worst-case probability of leaving the operational volume of:

$$P_{High}(ADJ|\neg OV) = 10^{-4} \quad (44)$$

Again, similar to the Low Robustness containment outcomes, this constant benefit equals the inherent containment for SAIL III or is exceeded by the inherent containment for SAIL IV or higher; hence, the inherent probability of leaving the operational volume will be used as the mitigated probability of leaving the operational volume for SAILs III and higher:

$$P_{High}(\neg OV) = \begin{cases} 10^{-4}, & \forall SAIL \leq II \\ 10^{-SAIL-1} & \forall SAIL \geq III \end{cases} \quad (45)$$

Table 23: Containment Robustness Objectives (overall)

	Low Robustness	Medium Robustness	High Robustness
SAIL Level	$P_{Low}(ADJ)$	$P_{High}(ADJ)$	$P_{Med}(ADJ)$
I	$10^{-4}$	$10^{-5}$	$10^{-6}$
II			
III	$10^{-SAIL-2}$	$10^{-SAIL-3}$	N/A
IV			
V			
VI			

Table 24: Containment Robustness Objectives (split across ADJ and  $\neg OV$ )

	Low Robustness		Medium Robustness		High Robustness	
SAIL Level	$P_{Low}(\neg OV)$	$P_{Low}(ADJ \neg OV)$	$P_{Med}(\neg OV)$	$P_{Med}(ADJ \neg OV)$	$P_{High}(\neg OV)$	$P_{High}(ADJ \neg OV)$
I	$10^{-3}$	$10^{-1}$	$10^{-3}$	$10^{-2}$	$10^{-4}$	$10^{-2}$
II						
III	$10^{-SAIL-1}$	$10^{-1}$	$10^{-SAIL-1}$	$10^{-2}$	N/A	N/A
IV						
V						
VI						

The requirements for terminating flight and defining the ground risk buffer are equivalent to the Medium Robustness containment requirements (i.e.,  $P_{High}(ADJ|\neg OV) = P_{Med}(ADJ|\neg OV)$ )

$$P_{High}(ADJ|\neg OV) = 10^{-2} \quad (46)$$

And the overall effects of enhanced containment are provided below:

$$P_{High}(ADJ) = P_{High}(\neg OV) \times P_{High}(ADJ|\neg OV) \begin{cases} 10^{-6}, & \forall SAIL \leq II \\ 10^{-SAIL-3} & \forall SAIL \geq III \end{cases} \quad (47)$$

Note that the High Robustness containment outcomes for SAILs III and greater are actually equivalent to that of Medium Robustness containment outcomes, hence High robustness containment is only applied to SAILs I and II (Medium Robustness containment provides equivalent outcomes for SAILs III and higher). In summary, Low, Medium, and High containment objectives provide the following outcomes for the containment functions:

### 5.2.8 Containment Objectives Based Upon the Risk of the Adjacent Area

We can now tabularise across various combinations of final GRC in the adjacent area and the SAIL in the Operational Volume and Ground Risk Buffers, for use in the SORA Main Body. From the overall requirement for the containment

We use the following equation for SAILs I and II, alongside the defined mitigation values for Inherent, Low, Medium, and High robustness containment:

$$P_{mit}(\neg OV) \times P_{mit}(ADJ|\neg OV) \leq \frac{1}{10^{fGRC_{adj}-1}} \quad (48)$$

A reminder that if no mitigations are applied, then the inherent probability of entering the adjacent area for SAIL I or II reverts to the value of  $P_{in}(ADJ) = 10^{-SAIL-1}$ . However, when any mitigations are applied, this relativity is subsumed by the absolute effectiveness of the mitigations used.

For SAIL levels at III or higher, we use the relative formula, taking into consideration the SAIL level of the operation's effect on the probability of leaving the operational volume:

$$P_{mit}(ADJ|\neg OV) \leq \frac{1}{10^{fGRC_{adj}-1} \times P_{mit}(\neg OV)} \quad (49)$$

$$P_{mit}(ADJ|\neg OV) \leq \frac{1}{10^{fGRC_{adj}-2}} \quad (50)$$

We can combine these two tables and remove the numbers to ease use (where N – No requirement, L – Low Robustness required, M – Medium Robustness Required, H – High Robustness required, and Out of Scope):

### 5.3 Alternative Method to Compute Ground Risk Containment Requirements

#### 5.3.1 Introduction

The containment requirements depend on the difference between the risk level of the operational volume and the adjacent volume. In order to derive it, the applicant is required to assess first the containment requirements of the adjacent area, then the containment requirements of the adjacent airspace and finally merge the 2 requirements to get the final containment requirements.

#### 5.3.2 Outcome

Alternative Method for identification of the applicable final containment requirements listed in Annex E – Section 4.

#### 5.3.3 Task Description

- (a) Establish the size of the adjacent area for the operation in accordance with step #8
- (b) Determine the **adjacent area final GRC**:
  - (i) Identify the applicable mitigations listed in Table 4 – Mitigations for Final GRC determination, that could lower the iGRC of the adjacent area.
  - (ii) Calculate the final GRC of the adjacent area after mitigations have been applied.
- (c) Using Table 27, identify the adjacent area containment requirement using the SAIL (identified in step #7) and the adjacent area final GRC from (b) where:
  - (i) N = No containment,
  - (ii) L = Low level of containment,
  - (iii) M = Medium level of containment,
  - (iv) H = High level of containment.
- (d) Annex A, section 3 contains further guidance on presenting the data supplementing the risk assessment to the authority.

Table 25: SAIL I and II Containment Requirements

		SAIL in the Operational Volume	
		I	II
Adjacent Area Final Ground Risk Class	<b>1</b>	1	1
	<b>2</b>	$10^{-1}$	$10^{-1}$
	<b>3</b>	$10^{-2}$	$10^{-2}$
	<b>4</b>	$10^{-3}$	$10^{-3}$
	<b>5</b>	$10^{-4}$	$10^{-4}$
	<b>6</b>	$10^{-5}$	$10^{-5}$
	<b>7</b>	$10^{-6}$	$10^{-6}$
	<b>8</b>	$10^{-7}$	$10^{-7}$
	<b>9</b>	$10^{-8}$	$10^{-8}$
	<b>10</b>	$10^{-9}$	$10^{-9}$
	<b>11</b>	$10^{-10}$	$10^{-10}$

Table 26: SAIL III, IV, V and VI Containment Requirements

		SAIL in the Operational Volume			
		III	IV	V	VI
Adjacent Area Final Ground Risk Class	<b>1</b>	$10^4$	$10^5$	$10^6$	$10^7$
	<b>2</b>	$10^3$	$10^4$	$10^5$	$10^6$
	<b>3</b>	$10^2$	$10^3$	$10^4$	$10^5$
	<b>4</b>	10	$10^2$	$10^3$	$10^4$
	<b>5</b>	1	10	$10^2$	$10^3$
	<b>6</b>	$10^{-1}$	1	10	$10^2$
	<b>7</b>	$10^{-2}$	$10^{-1}$	1	10
	<b>8</b>	$10^{-3}$	$10^{-2}$	$10^{-1}$	1
	<b>9</b>	$10^{-4}$	$10^{-3}$	$10^{-2}$	$10^{-1}$
	<b>10</b>	$10^{-5}$	$10^{-4}$	$10^{-3}$	$10^{-2}$
	<b>11</b>	$10^{-6}$	$10^{-5}$	$10^{-4}$	$10^{-3}$

Table 27: SORA Containment Requirements

		SAIL in the Operational Volume					
		I	II	III	IV	V	VI
Adjacent Area Final Ground Risk Class	≤3	N					
	4	L	N				
	5	L	L	N			
	6	M	M	L	N		
	7	H	H	M	L	N	
	8	Out of scope	Out of scope	Out of scope	M	L	N
	9				Out of scope	M	L
	10					Out of scope	M
	11						Out of scope

### 5.3.4 Additional Guidance

- (a) Although the SORA process does not support a final GRC higher than 7, the value is acceptable for the adjacent area, since the operation is not expected to happen in this area.
- (b) Conservative simplifications for calculating the average population density should be accepted to allow more practical calculation means. In contrast to the iGRC of the operational area, the Adjacent Area uses an weighted average value as it is a reasonable assumption that the likelihood of an excursion from the operational volume occurring in different portions of the Adjacent Area is close to uniform.

### 5.3.5 Guidance on the application of the ground risk mitigations in the adjacent area

- (a) Mitigations might be applied to reduce the GRC of the adjacent area. Please note that not all ground risk mitigations used for the operational area are effective in the adjacent area. In order to fly above the adjacent area, a loss of control of the operation event must have occurred, which includes likely the loss of certain types of mitigation means. Mitigations that are assumed to be effective in the adjacent area:
  - (i) M1(A) - sheltering arguments: Works assuming the sheltering arguments are generalizable.
  - (ii) M1(B) - restricting the operation to times of day with less people outside (i.e. night): Works assuming the same analysis is generalizable.
  - (iii) M2 - frangible design features of an UA: passive mitigation means based designs or inherent UA characteristics, like frangibility are still effective in a fly-away situation. M2 mitigations like parachutes or special descent manoeuvres may not be used by default.
- (b) Ground Risk Mitigations that are **not** considered to be effective in the adjacent area include:
  - (i) M1 (B) - route restrictions, exposure arguments: at the point breaching the Operational Volume, flight path planning is assumed not to be effective at reducing the population at risk.
  - (ii) M1 (C) - Tactically mitigating the ground risk by observing the overflown area. The operator will not likely have vision of all potential areas in the adjacent area.
  - (iii) M2 - active means to enable a reduced energy descent, e.g. parachute or stabilised stall that rely on the systems that can fail to result in a loss of containment event: It can be conservatively assumed that these functions are a fundamental part of the UA containment means. When the UA starts flying over the adjacent area, the containment means must have failed and cannot be available to mitigate a crash in the adjacent area.
- (c) Applicants may provide justification to the Competent Authority for additional mitigations as long as they are still applicable in a fly away scenario.
- (d) If a failure of an M2 mitigation would lead to a malfunction of flight termination resulting in a fly away scenario, this mitigation cannot be used for computing the adjacent area final GRC. For example, if the flight termination system triggers a parachute, in the event of a fly away, it is assumed the parachute system has failed, unless proven otherwise by the applicant.

## Appendices

### A Critical Area to Wingspan and Speed Calculations

The iGRC table derived in Section 2 is actually based on the critical area  $A_C$ , as this variable (alongside population) is one of the two key variables determining TLOS. However, the calculation of critical areas is not necessarily straightforward for operators or regulatory authorities, as it is based on multiple variables, and oftentimes, the data is not readily available to support its calculation for individual use cases.

To resolve this, the iGRC table in the SORA main document uses wingspan (or, more generally, maximum characteristic dimension) and Maximum Speed<sup>16</sup> as predictors for critical areas. This appendix details how the values for wingspan and speed values support the iGRC table values and the underpinning assumptions. The Appendix is structured as follows:

- In A.1, we argue for the use of velocity instead of kinetic energy in the iGRC as limits on the aircraft size classes.
- In A.2, we discuss what parameters are important for determining the size of the critical area and conclude that impact speed and angle are the two main free variables that need to be determined. We propose three different descent angles for determining appropriate speed limits.
- In A.3, we determine all the parameters that are needed in order to use the JARUS model on the scenario for relating speed and angle.
- In A.4, we then plot scenario outcomes and determine the speed limits.
- In A.5, special cases are considered to ensure that the model better reflects realistic impact scenarios.
- In A.6, we combine all of the previous work to produce the final iGRC table.

If an operator or regulatory authority deems the iGRC is non-representative for the aircraft operation under regulatory consideration, they can use the models described in Appendix B, or any other model accepted by the regulator that more accurately reflects the operation, to determine a critical area that is more representative of the operation and the allowable population density that can be overflown.

#### A.1 Addition of Velocity Constraints in the Column Headers

In the previous version of the SORA, kinetic energy was used as a column limit along with wingspan to move fast and/or heavy drones into higher iGRC categories.

However, it was decided that Maximum Speed<sup>17</sup>, in combination with Wingspan, had greater utility for supporting the safe and accurate determination of critical area. It can be shown that the speed of the aircraft at impact is a good descriptor of the critical area when teamed with wingspan.

---

<sup>16</sup>The SORA 2.5 Main Body defines Maximum speed as maximum possible commanded airspeed of the UA, as defined by the designer. This is not the mission specific maximum commanded airspeed of the UA as reducing the mission airspeed may not necessarily reduce the impact area

<sup>17</sup>defined as the maximum possible commanded airspeed of the UA, as defined by the designer

## A.2 Determining Appropriate Values for the iGRC Table

In order to assess the appropriate coupling between the critical area and the more easily calculated wingspan and speed using the JARUS model, a number of parameters have to be determined. These include:

- Impact speed (see section [A.3.1](#) and [A.3.2](#))
- Impact angle
- Friction coefficient for ground (see section [A.3.4](#))
- Loss of energy at impact through the coefficient of restitution (see section [A.3.3](#))
- Height and width of a standard person
- Width or wingspan of the aircraft (given by iGRC columns)
- Lethal kinetic energy (see section [A.3.5](#))

The values used in the JARUS model and the reasoning behind them are described below,

### A.2.1 Impact Angle and Speed

The descent angle plays a central role in all the models, and it is important to determine a realistic range for the impact angle for the given type of aircraft used. Relatively shallow impact angles will result in larger critical areas due to longer glides as well as longer skidding across the terrain. Slightly higher angles of attack result in a shorter glide area. High angles of impact typically come from a ballistic, deep stall, or spiraling descent and will typically have a higher impact velocity than more shallow impacts.

Impact velocity and impact angle affect how long the slide after impact will be. Note that in all models, the velocity used for the slide is the horizontal component of the impact velocity. Furthermore, the glide part of the critical area does not depend on the impact velocity. Additional considerations include the failure mode prior to impact (including CFIT), adopting the best glide after engine failure, and whether it is a ballistic collision. Whilst many permutations are possible, we examined three different descent scenarios, as shown in Figure [26](#).

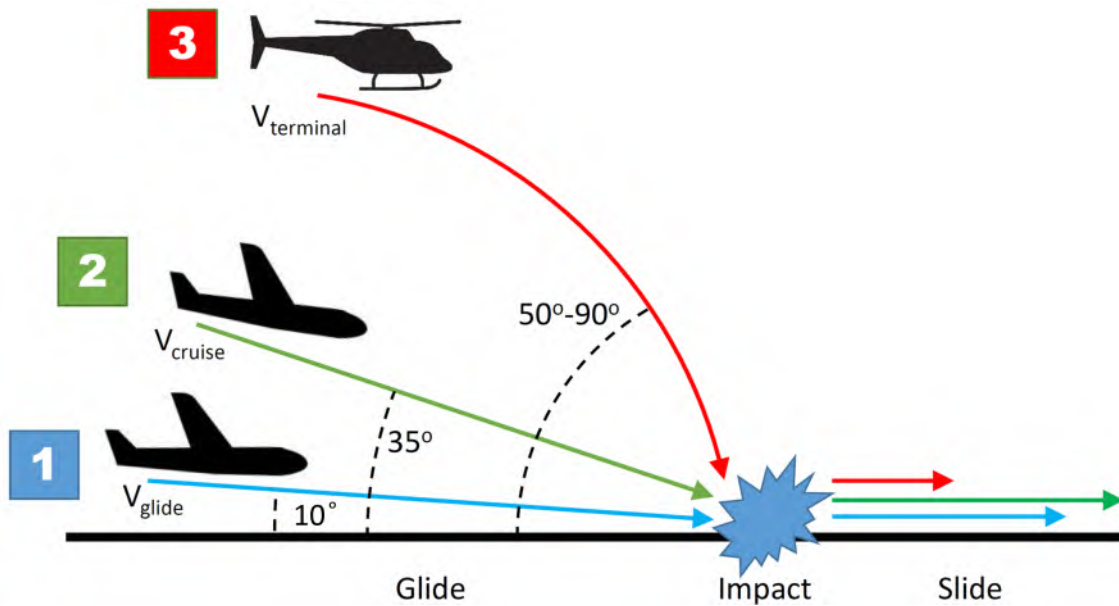


Figure 26: The three different descent scenarios used to compute critical areas. The illustration is conceptual only, with the aircraft, distances, and angles not to scale. We emphasize also that we make no distinction between fixed wing, rotorcraft, or other types of aircraft, even though different silhouettes are used in the figure. The altitude used for ballistic trajectories is provided in Table 29.

Note that this graphic is not to scale and only serves to depict the concept of the descent scenarios. The glide angles, slide distances, aircraft type and size, etc. will vary depending on the situation. Since the direction of travel of the aircraft is separately specified in the models, the velocity is sometimes referred to as speed in this document.

### A.2.2 Altitude for ballistic descent

The altitudes used for the computation of impact angle and impact speed for the ballistic descent vary between the classes, with 1 m being the lowest and 40 m the highest. The actual values are shown in Table 29. While there obviously can be a large variance in operational altitude for different flights, a change in altitude does, in fact, not change the resulting critical area very much, as long as the altitude is not very low (in which case the descent is more like a glide scenario). This is because ballistic descent relatively quickly becomes steep and close to terminal velocity. Consequently, any further descent does not change the impact speed and impact angle very much. In addition, as can be seen from Table 32, the critical areas for ballistic descent are significantly smaller than for scenario 1 and 2. Therefore, the altitude chosen for the ballistic descent becomes irrelevant for the critical areas used in the iGRC table.

### A.2.3 Descent scenarios

The three scenarios cover different expected types of descents for a loss of control event.

- **Scenario 1** is a glide, which could result from an engine-out event with the aircraft still capable of actuating its control surfaces and coming in at glide speed. Glide speed is used for this scenario, and the impact angle assumed is 10 degrees. Glide speed is approximated to be 0.65 times maximum speed
- **Scenario 2** represents a complete system failure during cruise, such as a battery failure, which

results in the aircraft impacting at maximum speed and at a steeper angle. Maximum Speed<sup>18</sup> is used for this scenario, and the impact angle is 35 degrees

- **Scenario 3** is a ballistic or near-ballistic descent, which can occur for rotorcraft in case of an engine-out resulting in stopped rotors or for fixed wing in case of structural disintegration or stall. For the ballistic descent, the velocity and impact angle are computed specifically based on a second-order drag equation. Section A.3.7 expands on the calculation of ballistic descent.

#### A.2.4 Lighter-than-air aircraft

The computations in Annex F are primarily for fixed and rotary-wing aircraft and do not specifically address lighter-than-air (LTA) aircraft. Such aircraft may, in some circumstances, behave differently from traditional aircraft during descent and crash. The formulas for critical area and iGRC values are still applicable in the sense that they will often be rather conservative because LTA may be coming down slower and at a steeper angle than especially fixed-wing aircraft. When using the iGRC table, the wingspan value for an LTA is the diameter of the hull. When using the JARUS model, the glide angle can be assumed to be similar to a ballistic descent, that is, around 60 degrees. The frontal area has to be estimated conservatively (i.e., an inflated hull), and the drag coefficient should be that of a sphere (i.e., 0.5). The ballistic descent is described in more detail in Section A.3.7.

### A.3 Critical Area Model Parameters

The JARUS model in Section B.3 is used to calculate the critical areas, with the parameters outlined in Table 28 employed.

Table 28: Values use for computations for the three descent scenarios. The impact angles and speeds for scenario 3 come from Table 29.

Descent scenario parameters							
Descent scenario	1	2	3 (Section A.3.7)				
Aircraft size	All	All	1 m	3 m	8 m	20 m	40 m*
Impact angle [deg]	10	35	76	64	57	51	59
Impact speed [m/s]	$0.65 \cdot v_{\text{max-speed}}$ (A.3.2)	$v_{\text{max-speed}}$ (A.3.1)	24	40	60	106	121
Height of person (m)	1.8						
Radius of a person (m)	0.3						
Coefficient of friction (Section A.3.4)	0.75						
Drag coefficient (Section A.3.6)	N/A		0.8				
Coefficient of restitution (Section A.3.3)	0.8	0.75	0.63	0.67	0.68	0.70	0.68

Below is an explanation for the main values chosen above and an explanation of why they are

<sup>18</sup>maximum possible commanded airspeed of the UA, as defined by the designer

expected to be slightly conservative. Operators and competent authorities can determine if these assumptions properly reflect the operation under consideration and can adjust as needed.

### A.3.1 Maximum Speed

Early versions of Annex F adopted *Maximum Cruise Speed* as the velocity value to be used within the iGRC table and corresponding calculations. However, this has since been depreciated and the current iGRC table used in Annex F and the Main Body employs the term *Maximum Speed*, where this is defined as

- The maximum possible commanded airspeed of the UA, as defined by the designer,
- The *Maximum Speed* is not the mission specific maximum commanded airspeed of the UA as reducing the mission airspeed may not necessarily reduce the impact area.
- Mitigations that limit airspeed below the maximum speed value during an impact can be accounted for in Annex B, part of Step #3.

Ideally, the maximum speed used in critical area calculation should be groundspeed, as this is subsequently translated into impact speed and the speed during the slide. However, since the actual speed may change depending on numerous factors, the maximum speed (denoted  $v_{\text{max-speed}}$ ) is an airspeed and not ground speed. This means that subject to wind, the ground speed may be higher or lower than the airspeed.

However, since it is relatively complicated to account for the wind during the planning of missions, and since a powered crash (which is the only situation where  $v_{\text{max-speed}}$  is relevant for a crash) may occur equally likely in any direction. In turn, the average wind speed is assumed to be 0, so the simplifying assumption used in this Annex is that the ground speed and airspeed are the same.

### A.3.2 Ratio of Glide to Maximum Speed

It is expected that for an aircraft to impact the ground at a 10 degree angle in a non-CFIT situation, that it would be gliding, thus, glide speed is used. Looking at aircraft where max speed, cruise speed and glide speeds were available, the ratio of these speeds for most aircraft fell between 0.65 and 0.50. Given the lack of data in this area for drones, a value of 0.65 times the max speed was conservatively used as that means the aircraft would be coming in at a faster speed, thus creating a larger slide area. It is expected that a larger glide speed ratio would come from higher wing loading and, thus, a steeper impact angle, potentially reducing the overall critical area.

### A.3.3 Coefficient of Restitution

The coefficient of restitution (CoR) expresses the reduction of velocity from before an impact to after an impact. For very stiff objects colliding, the velocity reduction is small, while for softer or breakable objects that may absorb energy during the impact, the velocity reduction is larger. In the modeling of ground impact, the two “objects” will be the unmanned aircraft and the ground. Unmanned aircraft tend to be somewhat stiff but certainly not unbreakable, so some loss of kinetic is to be expected on impact. The ground may obviously vary from very stiff, such as concrete or asphalt, to rather soft, such as grass, soil, sand, etc.

The assumption in the JARUS model is that for any impact, the aircraft is going to deform and not going to bounce back up and become airborne again. So the assumption is that any vertical velocity

is lost to the deformation of the aircraft and/or the ground. For the horizontal velocity, the JARUS model has the parameters  $e$  that allow for choosing a CoR value smaller than 1 (see Section B.3). The horizontal CoR in the calculations in Section A.4 varies the CoR linearly from 0.8 to 0.38, as the impact angle  $\theta$  varies from 10 to 80 degrees, i.e.,

$$e = 0.8 - \frac{0.42}{70}(\theta - 10) \quad (51)$$

### A.3.4 Coefficient of Friction

Friction is the force resisting the relative motion of two surfaces as they slide against each other. In this setup, the two surfaces will be the ground and the aircraft, and only the kinetic or sliding friction will be considered (i.e., not static friction). The force of sliding friction between two surfaces is the product of the coefficient of friction, and the normal force, which under the assumption that the ground is level, is simply mass times gravity. Consequently, the friction force  $F$ , which will slow down the sliding aircraft, is given by

$$F = mgC_g, \quad (52)$$

where  $C_g$  is the coefficient of friction. The value of  $C_g$  depends on the type of ground and the materials of the aircraft. Values for the friction coefficient for combinations of materials can be found in the literature for relatively flat surfaces parallel to each other, starting around 0.15 for wet grass against glass fiber and increasing to 0.7-0.8 for soft rubber against asphalt. In addition, the movements of the aircraft may affect friction, as bouncing and rolling will inevitably change the interaction between the ground and the aircraft, as well as the lack of uniformity between the two surfaces. In this document, a conservative value of 0.65 has been chosen and used throughout.

The CasEx package details CoF for a range of combinations of materials, which can be used in specific cases to get more accurate friction (and thus critical area).

### A.3.5 Lethal kinetic energy

Not all impacts between drones and people are fatal. It is desirable to accommodate this observation in the fatality rate modeling. However, the level of injury sustained relative to the impact parameters is a complex topic beyond the scope of this Annex. Albeit kinetic energy is not an optimal measure for lethality, it is found to be a useful middle ground between the true injury dynamic and the simple "all impacts are fatal."

The JARUS model includes the threshold parameter "Non-Lethal Kinetic Energy" or  $K_{\text{non-lethal}}$ , which reduces the critical area only to the area within which the impact is fatal. For the purposes of the iGRC model, it will be assumed that impacts below 290 Joules of kinetic energy during a slide are non-fatal. For the case of the  $< 1$  m platforms, it can be reasonably assumed that the entire slide will be non-lethal, and hence can be ignored. For larger than 1m platforms the reduced distance of slide will be calculated using the 290 Joule limit.

The 290 J threshold below which the kinetic energy is assumed non-fatal upon impact is a 10% probability of fatality for the limbs using the Janser Kinetic Energy Threshold for limbs [53].

### A.3.6 Drag coefficient

The drag coefficient  $C_d$  is a dimensionless quantity that describes the drag or resistance of an object in air. It is used in the drag Equation (53) in which a lower drag coefficient indicates the object will have less aerodynamic drag. For most objects, the drag coefficient is between 0.2 (quite low) and

1.2 (quite high). Determining the actual drag for a ballistically descending aircraft is difficult and may vary somewhat. However, it is unlikely to be at the low end due to the presumably less-aerodynamic shape of a descending aircraft. Setting it to high will yield more optimistic results (slower descent speed). As such, an intermediate value of 0.8 has been chosen.

It is worth noting that the ballistic descent scenarios achieve an impact speed close to the terminal velocity, which in turn depends on the reciprocal of the square root of the drag coefficient. Therefore, even moderate variations of the drag coefficient have limited effect on the impact speed and impact angle.

Note that the drag coefficient is not to be confused with the friction coefficient described above.

### A.3.7 Ballistic Descent Calculations

The ballistic descent is the case where the aircraft has no lift, and only gravity and drag affect the aircraft. It is assumed that the ballistic descent is governed by gravity acting vertically and the standard second-order drag equation

$$F_{drag} = \frac{1}{2}\rho C_d v^2 A, \quad (53)$$

acting in the direction of travel. Here the frontal area  $A$  is approximately equal to the smallest cross-section of the aircraft (i.e. a conservative value). The drag coefficient  $C_d$  is 0.8, as described in Section A.3.6. The density of the air  $\rho$  is always set to 1.225 kg/m<sup>3</sup>. The velocity is  $v$ .

For given values of initial altitude, horizontal speed, and vertical speed, it is possible to determine both impact angle and speed. The CasEx package (see Appendix E) incorporates the necessary functionality for determining these values.

The terminal velocity resulting from the drag equation is easy to determine by setting  $F$  to gravity. The equation rearranged to

$$v = \sqrt{\frac{2mg}{\rho A C_d}}, \quad (54)$$

where  $m$  is mass and  $g$  is the gravitational constant.

To support an awareness of the importance of key variables, five descent scenarios, one for each set of values of Wingspan and Velocity, have been computed and are summarized in the Table 29. The first part of the table gives the parameter values used. The scenario velocities (cruise speeds) are also listed and used as initial horizontal velocities. The initial vertical velocity is zero in all cases. Then the terminal velocities for the five scenarios are calculated. The kinetic energy at cruise speed is also listed for later comparison with the impact kinetic energy. The last part of the table then shows the results when applying gravity and second-order drag, giving impact speed and angle as well as horizontal distance traveled during descent, the time the descent takes, and finally, the kinetic energy at impact.

Table 29: The first part of the table is the parameters used for computing ballistic descent, and the second part is the resulting values.

Ballistic descent						
Characteristic Dimension		1 m	3 m	8 m	20 m	40 m
Parameters for ballistic descent	Frontal area [m <sup>2</sup> ]	0.1	0.5	2.0	8.0	14.0
	Mass [kg]	3	50	400	5,000	10,000
	Drag coefficient	0.8				
	Air density [kg/m <sup>3</sup> ]	1.225				
	Gravity Acceleration [m/s <sup>2</sup> or kg m/s <sup>2</sup> ]	9.81				
	Initial altitude [m]	75	100	200	500	1,000
	$V_{\text{max-speed}}$ [m/s] (iGRC table)	25	35	75	150	200
$V_{\text{terminal}}$ [m/s] (infinite vertical drop)		25	45	63	112	120
Kinetic energy at $V_{\text{max-speed}}$ [kJ]		1	31	1,125	56k	200k
Ballistic descent starting at $V_{\text{max-speed}}$	Ballistic impact velocity [m/s]	24	40	60	106	121*
	Ballistic impact angle [deg]	76	64	57	51	59
	Coefficient of restitution	0.63	0.67	0.68	0.70	0.68
	Hori dist traveled before impact [m]	63	123	335	1043	1690
	Descent time [s]	4.7	4.9	6.9	10.8	15.9
	Ground impact Kinetic energy [kJ]	1	39	719	27,976	73,106

\* The impact velocity is a little higher than terminal velocity. This is because the aircraft reaches terminal velocity during descent, and impact velocity is computed using an approximation [54], which gives a small error.

### A.3.8 Concession on smaller critical area for rotorcraft

In the calculations in the previous sections, there is a distinction between a glide descent, flight into terrain, and a ballistic descent. It is obvious that a ballistic descent will almost always have a higher impact angle, and thus comparatively smaller critical area, because the horizontal velocity is smaller. Since rotorcraft are more likely to have a ballistic descent than fixed wing aircraft, it may be reasonable for competent authorities to allow applicants to claim a smaller critical area and hence lower iGRC for rotorcraft.

However, this is not incorporated into the iGRC table for the following reasons. Firstly, while there is indeed a reduction in critical area for higher impact angles, it is often in the order of a factor 2 compared to a glide impact, and thus not near the needed factor 10 to reduce to a lower iGRC value. Secondly, rotorcraft are indeed able to glide (using autorotation) and of controlled flight into terrain, which for some rotorcraft may even be more likely than loss of thrust. Thirdly, any operator can conduct individual computation using a given probability distribution between various descent scenarios and determine a likely critical area, which in turn can be converted to an iGRC value. If a ballistic descent can be shown or argued to be much more likely than other types of descent, the operator may claim the ballistic descent as a more appropriate method for determining the critical area.

If an operator can indeed show that ballistic descent is far more likely than CFIT and autorotation, the applicable critical area can then be argued to be what results from this ballistic descent. The operator must then determine this critical area by using the JARUS model, see Section B.3, along with the appropriate impact angle and velocity. As can be seen from Table 29, typical ballistic impact angles from moderate altitude is around 50 to 70 degrees, and the impact speed should be determined as the terminal velocity, see Equation (54), since this is often quite close to the actual impact speed.

## A.4 Mapping Impact Speed and Impact Angle

### A.4.1 Speed and angle relation for fixed critical area

Figure 27, illustrates sensitivity of critical area to variation in impacts speed and impact angle for a 3m wingspan UAV. The following scenarios were chosen to illustrate the impact:

- A glide impact at 10 degrees, with a horizontal velocity component of 24.5 m/s (red line).
- A cruise<sup>19</sup> impact at 35 degrees, and horizontal velocity component of 35 m/s (yellow line).
- A ballistic impact at 64 degrees, and horizontal velocity component of 40 m/s (cyan line).

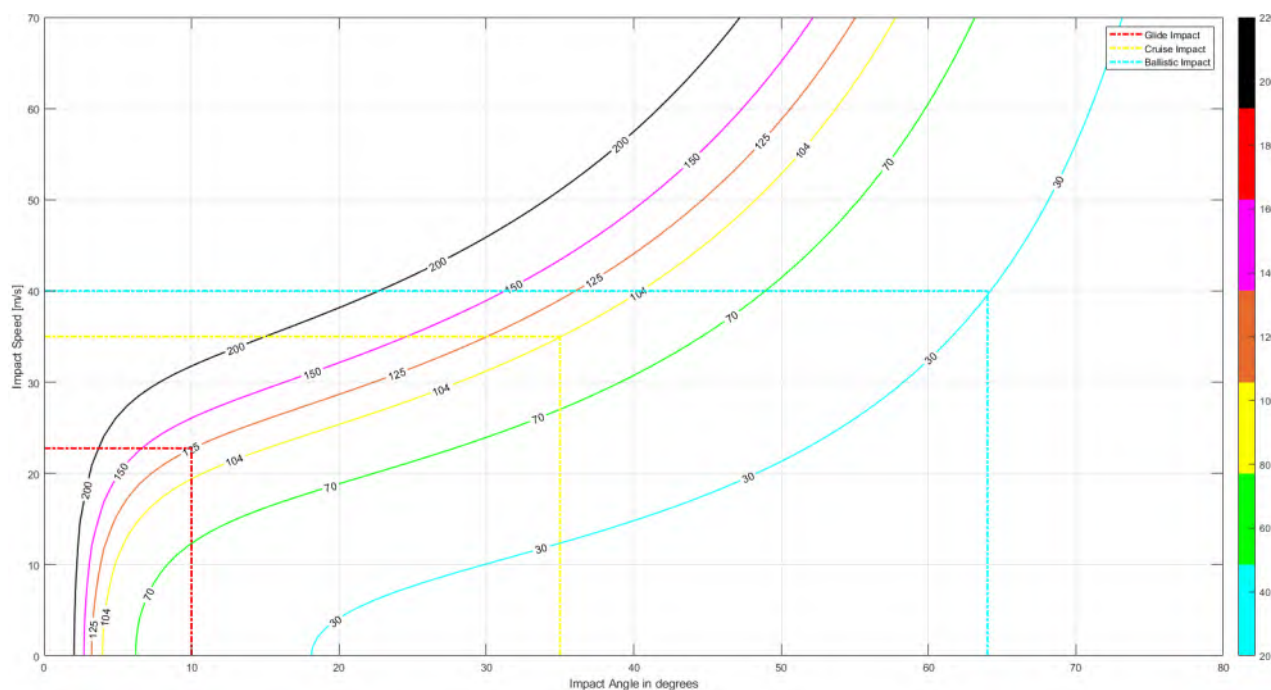


Figure 27: Critical area variations for the 3 m class. The curves shows where there is a constant critical area size for varying impact angle and impact speed. The target of 104.5 m<sup>2</sup> is shown in yellow. The three scenario values are also shown. Whilst the figure shown was generated in Matlab, a similar figure can be created via Python, using `figures.figure_angle_vs_speed()` method in the CasEx package.

Glide impact velocities were calculated according to the following assumption:

$$v_{\text{glide}} = 0.65 \cdot v_{\text{max-speed}} \cdot \quad (55)$$

<sup>19</sup>For these calculations it is assumed the aircraft is travelling at max possible commanded airspeed for the UA, as defined by designer

Review of Figure 27 reveals the Critical Area for the cruise impact scenario (35 degrees) is approximately 104 m<sup>2</sup>, glide impact (10 degrees) is 125 m<sup>2</sup>, and the ballistic impact, as expected, has a significantly smaller critical area. Similar results can be observed for the 1 m, 8 m, 20 m and 40 m classes. The cruise scenario and parameters was chosen as the most representative for use in the calculations in the iGRC table in Section 2.

It is worth noting that the ballistic impact has a somewhat smaller critical area for a given platform compared to the glide or flight descents. However, the critical area for the ballistic trajectory can vary significantly from that shown in 27, subject to variables used (see Table 29 for example). Any change to the assumed critical area will be subject to a substantiation of variable values with the competent authority, with further detail outlined in Section A.3.8.

## A.4.2 iGRC Maximum Speed Limit Values

To maximise alignment with the previous version of the SORA and the impact on aircraft manufacturers, this version of the SORA maintains the wingspan cutoffs at 1, 3 and 8 m respectively. The column previously associated with 8+ m has now been replaced with a representative value of 20m, and a new column added for 20m+ platforms, which for calculation purposes uses a value of 40m.

The velocity limits for Critical Area/Wingspans doublets embedded in the iGRC are as follows:

- **6.5 m<sup>2</sup> (1 m)**: This coincides with a maximum possible commanded speed of 25 m/s. Further details on the derivation of critical area is provided in Section A.5.1
- **104.5 m<sup>2</sup> (3 m)**: This coincides with a maximum possible commanded speed of 35 m/s, as illustrated in Figure 27.
- **1013 m<sup>2</sup> (8 m)**: The coinciding velocity was approximately 75 m/s,
- **6,108 m<sup>2</sup> (20 m)**: The coinciding velocity was approximately 120 m/s. For computational purposes.
- **32,720 m<sup>2</sup> (40 m)**: Because this column is the upper limit to the iGRC table, it is more difficult to generate. Using a velocity of 200 m/s, the critical area shown was generated.

Note these critical area values are the values used before any reduction due to obstacles is applied. Obstacle reductions were not applicable for aircraft greater than 20m.

## A.5 Special Cases

### A.5.1 The First iGRC column (UAS characteristic dimension < 1 m)

Initially when applying the simplistic wingspan and velocity critical area calculations to this column, the results were implausible, and these small aircraft were travelling extreme distances. The group determined that a more appropriate and realistic case for aircraft of this size was to demonstrate that the slide portion of the impact was non-fatal.

The following assumptions were made:

- The aircraft is travelling at maximum possible commanded airspeed of the UA<sup>20</sup>,

---

<sup>20</sup>as defined by the designer

- The angle of impact is 35 degrees (corresponding to cruise scenario), as this category contains a significant amount of multi rotors and these smaller aircraft would have higher wing loading and thus a steeper glide angle.
- During the glide phase of impact, the aircraft will fatally injure if the aircraft hits a person.
- The coefficient of restitution when the aircraft hits the ground is 0.65.
- During the slide portion of the impact, the aircraft will only impact the lower limbs.
- The fraction of energy absorbed by the lower limbs on impact during the slide is 0.5. This is a combination of an assumption of a non ideal impact (such as the two centre of masses of the objects not being aligned) and the coefficient of restitution on impact with a human. Additionally the energy thresholds in [53, Figure 4, p.1518] are derived from previous sources such as [55, Table 1, p.431] which deal with the results of impacts with piercing type injuries due to explosive debris (i.e. Feinstein calculates the energy required for a 10% chance to “fracture large bones” in the limbs causing “near lethality” from spherical bullets is approximately 213 J). This is expected to be overly conservative.

It can be shown that the allowable cruise velocity before impact, in order to meet these assumptions, is

$$v_{\text{cruise}} = \frac{\sqrt{\frac{2E_{\text{lethal}}}{\beta_{\text{transfer}}m_{90}}}}{e \cos \gamma} \quad (56)$$

where

- $E_{\text{lethal}} = 290 \text{ J}$  (see section A.3.5)
- $\beta_{\text{transfer}} = 0.5$
- $m_{90} = 3 \text{ kg}$ . This is the 90th percentile mass based on a statistical analysis of AUVSI data for unmanned aircraft physical characteristics. The 90th percentile was chosen to ensure the majority of platforms were represented by this calculation.
- $e = 0.65$ .
- $\gamma = 35 \text{ degrees}$ .

In this case, the maximum possible commanded airspeed should remain below 25 m/s in order to ensure the slide is non-fatal. At 35 degrees, the glide critical area is approximately 6.5 m<sup>2</sup>. Additionally, an aircraft of this mass and speed is unlikely to be able to penetrate a single person and then continue traveling such that a second person would be struck and killed. We can solve for the population density that coincides with the tightest grouping of people that results in 1 person every 6.5 m. This converts to a population density of approximately 150,000 ppl/km<sup>2</sup>.

## A.5.2 Obstacles stopping an aircraft

The JARUS model for computing the critical area is based on ground friction and dissipation of energy into deformation of the ground and the aircraft as the means to bring the aircraft to standstill after impact. The basic assumption is that the aircraft crashes in an area unimpeded by anything but people. However, in many operational areas, there will be numerous obstacles that will stop an aircraft that is either gliding close to the ground or sliding along the ground. This could be cars, trees, road signs, houses, and so on. And when such an obstacle stops the aircraft, the critical area

will be reduced in size, and consequently, the probability that the aircraft will impact a person is also reduced.

Although this could technically be used in any operational scenario, the group felt it best to be conservative and assume that in less populated environments, the aircraft does not encounter obstacles. An applicant could utilise the following models to justify a reduction in lethal area using M2 in these sparsely populated environments.

This effect will reduce  $P(\text{fatality}|\text{collision}, \text{GI})$  in Equation (2). For the iGRC table, this value is assumed to be the density of people on the ground. But when introducing obstacles, this value can be reduced since there is a certain probability that the aircraft will impact an obstacle, reducing the critical area.

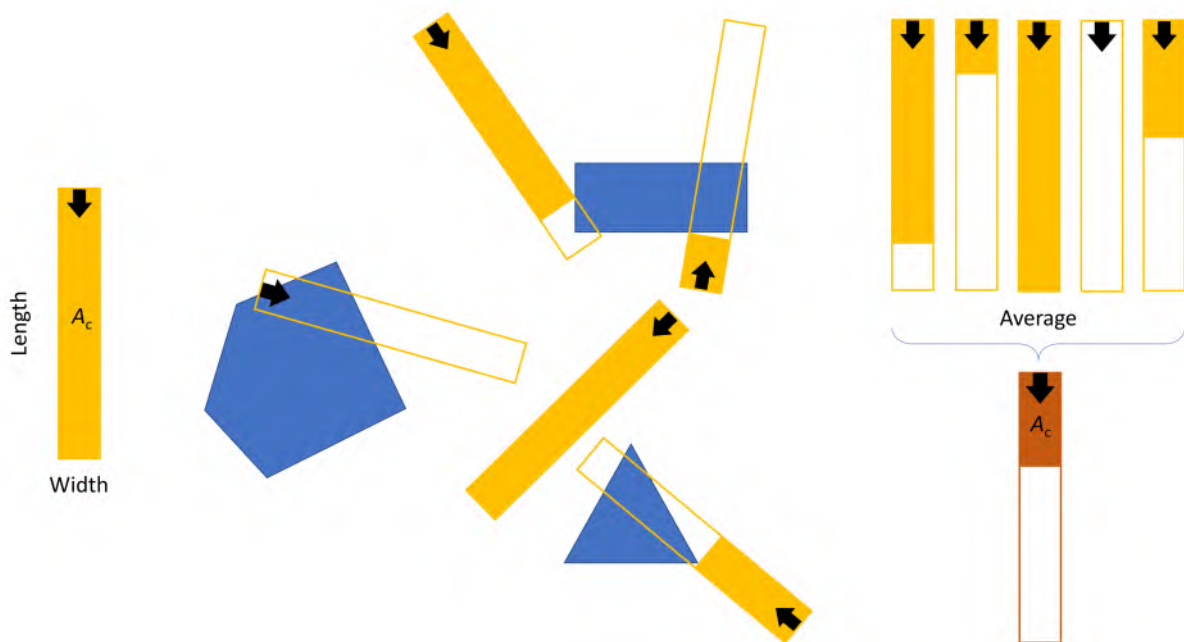


Figure 28: The concept of reduced CA due to obstacles: The nominal critical area is shown on the left. The yellow rectangle represents the ground area covered by the aircraft and the black arrow the direction of travel. In the middle are three obstacles (convex polygons) and 5 random crashes. The "empty" part of the CAs are discounted due to the obstacle stopping the aircraft. On the right, the 5 effective CAs are averaged to get the reduced CA (dark orange).

The actual reduction in the critical area can be determined either through simulation or through derivations. The concept of reduction is shown in Figure 28. Here the nominal critical area from the JARUS model is shown on the left. We will then assume that there are a number of obstacles of varying shape and size scattered randomly across the ground area. In the figure, these are represented by three blue polygons. If a critical area touches one of the obstacles, we will assume that this stops the aircraft, and the critical area is reduced to extend from the black arrow to where it hits the obstacle. Five examples of different reductions in the critical area are shown.

Assuming also that the aircraft may crash with equal probability at any location and equal probability in any direction, we scatter a number of crashes across the map. We then measure the reduction in each case and take the average. The result is a reduced critical area, which will be used in the continued computation instead of the nominal critical area.

Note that the implemented process is more involved. The following must all be observed

1. Since the area has a number of obstacles added, the effective area where people can be hit is reduced by the joint area of the obstacles, which in the fatality computations is addressed by a comparative increase in population density.
2. The determination of the average involves thousands of examples, and not just five.
3. It is possible to determine distribution of CA sizes for a given set of obstacles through modeling rather than simulation with thousands of examples.
4. The reduced size of the CA is not only a function of the average size and shape of obstacles, it is also possible to vary the critical area as a function of width and length of the aircraft.

These items are explained in more detail in section [B.4](#).

### A.5.3 Obstacles versus sheltering

In the initial equations (2) and (3) for the fatality rate, there is a factor to account for sheltering of people. With this factor, it is possible to include an assumption on the fraction of the population that is sheltered in some fashion. Any sheltered person is considered safe from a descending aircraft and thus cannot be impacted. A typical shelter is a normal house, and an assumption of people being indoors, for instance, during nighttime, would result in a sheltering factor of less than 1.

Sheltering effectively means that a person who would be in the path of a descending aircraft is not impacted because the aircraft impacts the house first and, thus, is stopped before reaching the person. Obstacles work the same way, i.e., arresting an aircraft such that it may not impact a person that would have been impacted if the obstacle was not present.

An obvious question is therefore: If assuming a sheltering factor  $F_{\text{exp}}$  less than 1 due to some fraction of people being indoors and assuming that the houses people are in are also obstacles, would this be taking credit for the same reduction twice? In other words, is it reasonable to assume both sheltering in houses and using the houses as obstacles at the same time?

**The answer is yes.**

This is because houses (and similar structures that people can be in) can serve a double and independent purpose as both sheltering and obstacles. So everyone that is indoors is excluded from the fatality rate in Equation (3) through the factor  $F_{\text{exp}}$ . But anyone outside is still subject to the risk of impact and can benefit from any obstacle in the area, including the houses that provide shelter to (other) people. Sheltering can also be seen as a reduction in the “people exposed” population density.

This is illustrated in Figure 29. There are 15 critical areas, which all present the same crash. The five columns each have different (semi) random distribution of people. There are only three people in every crash to make the figure simple, but they could represent, say, a density of 3,000 ppl/km<sup>2</sup>. The first row shows how the CA, in some cases, will coincide with one or more people. The second row shows how the CA is reduced in size because we have introduced an obstacle. And the third row shows the case when 1/3 of the people have gone indoors (and are thus sheltered). If we let the blue box be a house, people may well be inside it. They may also have gone elsewhere to be indoors. Or they may, in fact, have left the area. In either case, it is irrelevant to the computation.

For all 5 cases in the first and second row, three people are exposed to the aircraft crashing. In some cases, no one is impacted. In other cases, one or more people are impacted. For the first row, we can, in fact, compute the average number of people impacted by a crash. This is simply the size of the CA times the population density (measured in ppl/m<sup>2</sup>).

In the second row, the obstacle will stop the aircraft short, and the effective CA is reduced compared to the nominal CA. This means that compared to the first row, of all the people impacted, some will still be impacted (if they are on the "wrong" side of the obstacle). But some will not because they now are now in the "shadow" of the obstacle. The average number of people impacted by a crash is still the size of the CA times population density, but the CA is now reduced, thus reducing the average number of people impacted.

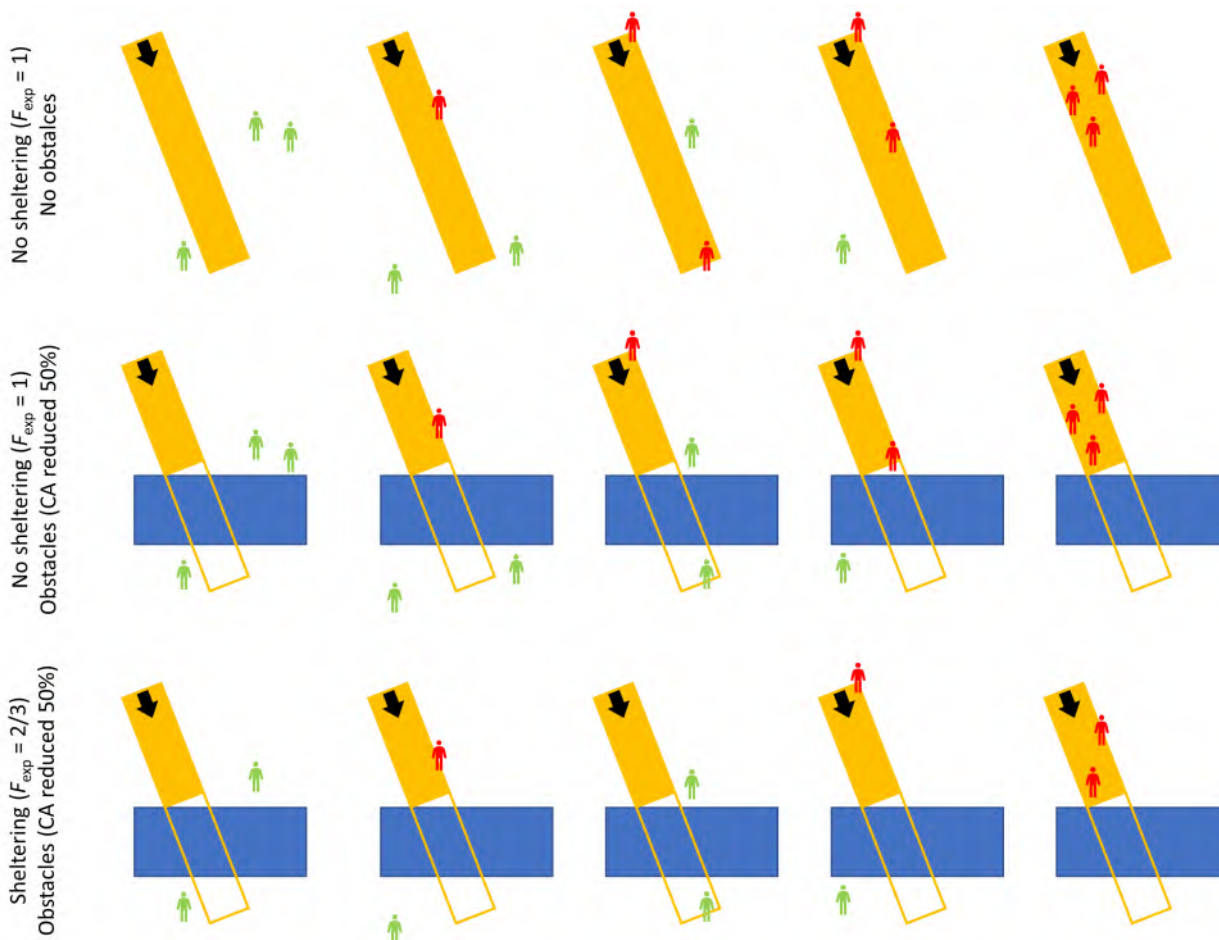


Figure 29: Progression from no sheltering and no obstacles in row 1, to introducing obstacles in row 2, to adding sheltering in row 3. Each column shows some (semi) random distribution of three people.

In the third row, one of the three people (picked at random) is now indoors and will, therefore, never get impacted. This effectively reduces the number of exposed people. The reduced CA is still the same as in row two, but the average number of people impacted is further reduced (by a factor  $F_{exp}$ ).

It is important to note that if we swap rows two and three, that is, doing sheltering before obstacles, the arguments remain the same. This is also seen from the fact that both sheltering and obstacles give a reduction in the fatality rate as a factor. And the order of factors does not alter the product.

In addition, if we do not have sheltering (omitting row three), or if we do not have obstacles (omitting row two), the argument for the other non-omitted row remains the same. Consequently, obstacles and sheltering are independent.

It is also important to note that green and red people in Figure 29 are NOT randomly placed (if so, the figure would most likely have no or only one red person). This is because the figure is meant to demonstrate the concept and not portray the result of actual random placement. In fact, the fifth column, where all people are impacted, has a much, much lower probability of occurring than the

first column, where no people are impacted.

#### A.5.4 Density of obstacles

The key question is, of course, how much this value is reduced for a given density of obstacles. To determine this, consider a critical area for a crash where there are a number of obstacles in the path of the aircraft. All considered obstacles have to be sufficiently sturdy to stop or significantly slow the aircraft in both glide and slide and will depend on the aircraft characteristics such as mass and speed (i.e., a bush may stop a 3 m aircraft but not an 8 m aircraft).

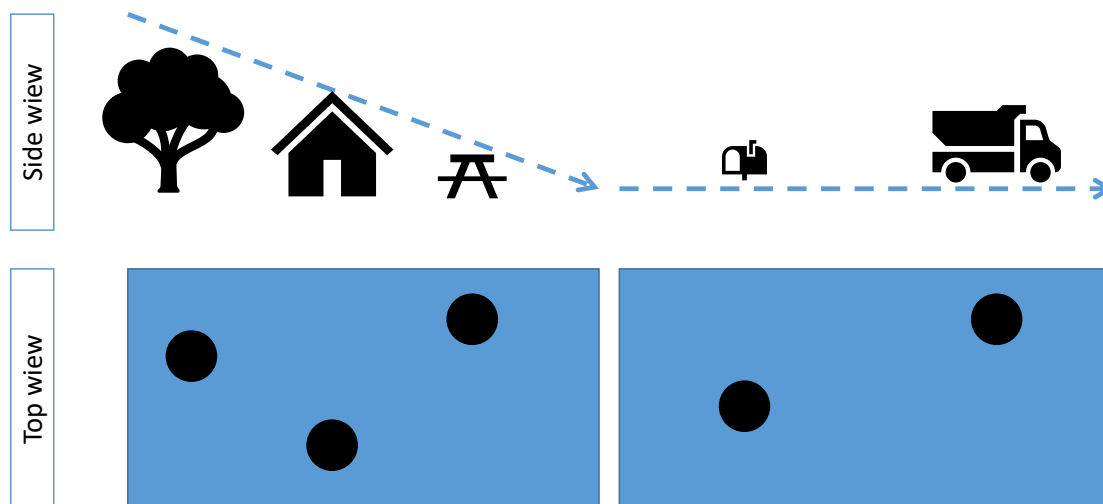


Figure 30: Illustration of the influence obstacles have on critical area

A simple conservative model was developed where obstacles were distributed randomly and evenly (i.e., according to a uniform distribution) in the area the aircraft is flying over as point masses tall enough to stop the aircraft's glide path. Thousands of crashes were simulated and projected onto this area where the aircraft would stop when it came into contact with an obstacle, and the critical areas were determined and summarized. The results showed that as the population density increases, the average critical area will decrease as expected. For a population density of 1,500 ppl/km<sup>2</sup>, it was shown that 70% of all critical areas for a 3 m wingspan aircraft was less than 120 m<sup>2</sup>.

For the 8 m wingspan, it was shown that 90% of all critical areas are less than 700 m<sup>2</sup>. This is expected to be conservative.

### A.6 Creating the Final iGRC Table

#### A.6.1 Introduction

Sections 1 and 2 described the development process for the iGRC Table, outlining how the variables in Equation (5) underpins an idealised iGRC table. It was also highlighted that there could be endless permutations of critical area and population that could produce integer increments in the iGRC. In Section 2, 2 a the pairings were multiples of 2 for critical area (eg 20, 200, 2000 etc) whilst population was incremented in multiples of 10. The final iGRC ultimately used multiples of 6.5 for critical area, and multiples of 5 for population as shown in Table 30 are derived.

Table 30: Raw iGRC Scores with Final Population and Critical Area values

<b>Max UAS Characteristic Dimension</b>	<b>1 m</b>	<b>3 m</b>	<b>8 m</b>	<b>20 m</b>	<b>40 m</b>	
<b>Maximum Speed</b>	<b>25 m/s</b>	<b>35 m/s</b>	<b>75 m/s</b>	<b>120 m/s</b>	<b>200 m/s</b>	
<b>Max critical area [m<sup>2</sup>]</b>	<b>6.5</b>	<b>65</b>	<b>650</b>	<b>6500</b>	<b>65000</b>	
<b>Intrinsic Ground Class Value</b>						
<b>Max population density [ppl/km<sup>2</sup>]</b>	<b>Controlled</b>	1	2	3	4	5
	< 5	2	3	4	5	6
	< 50	3	4	5	6	7
	< 500	4	5	6	7	8
	< 5000	5	6	7	8	9
	< 50,000	6	7	8	9	10
	> 50,000	7	8	Not part of SORA		

**Note:** Maximum Speed is the maximum possible commanded airspeed of the UA, as defined by the designer.

### A.6.2 Critical Area Calculations

Section A.2.3 described three descent scenarios which were examined to establish suitable critical area values for the iGRC Table. These were a glide descent, cruise descent, and ballistic descent and are illustrated in Figure 26. The determination of critical area values for each of these scenarios is based on the JARUS Critical Area model which is presented in Section B.3. The difference between the descent scenarios, relative to the JARUS model, is impact speed, impact angle, and coefficient of restitution (which depends solely on the impact angle). These values are shown in Table 28 and explained in more detail in section A.3.

The final calculation in Table 31 is the application of the obstacles model reduction to the raw critical area in Row 13 to achieve the final value shown in Row 14. Put simply, a 40% reduction is applied to raw value, for all wingspans greater than 1 m and less than or equal to 20 m. More details on the obstacle model and basis for the reduction is provided in Appendix B.4.1. It is important to note that the calculations shown in Table 31 are based on variable choices that produced Critical Areas in multiples of 8 (8, 80, 800 etc). In contrast, the final iGRC results for Critical Area values in multiples of 6.5. The results for these calculations are not shown.

It is also emphasised that the critical area for 1 m wingspan UAs only considers the glide and not slide, as the slide is considered non-lethal. The influence of obstacles on larger wingspan platforms (>20 m) is not easily modelled, so no obstacle reductions are used for this column.

Table 31: Critical area calculations for the three scenarios. When there is one row, the values are identical for all scenarios. When there are three rows, each row represents the three scenarios. The variable names refer to the JARUS model. The numbers in parentheses refer to the equation used for computing the variable. This table can be generated using `AnnexFTables.scenario_computation_table()` in CasEx.

Row	Name	Variable	Values				
1	Maximum UAS Characteristic Dimension [m]	$w$	1	3	8	20	40
2	Mass [kg]	$m$	3	50	400	5,000	10k
3	Maximum Speed [m/s]	$v$	25	35	75	150	250
4	Impact angle [deg]	$\theta$	35	10	10	10	10
			35	35	35	35	35
			35	35	35	35	35
5	Impact speed [m/s]	$v$	16	23	49	98	130
			25	35	75	120	200
			24	40	60	106	121
6	Aircraft width + buffer [m]	$2r_D$ (59)	1.6	3.6	8.6	20.6	40.6
7	Glide Distance [m]	$d_{\text{glide}}$ (58)	3	10	10	10	10
			3	3	3	3	3
			0	1	1	1	1
8	Non-lethal speed [m/s]	$v_{\text{non-lethal}}$ (70)	N/A	3.4	1.2	0.3	0.2
9	Horizontal Speed at impact [m/s]	$v_{\text{horizontal}}$ (57)	13	22	48	96	128
			20	29	61	123	164
			6	18	33	66	63
10	Coefficient of restitution [-]	$e$ (51)	0.74	0.80	0.80	0.80	0.80
			0.74	0.74	0.74	0.74	0.74
			0.63	0.67	0.68	0.70	0.68
11	Horizontal speed after impact [m/s]	$e v_{\text{horizontal}}$	10	18	38	77	102
			15	21	45	91	121
			4	12	23	46	43
12	Reduced slide distance [m]	$d_{\text{slide, reduced}}$ (72)	0	26	123	492	874
			0	34	161	643	1,141
			0	16	58	243	210
13	Time to safe speed [s]	$t_{\text{safe}}$ (71)	0.0	2.4	6.0	12.4	16.5
			0.0	2.8	6.9	14.1	18.9
			0.0	1.7	4.1	8.5	8.1
14	Raw critical area [m <sup>2</sup> ]	$A_C$ (69)	5	140	1,202	11k	37k
			5	143	1,462	14k	48k
			2	69	568	5,177	9,860
15	Critical Area reduced by 40% for obstacles [m <sup>2</sup> ]	$0.6A_C$	N/A	84	721	6,402	N/A
				85	877	8,182	
				42	341	3,106	

### A.6.3 Finalisation of iGRC Table

The final critical area values across glide, cruise and ballistic descent were recalculated using the finalised variable values in Table 3 with results shown in Table 32. Note the critical areas do not include skid for the 1<sub>st</sub> column, with the last column not including obstacle reductions.

Table 32: Final Critical Area Calculations using variable values from 3

Descent Configuration	Wingspan				
	1	3	8	20	40
Glide (scenario 1)	10.2	59.3	429.3	6002	20835
Cruise (scenario 2)	2.5	62.7	607.8	5595	32719
Ballistic (scenario 3)	2	42	314	3,106	9,860
<b>Final Critical Area Values</b>	6.5	65	650	6,500	65000

The bottom row of the table captures the critical area value employed in determining the allowable iGRC scores that maintain TLOS, given population multiple of 5, 50 etc. As can be seen, these critical areas are some multiple of 6.5 (i.e. 6.5, 65, 650 etc). These were then used to calculate raw iGRC scores shown in Table 33. These were rounded down in accordance with the rounding policy in Section 2 to produce the final iGRC table used in the main body of SORA 2.5.

It should be noted that the Glide and Cruise Impacts, generally produce similar critical areas, as the impact angle and the horizontal component of the impact velocity vary inversely. For the Cruise Scenario, its assumed that the Cruise is conducted at the maximum possible commanded airspeed

Table 33: Final iGRC Table with Critical Areas included

Max UAS Characteristic Dimension	1 m	3 m	8 m	20 m	40 m	
Maximum Speed	25 m/s	35 m/s	75 m/s	120 m/s	200 m/s	
Max critical area [m <sup>2</sup> ]	6.5	65	650	6500	65000	
Intrinsic Ground Class Value						
Max population density [ppl/km <sup>2</sup> ]	Controlled	1.0	1.0	2.0	3.0	3.0
	< 5	2.50	3.50	4.50	5.50	6.50
	< 50	3.50	4.50	5.50	6.50	7.50
	< 500	4.50	5.50	6.50	7.50	8.50
	< 5000	5.50	6.50	7.50	8.50	9.50
	< 50,000	6.50	7.50	8.50	9.50	10.50
	> 50,000	7.50	8.50	9.50	10.50	11.50
	> 250,000	7.50	8.50	Not part of SORA		

## B Critical area modelling

This appendix describes the math behind the models that form the basis of the JARUS critical area model. First, in section B.1, the models from literature referenced in 2.3 are described in some detail, followed by explanations for the various model components. The actual math for each model is presented in section B.2, and the math for the JARUS model is presented in section B.3.

### B.1 Existing Model Comparison

We have considered a few models for computing the critical area. Below is a review of these models. There are more models in the literature, but they are generally similar to one of the models described below, and as such not included here.

- RCC model [3, p. D-4]  
This model is relatively simple consisting of a glide distance plus a slide distance multiplied by the width of the aircraft, effectively computing the area swept by the aircraft.
- RTI model [4, p. 3-11, 53]  
This model is developed for critical area for falling inert debris from failed rocket launches. It includes the following components; glide, slide, bounce, and splatter. The glide part is similar to the RCC model. The bounce and splatter are relatively complicated models for the dynamics of fragments moving across terrain in a non-sliding way. These two components will not be discussed in this annex for reasons given above.
- FAA model [5, p. 99-103]  
This model is for falling inert and explosive debris from launch vehicles. It includes secondary effects, which can be significant for launch vehicles. For this annex only the inert debris part is used. The model only includes glide (no slide), and is equal to the RTI glide model plus the secondary effects.
- NAWCAD model [6, p. 11-47]  
This model is actually a collection of models for fixed wing dive and glide plus skid (slide), and rotary wing dive and autorotation. The fixed wing model is similar to the RCC model, although the slide length is from impact to a safe speed (no longer injuries to people) rather than to zero speed. Note that this difference is negligible for larger aircraft. The rotary wing dive model is similar to the fixed wing dive except it assumes terminal velocity (see below), and the rotary wing autorotation model is a pure glide based on autorotation properties of rotorcraft. This source also has a blade throw model, which is a ballistic model (differential equations) that includes drag and air tumbling. Finally, this source also has a model for deflagration (damage/injury due to heat).
- Deflagration model [7, p. 84–89]  
This model basically predicts the distance from the center of deflagration where it is lethal to be. This computation uses the energy density in the fuel for determining the potential heat production. Lethality can occur either through thermal radiation or by actually being inside the fireball. Since either are lethal the singular distance predicted is the maximum of the two distances.

#### B.1.1 Bounce and splatter/cratering

Aircraft or pieces of debris that remain largely intact after impact may bounce (or ricochet) along the ground, thus increasing the critical area. A piece may have multiple bounces before coming to

rest. Splatter is the aircraft breaking up upon impact and cratering is deformation of the impacted ground. Some part of the initial kinetic energy may be spent in this process. This is expressed by the coefficient of restitution. The dispersing of fragments from splatter will cover a certain area, which then becomes part of the critical area.

The slide, bounce, and splatter all take energy from the initial kinetic energy in the aircraft just prior to ground impact. As such, if some energy is consumed by splatter, comparatively less is available for bounce and slide. In addition, these components are, for individual pieces of debris, mutually exclusive, since a piece cannot simultaneously slide and bounce, nor splatter.

To what extent an unmanned aircraft will exhibit slide, bounce, and/or splatter depends to a large extent on the aircraft size, type, construction and the surface being impacted. Smaller fixed wing aircraft may bounce, while larger rotorcraft may mostly splatter, and larger fixed wing may break up, but still largely slide. Since we cannot reasonably determine an appropriate one-size-fits-all distribution of energy between these three components, this annex will use slide combined with the assumption of dissipation of energy on impact as expressed by the coefficient of restitution (dissipated to cratering and aircraft deformation). In addition, slide is by far the simplest of the three components to model for a generic situation.

### **B.1.2 Secondary effects**

Only the FAA model for falling inert debris includes the secondary effects, that is, fatalities resulting from debris being scattered around the impact area. The scattering area is modelled as a disc around the impact point, and is in general significantly smaller than the slide area in the other models. The scattering depends on how hard the impact surface is, and works best for more steep descent. Since slide area typically is significantly larger than secondary effects, secondary effects will be disregarded.

### **B.1.3 Explosions**

Explosions are defined as rapid increase in volume and release of energy in an extreme manner, typically resulting in a supersonic shock waves. The pressure from this shock wave (overpressure) can be lethal. When an explosion is relatively slow, it is called deflagration. This is subsonic combustion propagating by means of heat transfer; hot burning material heats the next layer of cold material and ignites it. This is how aviation propellant such as gasoline and jet fuel typically burns. Burning such fuels requires oxidizer (unlike explosives). Since there is typically little oxygen in the fuel tank, the fuel has to be released from the tank and vaporized in order to burn. While it is possible with the correct fuel vapor and air mixture to get a violent deflagration akin to an explosion, this state is rarely present in crashes of unmanned aircraft. As a consequence, a model for fatalities resulting from pressure change due to a shock wave (i.e. explosion) is typically not applicable for aviation fuel “explosions” and thus not used in the JARUS model. [6, p. 55]

If the aircraft is carrying explosives, the blast effects of an explosion can be modelled according to [56, p. 31–33].

### **B.1.4 Deflagration**

The primary release of energy in deflagration is through heat rather than pressure. As a result the critical area will typically be much smaller than for an explosion with the same energy release. There are two components in deflagration lethality; the fireball itself and the thermal radiation. We will assume that being inside the fireball is lethal, and we will assume that being exposed to a



Figure 31: Examples of gasoline “explosion” (deflagration) on the left and true explosion (notice the shock wave on the ground) on the right. Right image is from United States Department of Energy.

certain amount of thermal radiation is also lethal. It is assumed that the deflagration component of the critical area will be within the slide area and thus it is not added to the JARUS model.

Deflagration is modelled in [7, p. 84–89].

### **B.1.5 Blade throw**

For rotorcraft blades may pose a danger due to their intrinsic high kinetic energy. Upon impact with terrain the blades may come loose and consequently be thrown quite far. While a loose blade indeed has the potential of inflicting substantial injury, the probability of being impacted by such a blade is relatively small. A rotor blade disconnecting from the rotor head at relatively high RPM will initially continue in a straight line with the leading edge first. However, since the center of gravity is typically towards one end of the blade the general motion will tend towards a dart-like motion, given the blade a relatively small frontal area upon impact (assuming some distance from the crash). Even for modest distances the probability of being impacted is negligible. For this reason, blade throw is not considered in this annex. However, if blade throw is required for obtaining a realistic critical area, a fairly comprehensive blade throw model is presented in [6, p. 35-47].

### **B.1.6 High-energy rotating parts**

Some aircraft will have internal or external parts that rotate fast as part of the power unit. These can be parts of the power unit, such as turbine or compressor wheels, parts of the trust/lift device, such as propellers and rotor blades, and parts of the drive train, such as gears and belts. Due to the kinetic energy stored in the rotating part, it may cause injury upon contact with a person. In this Annex, the nominal assumption is that any contact with the aircraft is lethal, and therefore the concern will only be for parts that have separated from the aircraft upon impact. For most unmanned aircraft, such parts would typically be relatively small and not very likely to separate, and since the critical area model is relatively conservative by construction, rotating parts are not included in the model.

## B.2 Mathematics behind models

This document gives an introduction to a range of models for determining the critical area for a descending aircraft. The models are presented with a unified terminology and use of variables rather than referencing the terminology and choice of variable names in the individual models. All variables used are also listed in Appendix D.

In addition, some derived variables are common to multiple models. The horizontal impact velocity and the glide length (airborne part of the "crash") are given as

$$v_{\text{horizontal}} = v \cos \theta , \quad (57)$$

$$d_{\text{glide}} = \frac{h_{\text{person}}}{\tan \theta} . \quad (58)$$

Note that  $d_{\text{glide}}$  is defined to be 0 for a vertical impact, i.e.  $\theta = 90$  deg. In addition, the combined 'aircraft radius' and person radius appear numerous times, so for convenience, we also define

$$r_{\text{D}} = r_{\text{person}} + \frac{w}{2} . \quad (59)$$

We will present the following models, which are here named after their primary reference:

- RCC [3]
- RTI [4]
- FAA [5]
- NAWCAD [6]
- Deflagration [7]
- JARUS

All units in this document are metric, which means that some of the formulas are different from the sources to accommodate this. References to equations and formula in the references are given as "equation x", while references to equations in this document are given as (x).

### B.2.1 RCC model

This model is found at the end of [3] on page D-4. It defines

$$A_{\text{C}} = 2r_{\text{D}}(l + d_{\text{glide}} + d_{\text{slide}} + 2r_{\text{person}}) ,$$

and states that typically  $r_{\text{person}} = 1$  ft and the glide distance is typically based on  $h_{\text{person}} = 6$  ft. This model does not provide any formula for determining the slide distance. For the purpose using this mode, we have computed  $d_{\text{slide}}$  in the same way as the RTI model, i.e. based on friction.

This model assumes a rectangular critical area both for glide and slide. It include the length of the aircraft to include the effect that a person may be impacted by the end of the aircraft during glide. Note that this is the only model that depends on the length of the aircraft.

## B.2.2 RTI model

The RTI model is from [4] and is for estimating casualty area for falling inert debris from missile and space vehicles. The model covers a range of effect for such debris, but this brief presentation will only include glide, slide, and the coefficient of restitution associated with bounce. The RTI model is combined from the glide model in equation 4 on page 6 in [4] and the slide model in equation 5 on page 8. It is given as

$$A_C = 2r_D(d_{\text{glide}} + d_{\text{slide}}) + \pi r_D^2 . \quad (60)$$

The slide distance is determined based on the standard friction equation

$$F = -C_g mg ,$$

where  $F$  is the friction force. This can be rewritten to

$$d_{\text{slide}} = \frac{(ev_{\text{horizontal}})^2}{2C_g g} , \quad (61)$$

where  $e$  is the coefficient of restitution from equation 7 on page 12. The RTI model explicitly states the following two assumptions on page 10 for a non-bounce impact:

- The vertical component of the impact velocity is zero after impact.
- The horizontal component of the impact velocity is unchanged after impact.

These assumptions are in fact also implicitly made in all the other models, except the FAA model. However, using the bounce equation the second assumption no longer holds, as the coefficient of restitution in Equation (61) reduces the horizontal velocity.

The friction coefficient is stated to often be between 0.5 and 0.7, although this is for space vehicle debris, and may be lower for especially a non-damaged aircraft fuselage.

This models uses a circular start and end of the critical area. This probably stems from the model being initially used to determine vertical impact of debris, which naturally does not have a travel direction. The different to the RCC model is negligible for wide set of parameter values, especially if  $l \approx w$ .

## B.2.3 FAA model

The FAA model [5] is also developed to capture debris from space vehicle launch and reentry. This model does not have slide, but uses secondary effects instead, which means fatalities resulting from debris from the initial impact ricocheting or sliding from the impact. The assumptions it that this happens equally in all directions.

The initial area for this model, as given by equation 12 and 13 on page 99, is the same as the glide area in the RTI model, i.e.

$$A_{\text{glide}} = \pi r_D^2 + 2r_D d_{\text{glide}} . \quad (62)$$

The additional area from the secondary effect is given by

$$A_{\text{secondary}} = \pi \left( r_{\text{person}} + \frac{w}{2} \sqrt{F_A} \right)^2 , \quad (63)$$

where  $F_A$  is defined as "the ratio of the area containing secondary debris impact effects and the projected area of the fragment". This number can vary significantly; a table with proposed numbers is provided in Table 6-5 on page 98.

The primary and secondary effect areas will overlap, and to determine the total critical area, this overlap needs to be determined, so as to not count twice. This is done on page 102-103 in equations 15 through 20 effectively by computing the additional area  $A'$  that Equation (62) gives beyond the secondary effect area in Equation (63). For this, first define

$$r_F = r_{\text{person}} + \frac{w}{2} \sqrt{F_A} .$$

Then this area is found by integrating

$$A' = 2 \int_0^u d_{\text{glide}} + \sqrt{r_D^2 - y^2} - \sqrt{r_F^2 - y^2} dy .$$

Assuming that  $u \leq r_D$  and  $u \leq r_F$ , we get

$$A' = 2ud_{\text{glide}} + r_D^2 \arcsin\left(\frac{u}{r_D}\right) + u\sqrt{r_D^2 - u^2} - r_F^2 \arcsin\left(\frac{u}{r_F}\right) - u\sqrt{r_F^2 - u^2} . \quad (64)$$

Note that Equation (64) corrects an error in equation 16 in [5]. Now,

$$u = \begin{cases} 0 & d_{\text{glide}} \leq r_F - r_D \\ r_D & d_{\text{glide}} > \sqrt{r_F^2 - r_D^2} \\ \frac{\sqrt{(2r_F d_{\text{glide}})^2 - (r_F^2 + d_{\text{glide}}^2 - r_D^2)}}{2d_{\text{glide}}} & \text{otherwise} . \end{cases}$$

Note that  $u = 0$  is for the scenario where the secondary effect critical area completely covers the glide critical area.

## B.2.4 NAWCAD model

This model is from [6], a report from the Naval Air Warfare Center Aircraft Division (NAWCAD). Unlike the previous models, this focuses on the critical area resulting from crash of an unmanned aircraft. It models the glide and slide similarly to the RCC model, uses friction for determining the slide distance, but also includes a reduction of the slide distance to accommodate the notion that a sliding aircraft becomes non-lethal before common to complete rest. The model is given in equations 9, 10, 14, 15, 16, together with equation 17 for fixed wing.

The maximum non-lethal kinetic energy is  $K_{\text{non-lethal}}$ , which gives the sliding aircraft a maximum non-lethal speed of

$$v_{\text{non-lethal}} = \sqrt{\frac{2K_{\text{non-lethal}}}{m}} . \quad (65)$$

Assuming that the acceleration of the aircraft during slide is  $-C_g g$ , the time from impact to this speed is reached is

$$t_{\text{safe}} = \frac{v_{\text{non-lethal}} - v_{\text{horizontal}}}{-C_g g} . \quad (66)$$

If  $t_{\text{safe}}$  becomes negative (which will happen if the horizontal impact speed is less than the lethal speed), it is set to zero. The slide distance during this time is

$$d_{\text{slide, reduced}} = v_{\text{horizontal}} t_{\text{safe}} - \frac{1}{2} C_g g t_{\text{safe}}^2 . \quad (67)$$

Note that Equations (66) and (67) correct errors in equation 15 and 14 from [6], respectively. The complete model is given in Equation B.2.4 for a fixed wing as

$$A_C = 2r_D(d_{\text{glide}} + d_{\text{slide, reduced}}) .$$

## B.2.5 Deflagration model

There are two models for lethality in relation to deflagration; fatality as a result of thermal radiation and lethality as a result of being inside the fireball. The models for these are found in [7] on pages 84-89. The purpose in this context is to model the effects of deflagration of the aviation fuel.

The lethal distance for thermal radiation is determined as ([7] equation 162)

$$d_{\text{thermal}} = Z(cM)^{1/3} ,$$

where  $Z$  is the thermal hazard factor (unit  $\text{m}/\text{kg}^{1/3}$ ),  $c$  is the TNT equivalent factor for the fuel, and  $M$  is the amount of fuel in kg. The hazard factor can be determined from Figure 10 in [7]

$$Z = \frac{\log\left(\frac{3663}{p} - 6952\right)}{14.839} , \quad (68)$$

where  $p$  is the probability of lethality. It is important to note that Equation (68) is only valid for  $p \leq 0.5$ , and that  $\log$  is the natural logarithm.

The TNT equivalent factor is found as the ratio of energy density in the fuel to that of TNT. For aviation fuel such as gasoline and jet A1 this ratio is typically round 10.

The radius of the fireball can be determined as (equation 164)

$$d_{\text{fireball}} = 1.496(cM)^{0.36} .$$

The lethal area is then determined as the size of the circle with a radius equal to bigger of the two distances, which will be the fireball except for very low values of  $p$ .

Do note that the above models are based on the assumption that all fuel is deflagrated immediately and ideally, which requires the fuel to be vaporized and in an ideal mix with oxidizer. This state is virtually impossible to achieve during a crash, and the models thus are somewhat conservative.

## B.3 JARUS critical area model

The model presented here is an attempt to take the best from the above models to suit the needs of the iGRC table. The goals for the JARUS models are

- as few parameters as reasonable, and
- cover all aircraft reasonably expected to be in the Specific category.

To this end, the JARUS model is a combination of the RTI and NAWCAD models, that both feature glide and slide. The former omits the length of the aircraft from the modelling, but largely maintains the modelling effect of this length by using a circular start and end of the glide/slide area. The NAWCAD model includes the reduction of the slide length, which is especially relevant for the smallest of the specific category aircraft. In addition, the RTI model uses the coefficient of restitution to account for energy dissipated to the environment and aircraft deformation.

Consequently, the model is given as Equation (60) with the reduced glide distance from Equation (67) and reduced residual horizontal speed as given by multiplication with coefficient of restitution, as in Equation (61). So,

$$A_C = 2r_D(d_{\text{glide}} + d_{\text{slide, reduced}}) + \pi r_D^2 , \quad (69)$$

where we have from Equations (65), (66), and (67)

$$v_{\text{non-lethal}} = \sqrt{\frac{2K_{\text{non-lethal}}}{m}}, \quad (70)$$

$$t_{\text{safe}} = \frac{v_{\text{non-lethal}} - e v_{\text{horizontal}}}{-C_g g}, \quad (71)$$

$$d_{\text{slide, reduced}} = e v_{\text{horizontal}} t_{\text{safe}} - \frac{1}{2} C_g g t_{\text{safe}}^2. \quad (72)$$

## B.4 Critical area reduction due to obstacles

When an aircraft crashes the ground is typically not just a flat plane with nothing but people. In most cases, there will also be a number of objects on the ground that will constitute obstacles for the crashing aircraft. This could be trees, houses, cars, masts, and so on. And the aircraft may impact obstacles both during the glide phase and the slide phase of the crash. Consequently, the CA of the aircraft may be shortened if the aircraft impacts an obstacle during the traversal of the length of the CA. This, in turn, reduces the probability that a person is impact by the aircraft. The aim of this section is to quantify this reduction. Obviously, there will be a significant diversity in the type of obstacles throughout various terrains and environments, and a useful model cannot faithfully capture all the details in this diversity.

The content of this section is an abbreviated version of "How obstacles may reduce the impact of a crashing unmanned aircraft" [57], which is an article written specifically to address the challenge of quantifying the effect of obstacles on a crashing aircraft. We will review two methods for determining a quantification of the CA reduction; through simulation and through modelling.

In Section B.4.1, we describe the processed used for modelling obstacles including properties and assumptions made. In Section B.4.2, the concept is demonstrated by mean of simulation, which provide some graphics to make the idea more tangible. And then in Section B.4.3 a mathematical model for computing the CA reduction is presented.

### B.4.1 Obstacles

An obstacle must be any object on the ground with the following properties:

- It is at least as high as a person (or close to, since a little less high has almost no effect on the modelling).
- It is sufficiently sturdy or heavy to stop the aircraft upon impact. For instance, a car will stop most aircraft, while a bicycle may not. Note that for smaller aircraft, more objects can be considered obstacles.
- The projection of the obstacles onto the ground can be represented well by a convex polygon.

For the purpose of simplicity, we will in the following use the term obstacle to mean the 2D convex polygon that represents the real world obstacle.

We will make the following assumptions on the set of all obstacles:

- It consists of obstacles with the same polygon shape. This could be a rectangle to represent houses.

- The size of the obstacles may follow a known distribution. This could be the length and width of houses, where both parameters are normally distributed.
- The location of the obstacles are uniformly distributed in two dimensions. That is, every obstacle can be anywhere with equal probability.
- It follows that the density of obstacles is the same everywhere.
- The density of obstacles (number of obstacles per area unit) is known.

It is important to note that there is no assumption that obstacles are disjoint. This means that two obstacles may overlap. This makes the derivations somewhat simpler, and will result in a more conservative estimation of the CA reduction (i.e. the actual reduction is higher than the method predicts). However, for realistic sets of obstacles, this effect is relatively small.

#### **B.4.2 CA reduction simulation**

The concept can be demonstrated with a simulation, as shown in Figure 32. Here we have distributed 800 rectangles representing obstacles in an area of 1,000 m by 1,000 m, which gives a density of 800 obstacles per square kilometer, or  $8 \times 10^{-4}$  obstacle per square meter. The obstacles are co-linear with each other, that is, they have the same orientation. The dimension of each obstacle is drawn from two normal distributions with mean 23 m and 9 m, for width and length, respectively. The standard deviations are 6 m and 2 m. The location of each obstacle inside the trials area is random and uniformly distributed. Note that obstacles may overlap, as described in the previous section. A fix-sized CA is used for the crash. This CA is 3 m wide and 67 m long, which coincides with the second column in the iGRC (which is limited to a CA of 200 m<sup>2</sup> for a 3 m wingspan aircraft). This CA has been added 200 times with random angles and random locations. Both are uniformly distributed. Every CA represents one possible crash. And for each crash, the intersection between the CA and any obstacle is determined. Since the CA has a direction, that is, a beginning and an end, we then remove the last part of the CA, as shown in Figure 28, resulting in 200 CAs which may or may not be reduced in size. All 200 CAs are shown in Figure 32. The part remaining after reduction is colored purple, while the reduced part is transparent (with black outline). Also, in the figure, any obstacle that resulted in a reduction of a CA is orange, while all other obstacles are green.

In this simulation, a few of the CAs do no impact any obstacle. There are also a fair number of CAs, which starts inside an obstacle, and are thus reduced to size 0, visualized as a purely transparent CA.

Note that while the number and size of obstacles attempts to replicate an actual suburban area, the number of crashes is arbitrary and serves only to demonstrate possible scenarios. There could have been 2000 crashes, but the graphics would be unnecessarily cluttered.

If the simulation is used to actually estimate a quantification of the CA reduction, significantly more CAs would have to be added. For this scenario size, at least some 100,000 crashes would be needed for a good estimation. By then making an accumulated histogram of over the sizes of the reduced CAs, it is possible to approximate the CDF for the size of a reduced CA. However, as a quicker and more flexible alternative, the mathematical model can be used.

If instead of the uniformly random distribution of houses, we use a distribution that mimics that of a suburban area, such as the one in Figure 33, the same simulation as above gives slightly higher values in terms of the CA reduction. As such, the random placement provides a conservative estimate of the CA reduction.

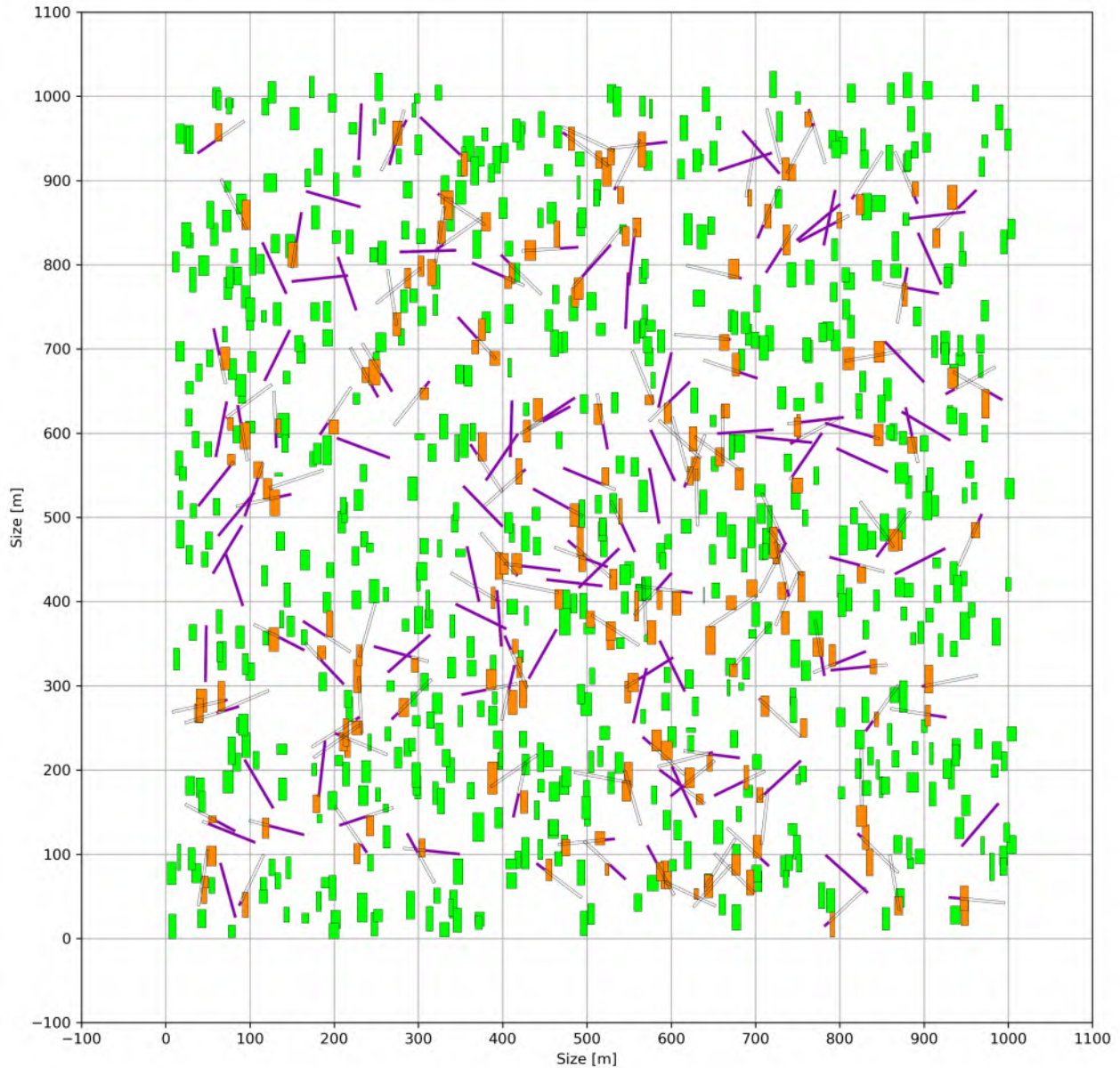


Figure 32: This image shows the result of 200 crashes. Each crash has the nominal CA (width 3 m and length 67 m) drawn as a rectangle. There are 850 obstacles as rectangles drawn in green (if not impacted by any crash) or orange (if impacted). The obstacles have width and length according to normal distributions  $N(17, 3)$  and  $N(8, 2)$ . Any part of a CA that "counts" is purple, while any part of CA that is inside or after an obstacle is transparent. Note that every CA in the simulation has a direction (a beginning and an end), but it is not shown in the image. The graph in Figure 34 is output of the mathematical model using the same parameters.

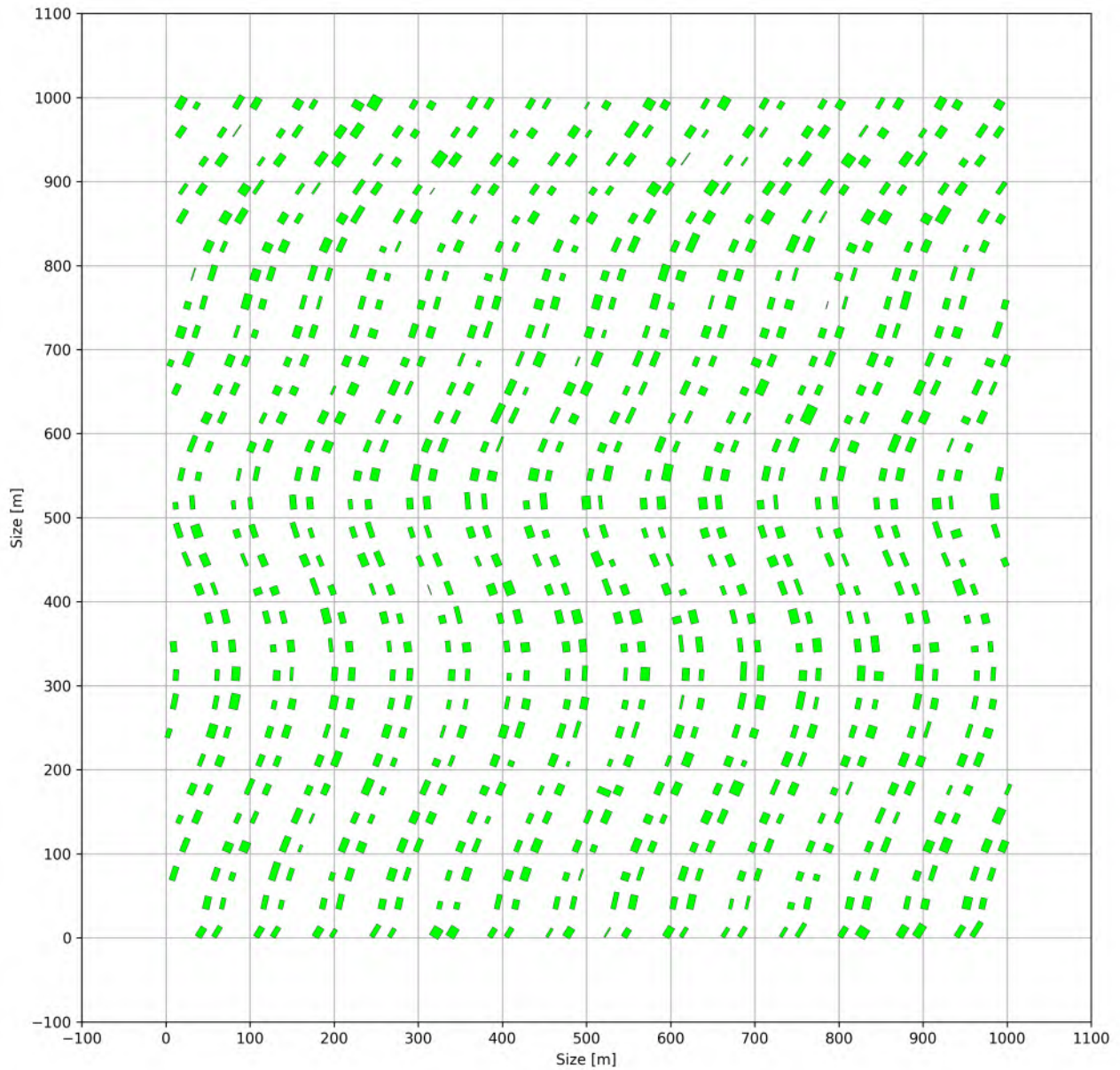


Figure 33: As an alternative to the random placement of obstacles, this shows a more realistic distribution if the obstacles are houses in a suburb.

It should be noted that in the following, all computations are based on 2D observations in the sense that the obstacles as well as the CAs are projected onto the ground. Consequently, there is an implicit assumption that all obstacles are 1.8 m tall, same as a human. Since most obstacles will be taller, the below computations are conservative, since taller objects will reduce the average CA more.

### B.4.3 CA reduction modelling

From [57], we get the following model for the probability of reducing the CA.

$$P(x) = \int \left[ 1 - \exp\left(-\mu \int |A_C^x \ominus A_{\Phi_{\text{ind}}, \Phi_{\text{com}}}| f_{\Phi_{\text{ind}}}(\phi_i) d\phi_i \right) \right] f_{\Phi_{\text{com}}}(\phi_c) d\phi_c . \quad (73)$$

The output of the model is the probability of the critical area being reduced to length  $x$ . The content of the models is as follows:

- $\mu$  is the obstacle density in obstacles per square meter.
- $A_C^x$  is a polygon of the critical area with length  $x$ . Effectively, this is a rectangle with side lengths equal to the wingspan and  $x$ .
- $A_{\Phi_{\text{ind}}, \Phi_{\text{com}}}$  is a convex polygon of an obstacle with size values (related to  $\Phi_{\text{ind}}$ ) and orientation value (related to  $\Phi_{\text{com}}$ ) drawn from the distributions  $f_{\Phi_{\text{ind}}}$  and  $f_{\Phi_{\text{com}}}$ .
- $f_{\Phi_{\text{ind}}}(\phi_i)$  is the distribution of the size parameters. For multiple parameters, this is a multidimensional function.
- $f_{\Phi_{\text{com}}}(\phi_c)$  is the distribution of the orientation parameter.

It is important to note that the distributions are in fact more general than described here, and can be interpreted as 'individual' and 'common' parameters which can pertain to other variables that size and orientation. For details on this, see [57]. However, for this presentation, the size and orientation interpretations will suffice.

In the model, the Minkowski difference  $\ominus$  is used. This is a particular way of combining two polygons, and relates to the detection of overlap between a critical area and an obstacle. The numerical value means the area of the polygon resulting from the Minkowski difference measured in square meters.

The CasEx package has a class that implements Equation (73) for rectangular obstacles where the lengths of the two side are given by normal distributions, the location is uniformly in 2D, and where the orientation of the obstacles is fixed to be co-linear with the coordinate system.

If we use the values from the simulation, that is, a wingspan of  $w = 3$  m, nominal CA length of 67 m, obstacle density of  $8.5 \times 10^{-4}$  (850 obstacles per square kilometer), and mean and variance for the normal distribution of the size of the obstacles as  $N(17, 3)$  and  $N(8, 2)$ , we can compute that  $P(120) = 0.55$ . This means that for this scenario, the probability that the CA is reduced to 120 m<sup>2</sup> or less is 55%.

If we switch from the random location in Figure 32 to the less random in Figure 33, we get  $P(120) = 0.64$ , that is, an increase of almost 10 percentage points over the random distribution of obstacles. This is based on simulation only, as we are still working on developing the theory for a non-random distribution.

The average value of the reduced CA can be computed from the CDF as

$$E[A_C] = w \int_0^{67} 1 - P(x) dx , \quad (74)$$

where the 67 is the length of the nominal CA and  $w$  is the width. For the random location scenario, we get  $E[A_C] = 109 \text{ m}^2$ . For the non-random scenario, we still do not have a  $P(x)$ , but estimated from simulation, we get  $E[A_C] = 90 \text{ m}^2$ , which is a significant reduction from the random scenario.

By running the model for multiple  $x$  values from 0 to the full length of the CA (67 m), we can draw a graph as shown in Figure 34. Since we do not (at the time of writing this) have a model for the more orderly placement of obstacles, we can simulate, and by simulating with sufficiently many crashes, it is possible to draw relatively smooth curve. This is also shown in the figure. Note that the graph

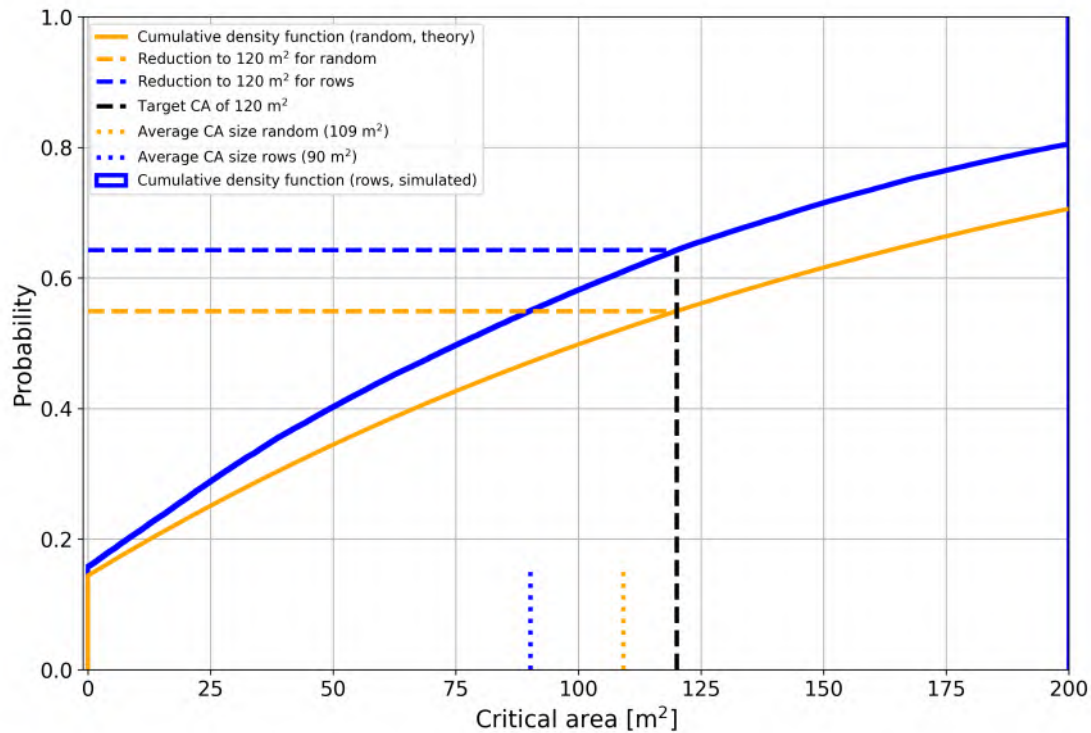


Figure 34: The orange curve shows the output of the model in Equation (73), which uses randomly located obstacles, while the blue curve shows the same concept using simulation for the neatly arranged obstacles (see Figure 33). The black dashed line shows the target of  $120 \text{ m}^2$ , with the orange and blue dashed lines showing the associated probabilities of 55% and 64%, respectively. The orange and blue dotted lines show the average CA sizes for the random obstacles and the obstacles in rows, respectively. The obstacle and CA parameters are identical to that of Figure 32 and Figure 33. This figure can be recreated with `figures.figure_obstacle_critical_area_reduction()`.

shows the CA size on the first axis, and not the CA length (but they are proportional by a factor  $w = 3$ ). From this graph we can see that approximately 15% of the critical areas are reduced to size 0, meaning that the crash was directly into an obstacle. We can also see that for the random placement of obstacles approximately  $1 - 0.71 = 29\%$  of the crashes are at  $200 \text{ m}^2$ , meaning that the aircraft is allowed to traverse the full CA without impacting an obstacle. The same parameter for the obstacles arranged in rows is  $1 - 0.8 = 20\%$  of the crashes. The  $120 \text{ m}^2$  is shown as a black dashed line, corresponding to the reduction used in the iGRC for the 3 m column.

#### B.4.4 Applying reduced CA

Since the distribution of CA lengths is not even close to linear (which would have given a straight line from  $(0, 0)$  to  $(200, 1)$  in Figure 34), the specific probability for being below  $120 \text{ m}^2$  critical area is

not very indicative of the actual effect of the reduction. Instead, the average size of the critical area after reduction is more interesting. This can either be computed as in Equation (74) or it can be computed in the simulation simply by adding the area of all CAs and divide by the number of CAs.

Once the reduced CA has been determined, it can be used in the normal computation for fatality rate, such as in Equation (3), where it will replace the nominal  $A_C$ .

## C Hazard terminology in the context of Annex F

As per SORA v1.0, the SORA bow-tie analysis defined a top-level event as "UAS operation out of control" which is defined as

**"An operation being conducted outside of the approved operations."**

In SORA v2.5, the term has been reworded to "Loss of Control of the Operation". This is further defined in the SORA semantic model as situations:

- Where the outcome of the situation highly relies on providence, or
- Which could not be handled by a contingency procedure.

This is a much wider concept than the loss of control of the UA, which usually refers to situations where there is an unintended departure from controlled flight. Loss of control of the operation instead refers to a point in a series of casual events that lead to one of the following.

- fatal injuries to third parties on the ground
- fatal injuries to third parties in the air (mid-air collision with crewed aircraft)
- damage to critical infrastructure

Due to the SORA semantic model and SORA bow-tie, we can infer that after a UAS operation out-of-control event occurs, there are four "kinds" of end states:

### Loss of control of the operation

- Within the operational volume and ground risk buffers:
  - 1 An event that will result in an eventual **ground impact** that cannot be prevented by contingency procedures. This includes flight termination initiated to ensure the aircraft impacts the ground within the ground risk buffers.
  - 2 A **loss of well clear** that eventually leads to a **Ground impact** due to an airspace event.
    - \* As a result of a loss of well clear, the aircraft impacts the ground. This could include events like a Mid-Air Collision that results in a ground impact, or a manoeuvre to avoid an NMAC or MAC that results in controlled flight into terrain.
  - 3 A **loss of well clear** only.
    - \* A well clear violation, Near Mid-Air Collision, or Mid-Air Collision that doesn't result in a ground impact.
- Within the adjacent area and adjacent airspace:
  - 4 A **Loss of containment**, potentially leading to an airspace event and leading to an eventual ground impact.

These four components of UAS operation out of control are deliberately defined to be mutually exclusive (note that the causes of these events may not be mutually exclusive or at least may be

difficult to delineate), hence we can attribute to each of these events a hazard rate (the probability of the hazard occurring, on the condition it has not occurred yet)

$$\lambda = \frac{P(T = t)}{P(T \geq t)} . \quad (75)$$

- $\lambda_{GI}$  is the hazard rate associated with a ground impact event only (no airspace event) within the operational volume and ground risk buffers.
- $\lambda_{AE}$  is the hazard rate associated with an airspace event only (no ground impact) within the operational volume.
- $\lambda_{AEGI}$  is the hazard rate associated with an airspace event that also results in a ground impact within the operational volume and ground risk buffer.
- $\lambda_{cont}$  is the hazard rate associated with any event (airspace and/or ground impact event) that occurs in the adjacent airspace or adjacent area.

The risk associated with ground impacts due to airspace events ( $\lambda_{AEGI}$ ) is considered part of the air risk model which will be detailed in Annex G <sup>21</sup>.

The risk associated with ground impacts due to a loss of containment ( $\lambda_{cont}$ ) is based on the analysis in of the "average" fGRC in the adjacent area, which uses concepts from this Annex.

The ground risk model in Annex F only deals with the red highlighted dot point (i.e. a ground impact not caused by an airspace event and not a ground risk due to a loss of containment). We will focus on the hazard rate related to ground risk within the operational volume and ground risk buffers ( $\lambda_{GI}$ ). The terms used throughout this Annex will reflect this categorization.

## C.1 UAS operation out of control in context

It is critical to note here that these hazard rates are not equivalent to the Target Level of Safety, as conditional, subsequent events must also occur for the target (third parties on the ground or in the air, critical infrastructure) to be affected by the hazard. For example, in an unmitigated ground risk case, to fatally injure a third party the aircraft must

- have a loss of control of the operation event,
- be on a collision course with a person (or persons), and
- upon collision with the person(s), fatally injure them.

We use the expected casualty equation to understand this:

$$E_C = \lambda_{GI} \cdot D_{pop} \cdot A_C \cdot F_{exp} \cdot P(fatality|impact) \quad (76)$$

To illustrate how a loss of control of the operation can subsequently lead to the fatalities on the ground referred to in Equation (2), an event sequence diagram, is provided in Figure 35.

---

<sup>21</sup>Annex G will be released at a later date

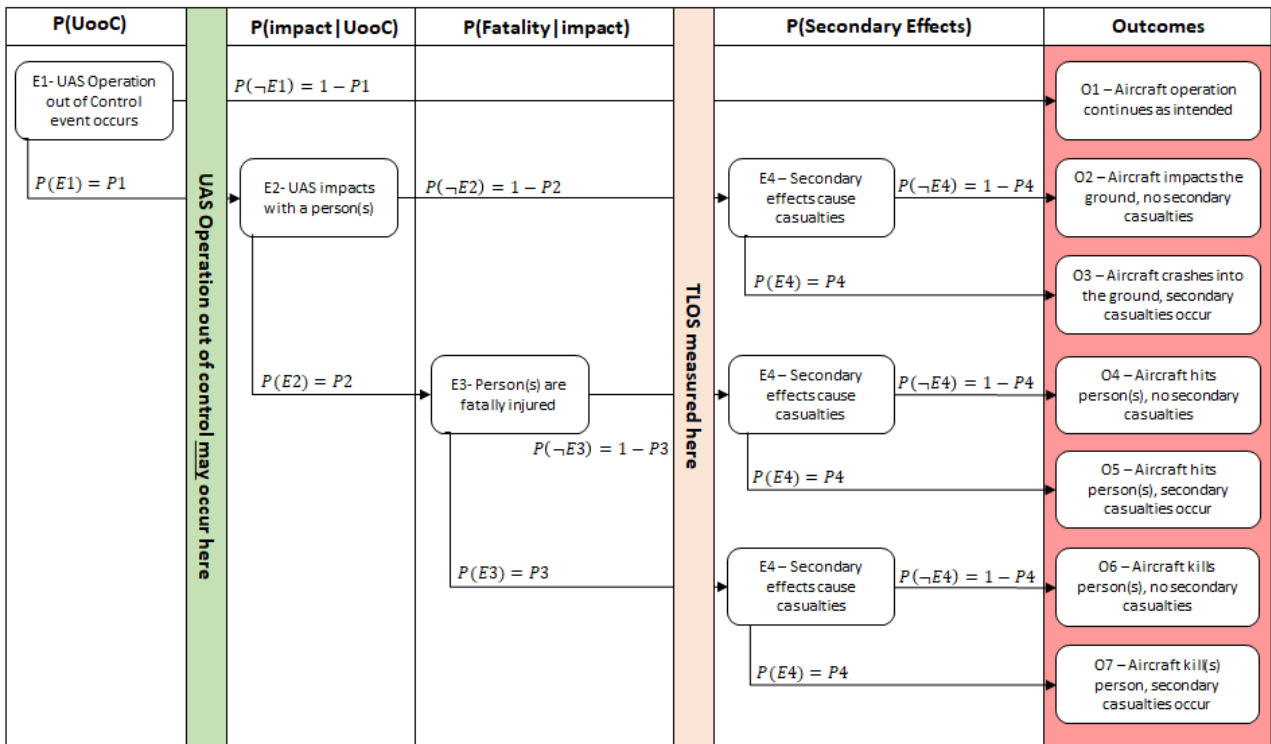


Figure 35: Generic SORA Event Tree.

Critical to note is that after a loss of control of the operation event, multiple (non-guaranteed) events also have to occur before the TLOS is measured. Additionally, OSO #8 of SORA requires that an applicant has an emergency response plan in place and validated, which acts on events after the TLOS is measured, to prevent secondary effects of crashes are managed effectively.

## D Abbreviations and variables

### D.1 Abbreviations

This is a list of used acronyms and abbreviations

Acronym	Description
AMC	Acceptable Means of Compliance
BVLOS	Beyond Visual Line of Sight
CA	Critical area
CFIT	Controlled Flight into Terrain
CoF	Coefficient of Friction
ConOps	Concept of Operations
CoR	Coefficient of Restitution
CV	Containment Volume
D&R	Durability and Reliability
DEGURBA	Degree of Urbanisation
FAA	Federal Aviation Administration
FH	Flight hour
GA	General aviation
GHSL	Global Human Settlement Layer
GPW	Global Population of the World
GRC	Ground risk class
HALE	High Altitude, Long Endurance
IDE	Integrated Development Environment
iGRC	intrinsic ground risk class (unmitigated risk)
JARUS	Joint Authorities for Rulemaking on Uncrewed Systems
KE	Kinetic Energy
LAU	Local Administrative Unit
LTA	Lighter than Air
M1	Mitigation type 1 (prior to flight)
M2	Mitigation type 2 (during flight)
MAUP	Modifiable Areal Unit Problem
NAWCAD	Naval Air Warfare Centre Aircraft Division
OSO	Operational Safety Objective
OV	Operational Volume
PFH	Per flight hour
RB	Risk Buffer
RCC	Range Commander's Council
RPAS	Remotely Piloted Aircraft System
RPM	Revolutions per Minute
RTI	Research Triangle Institute
SAIL	Specific Assurance and Integrity Level
SORA	Specific Operations Risk Assessment
TLOS	Target level of safety (fatality rate)
TNT	Trinitrotoluene
UA	Uncrewed Aircraft
UAS	Uncrewed Aircraft System
UAV	Uncrewed Aerial System
UTM	UAS Traffic Management
VLOS	Visual line of Sight
WG-SRM	Working Group - Safety Risk Management

## D.2 Variables

This is a list of variables used in the math throughout the document.

Variable	Unit	Description
$A$	$m^2$	Drag area for aircraft (area of aircraft projected along direction of travel).
$A_C$	$m^2$	Critical area.
$C_d$	-	Drag coefficient for aircraft.
$C_g$	-	Friction coefficient between aircraft and ground.
$d_{\text{fireball}}$	m	Radius of fireball.
$d_{\text{glide}}$	m	Glide distance (horizontal distance).
$D_{\text{pop}}$	ppl/ $m^2$	population density (Note that while this value is given as pp/ $km^2$ in the GRC tables for easy reference to available data, it does need to be in unit ppl/ $m^2$ in the formulas).
$d_{\text{slide}}$	m	Slide distance.
$d_{\text{thermal}}$	m	Radius of thermal radiation.
$e$	-	Coefficient of restitution.
EC	ppl	Expected number of casualties.
$F_{\text{exp}}$	-	Fraction of people/population exposed to crashing aircraft (also known as sheltering factor).
$\lambda_{\text{fatality}}$	ppl/h	Fatality rate measured in fatalities (of people) per hour.
$g$	$m/s^2$	Gravitational acceleration.
$\lambda_{\text{survival}}$	ppl/h	Rescue rate measured in people rescue (from fatality) per hour.
$h_{\text{person}}$	m	Height of a person.
$K_{\text{non-lethal}}$	J	Non-lethal kinetic energy (highest non-lethal KE at impact).
$l$	m	Length (size of aircraft parallel to the direction of travel).
$m$	kg	Aircraft mass.
$\mu$	$1/m^2$	Obstacle density.
$N_{\text{fatality GA}_{\text{Accident}}}$	-	Expected number of ground fatalities per manned general aviation aircraft accident.
$N_{\text{people}}$	-	Expected number of people a UA collides with during a loss of control event.
$P(\text{fatality collision, GI})$	-	Probability of fatality given a loss of control followed by collision with a person.
$\lambda_{\text{GA}_{\text{Accident}}}$	1/FH	Minimally defined accident rate for manned general aviation.
$\rho$	$kg/m^3$	Air density.
$\lambda_{\text{GI}}$	1/FH	Rate of failure of an aircraft.
$r_{\text{person}}$	m	Radius of a person (same as 'buffer' in some models).
$r_D$	m	'Radius' of the critical area, defined in Equation (59).
$\theta$	def	Impact angle (between direction of travel and ground).
$v$	m/s	Impact velocity (in the direction of travel at impact).
$v_{\text{horizontal}}$	m/s	Horizontal speed (horizontal component of $v$ ).
$v_{\text{non-lethal}}$	m/s	Non-lethal velocity (derived from $K_{\text{non-lethal}}$ ).
$v_{\text{no}}$	m/s	Maximum structurally safe cruising speed.
$w$	m	Wingspan (size of aircraft orthogonal to the direction of travel).

## E CasEx package

### E.1 Introduction

As part of the development of this document, quite a lot of programming in Matlab and Python has been done to test out different ideas, verify assumptions, plot graphs, etc. Some of this code work might be useful to other people, and may also serve to document how the various models and math implementation have been used in the development of this Annex.

Therefore, we decided to spend the effort to convert some of the code into a publicly available toolbox that can be used to apply the methods described without having to implement it all from scratch. The toolbox also reproduces some of the figures in this Annex.

The toolbox is called CasEx, and it is intended as a supplement to this Annex. It is important to note that it is still the responsibility of the operator or authority using the toolbox to make sure that any computed value and use of such values is in compliance with the SORA.

### E.2 Installation and use

In order to install the package, you need to have installed Python 3.6 or later. In addition, it is highly recommended to have an IDE for editing and running the code as well. Please refer to the appropriate documentation for installing Python.

Once installed, the CasEx package can be downloaded and installed using the following on the command prompt:

```
pip install casex
```

There is full documentation for the package, and this can be found at

<https://casex.readthedocs.io>

This documentation includes references for all the features of the toolbox, plus a series of eight examples that can be used to understand how the toolbox works. Do note that it will require some basic skills in Python to use the toolbox.

As referenced a number of times in the previous chapters, the toolbox also contains code for reproducing some of the figures, specifically Figures 2, 3, 27, and 34. In addition, the computed ballistic values in Table 29 can also be computed. See example 8 for details.

### E.3 Online calculator

We have also created an online calculator that allows users to use the JARUS model to compute a critical area and associated iGRC value. This is simply an online implementation of the CasEx toolbox with a simple graphical user interface. The calculator can be found at

<http://www.casex.one>

Note that this online functionality is still in development, and bugs are still being fixed.

## References

- [1] JARUS, "UAS Operational Categorisation," JARUS, Tech. Rep., 2019. [Online]. Available: [http://jarus-rpas.org/sites/jarus-rpas.org/files/jar\\_doc\\_09\\_uas\\_operational\\_categorization.pdf](http://jarus-rpas.org/sites/jarus-rpas.org/files/jar_doc_09_uas_operational_categorization.pdf)
- [2] —, "Scoping paper to amc rpas 1309 issue 2," JARUS, Tech. Rep., 2015. [Online]. Available: <http://jarus-rpas.org/content/jar-doc-04>
- [3] Range Commanders Council, "Range safety criteria for unmanned air vehicles - rationale and methodology supplement. Supplement to document 323-99," Range Commanders Council, Tech. Rep., 2001.
- [4] R. M. Montgomery and J. A. Ward, "Casualty Areas from Impacting Inert Debris for People in the Open - RTI Report No. RTI/5180/60-31F," Research Triangle Institute, Tech. Rep., 1995.
- [5] Federal Aviation Administration, "Flight Safety Analysis Handbook Federal Aviation Administration," Federal Aviation Administration, Tech. Rep., sep 2011. [Online]. Available: [https://www.faa.gov/about/office\\_org/headquarters\\_offices/ast/media/Flight\\_Safety\\_Analysis\\_Handbook\\_final\\_9\\_2011v1.pdf](https://www.faa.gov/about/office_org/headquarters_offices/ast/media/Flight_Safety_Analysis_Handbook_final_9_2011v1.pdf)
- [6] J. A. Ball, M. Knott, and D. Burke, "Crash Lethality Model - Report no. NAWCADPAX/TR-2012/196," Naval Air Warfare Center Aircraft Division, Tech. Rep., 2012.
- [7] M. J. Harwick, J. Hall, J. W. Tatom, and R. G. Baker, "Approved Methods and Algorithms for DoD Risk-Based Explosives Siting," DDESB, Tech. Rep., jul 2009. [Online]. Available: <http://www.dtic.mil/docs/citations/ADA463571>
- [8] Federal Aviation Administration, "System Safety Analysis and Assessment for Part 23 Airplanes," Federal Aviation Administration, Tech. Rep., 2011. [Online]. Available: [https://www.faa.gov/documentLibrary/media/Advisory\\_Circular/AC\\_23\\_1309-1E.pdf](https://www.faa.gov/documentLibrary/media/Advisory_Circular/AC_23_1309-1E.pdf)
- [9] N. Wardrop, W. Jochem, T. Bird, H. Chamberlain, D. Clarke, D. Kerr, L. Bengtsson, S. Juran, V. Seaman, and A. Tatem, "Spatially disaggregated population estimates in the absence of national population and housing census data," *Proceedings of the National Academy of Sciences*, vol. 115, no. 14, pp. 3529–3537, 2018.
- [10] WorldPop, *WorldPop Methods for Creating Population Density Maps and grid based count data*, (Accessed Jan 10, 2021), available at <https://www.worldpop.org/methods>.
- [11] —, *WorldPop Population Density Data*, (Accessed Jan 10, 2021), available at <https://www.worldpop.org/project/categories?id=18>.
- [12] Facebook/CEISIN, *Methods for Development FaceBook Data for Good Population Density Maps*, Accessed Jan 10, 2021, <https://dataforgood.fb.com/docs/methodology-high-resolution-population-density-maps-demographic-estimates/>.
- [13] M. Li, H. Zhang, and J. Chen, "Fine-grained dynamic population mapping method based on large-scale sparse mobile phone data," in *2019 20th IEEE International Conference on Mobile Data Management (MDM)*. IEEE, 2014, pp. 473–478.
- [14] D. Trewin, "Information paper: Mesh blocks australia," 2003.
- [15] C. for International Earth Science Information Network (CIESIN), "Documentation for the gridded population of the world, version 4 (gpwv4), revision 10 data sets," NASA Socioeconomic Data and Applications Center (SEDAC) Palisades, NY, Tech. Rep., 2017.
- [16] W. R. Tobler, "Smooth pycnophylactic interpolation for geographical regions," *Journal of the American Statistical Association*, vol. 74, no. 367, pp. 519–530, 1979.

- [17] W. Kongko, T. Schlurmann, and R. Khomarudin, "Tsunami model of cilacap-indonesia: Inundation and its mitigation," *AGUFM*, vol. 2009, pp. NH31B–1114, 2009.
- [18] H. Kim and X. Yao, "Pycnophylactic interpolation revisited: integration with the dasymetric-mapping method," *International Journal of Remote Sensing*, vol. 31, no. 21, pp. 5657–5671, 2010.
- [19] A. J. Tatem, A. M. Noor, C. Von Hagen, A. Di Gregorio, and S. I. Hay, "High resolution population maps for low income nations: combining land cover and census in east africa," *PloS one*, vol. 2, no. 12, p. e1298, 2007.
- [20] Oak Ridge National Laboratory, *LandScan - Geographic Information Science & Technology*, 2019, <https://landscan.ornl.gov>.
- [21] E. E. Agency, "Clc2006 technical guidelines," *EEA Technical report No 17/2007*, 2006. [Online]. Available: [https://land.copernicus.eu/user-corner/technical-library/copy\\_of\\_CLC2006\\_technical\\_guidelines.pdf](https://land.copernicus.eu/user-corner/technical-library/copy_of_CLC2006_technical_guidelines.pdf)
- [22] European Commission. (2019) GHSL - Global Human Settlement Layer. [Online]. Available: <https://ghsl.jrc.ec.europa.eu>
- [23] C. Frie, "White paper: ESRI's 2016 World Population Estimate Methodology," ESRI, Tech. Rep., 2017. [Online]. Available: [https://www.esri.com/content/dam/esrisites/en-us/media/whitepaper/Esri\\_2016\\_WPE\\_Methodology\\_WhitePaper.pdf](https://www.esri.com/content/dam/esrisites/en-us/media/whitepaper/Esri_2016_WPE_Methodology_WhitePaper.pdf)
- [24] F. Sergio, K. MacManus, M. Pesaresi, E. Doxsey-Whitfield, and J. Mills, "Development of new open and free multi temporal global population grids at 250 m resolution," *Geospatial Data in a Changing World*, 2016. [Online]. Available: [https://agile-online.org/conference\\_paper/cds/agile\\_2016/shortpapers/152\\_Paper\\_in\\_PDF.pdf](https://agile-online.org/conference_paper/cds/agile_2016/shortpapers/152_Paper_in_PDF.pdf)
- [25] Oak Ridge National Laboratory, *LandScan - Documentation*, 2021, <https://landscan.ornl.gov/documentation>.
- [26] P. Deville, C. Linard, S. Martin, M. Gilbert, F. R. Stevens, A. E. Gaughan, V. D. Blondel, and A. J. Tatem, "Dynamic population mapping using mobile phone data," *Proceedings of the National Academy of Sciences*, vol. 111, no. 45, pp. 15 888–15 893, 2014.
- [27] M. Li, H. Zhang, and J. Chen, "Fine-grained dynamic population mapping method based on large-scale sparse mobile phone data," in *2019 20th IEEE International Conference on Mobile Data Management (MDM)*. IEEE, 2019, pp. 473–478.
- [28] U. L. de Bruxelles, "First dynamic national-scale population map based on mobile phone data." *Science Daily*, 2014, [www.sciencedaily.com/releases/2014/10/141028101306.htm](http://www.sciencedaily.com/releases/2014/10/141028101306.htm).
- [29] L. Dijkstra and H. Poelman, "A harmonised definition of cities and rural areas: the new degree of urbanisation," *Regional Working Paper*, vol. 1, p. 2014, 2014.
- [30] L. Dijkstra, A. J. Florczyk, S. Freire, T. Kemper, M. Melchiorri, M. Pesaresi, and M. Schiavina, "Applying the degree of urbanisation to the globe: A new harmonised definition reveals a different picture of global urbanisation," *Journal of Urban Economics*, p. 103312, 2020.
- [31] European Commission Joint Research Centre, *GHS-SMOD: Country Fact Sheets based on the Degree of Urbanisation*, (accessed Feb 7, 2021), <https://ghsl.jrc.ec.europa.eu/CFS.php>.
- [32] —, *DEGURBA Simple Visualisation of Classes*, (accessed Feb 7, 2021), <https://ghsl.jrc.ec.europa.eu/degurbaDefinitions.php>.
- [33] —, *GHS-Tools*, (accessed Feb 7, 2021), <https://ghsl.jrc.ec.europa.eu/tools.php>.

- [34] L. Dijkstra, A. Florczyk, S. Freire, M. Pesaresi, and T. Kemper, "Applying the Degree of Urbanisation To the Globe : A New Harmonised Definition Reveals a Different Picture of Global Urbanisation," *16th Conference of International Association of Official Statisticians*, no. September, pp. 19–21, 2018.
- [35] NASA SEDAC, *NASA SEDAC Popgrid Viewer*, (Accessed Feb 10, 2021), available at <https://sedac.ciesin.columbia.edu/mapping/popgrid/>.
- [36] CEISIN, *Global Rural Urban Mapping Project Version 1-Download*, (accessed December 3, 2020), <https://sedac.ciesin.columbia.edu/data/set/grump-v1-urban-extents/data-download>.
- [37] Schiavina, Marcello and Freire, Sergio and MacManus, Kytt, *GHS population grid multitemporal (1975, 1990, 2000, 2015)*, (accessed December 3, 2020), <http://data.europa.eu/89h/0c6b9751-a71f-4062-830b-43c9f432370f>.
- [38] Florczyk, Aneta J. and Corbane, Christina and Ehrlich, Daniele and Freire, Sergio and Kemper, Thomas and Maffeni, Luca and Melchiorri, Michele and Pesaresi, Martino and Politis, Panagiotis and Schiavina, Marcello and Sabo, Filip and Zanchetta, Luigi, "JRC-Technical Report: GHSL Data Package 2019," [https://ghsl.jrc.ec.europa.eu/documents/GHSL\\_Data\\_Package\\_2019.pdf?t=1478q532234372](https://ghsl.jrc.ec.europa.eu/documents/GHSL_Data_Package_2019.pdf?t=1478q532234372), 2019, [Online; accessed 10-Jan-2021].
- [39] European Commission Joint Research Centre, *GHS-SMOD Dataset Epoch 2015*, (accessed December 3, 2020), <https://ghsl.jrc.ec.europa.eu/download.php?ds=smod>.
- [40] A. Florczyk, C. Corbane, D. Ehrlich, S. Freire, T. Kemper, L. Maffeni, M. Melchiorri, M. Pesaresi, P. Politis, M. Schiavina *et al.*, "Ghsl data package 2019," *European Commission Joint Research Center*, vol. 29788, 2019. [Online]. Available: [https://ghsl.jrc.ec.europa.eu/documents/GHSL\\_Data\\_Package\\_2019.pdf?t=1478q532234372](https://ghsl.jrc.ec.europa.eu/documents/GHSL_Data_Package_2019.pdf?t=1478q532234372)
- [41] Eurostat, *GeoStat database*, Accessed Jan 10, 2021, <https://ec.europa.eu/eurostat/web/gisco/geodata/reference-data/population-distribution-demography/geostat>.
- [42] European Forum for GeoStatistics (EuroStat), *Method Summary for Creating GeoStat Database*, (accessed December 3, 2020), also available as [https://ec.europa.eu/eurostat/statistics-explained/index.php/Population\\_grids#Methodology](https://ec.europa.eu/eurostat/statistics-explained/index.php/Population_grids#Methodology).
- [43] European Forum for GeoStatistics V7.0, *GEOSTAT 1A – Representing Census data in a European population grid*, (accessed December 3, 2020), available at [https://ec.europa.eu/eurostat/statistics-explained/index.php/Population\\_grids#Methodology](https://ec.europa.eu/eurostat/statistics-explained/index.php/Population_grids#Methodology).
- [44] C. Corbane, M. Pesaresi, T. Kemper, P. Politis, A. J. Florczyk, V. Syrris, M. Melchiorri, F. Sabo, and P. Soille, "Automated global delineation of human settlements from 40 years of landsat satellite data archives," *Big Earth Data*, 2016.
- [45] Florczyk, Aneta; Pesaresi, Martino; Politis, Panagiotis; Syrris, Vasileios, *GHS built-up grid, derived from Landsat, multitemporal (1975-1990-2000-2014)*, (accessed December 3, 2020), <http://data.europa.eu/89h/jrc-ghsl-10007>.
- [46] , *CORINE LAND COVER DATA 2018*, (accessed February , 2021), <https://land.copernicus.eu/pan-european/corine-land-cover/clc2018>.
- [47] Copernicus, *European Settlement Map Data*, (Accessed Feb 10, 2021), available at <https://land.copernicus.eu/pan-european/GHSL/european-settlement-map>.
- [48] F. Sabo, C. Corbane, P. Politis, M. Pesaresi, and T. Kemper, "Update and improvement of the european settlement map," in *2019 Joint Urban Remote Sensing Event (JURSE)*. IEEE, 2019, pp. 1–4.

- [49] F. Sabo, C. Corbane, P. Politis, and T. Kemper, "The European Settlement Map 2019 release," *Luxembourg, EUR*, 2019.
- [50] T. G. Tiecke, X. Liu, A. Zhang, A. Gros, N. Li, G. Yetman, T. Kilic, S. Murray, B. Blankspeer, E. B. Prydz *et al.*, "Mapping the world population one building at a time," *arXiv preprint arXiv:1712.05839*, 2017.
- [51] CIESIN, *CIESIN High Resolution Settlement Layer*, (Accessed Feb 10, 2021), available at <https://www.ciesin.columbia.edu/data/hrsl/>.
- [52] —, *CIESIN HRSL Viewer*, (Accessed Feb 10, 2021), available at <https://columbia.maps.arcgis.com/apps/View/index.html?appid=ce441db6aa54494cbc6c6cee11b95917>.
- [53] P. W. Janser, "Lethality of unprotected persons due to debris and fragments," *Twentieth Explosives Safety Seminar*, no. 164, 1982.
- [54] A. la Cour-Harbo, "Ground impact probability distribution for small unmanned aircraft in ballistic descent," in *2020 International Conference on Unmanned Aircraft Systems (ICUAS)*. IEEE, 2020, pp. 1442–1451.
- [55] D. I. Feinstein, "Fragment hazard criteria," Defence Documentation Explosives Safety Board, Tech. Rep., 1974.
- [56] Department of Defense, "DoD Ammunition and Explosives Safety Standards: General Explosives Safety Information and Requirements - DOD 6055.09-M, Volume 1," DoD, Tech. Rep., 2012.
- [57] A. la Cour-Harbo and H. Schioler, "How obstacles may reduce the impact of a crashing unmanned aircraft," *Preprint*, 2021.